Mechanisms and functions of adaptation in the *D. melanogaster* olfactory system

Dissertation
Zur Erlangung des Grades
Doktor der Naturwissenschaften

Am Fachbereich Biologie
Der Johannes Gutenberg-Universität Mainz

Ana Sofia de Castro Brandão
geb. am 02.02.1994 in Porto, Portugal

Mainz, 2025

Dekan: Prof. Dr. Eckhard Thines

1.Berichterstatter:

2.Berichterstatter:

Tag der mündlichen Prüfung:

Table of Contents

1 Abstract 4

2 Zusammenfassung 5

3 Introduction 7

3.1 Plasticity, adaptability and robustness in olfaction 7

3.2 Adaptation in olfactory receptor neurons 9

3.3 Mechanisms for response and adaptation in olfactory receptor neurons 10

3.4 Organization of the olfactory system 12

3.5 Antennal lobe computations 13

3.6 Aims of the dissertation and summary of the findings 15

4 Manuscripts 16

4.1 Adaptive temporal processing of odor stimuli 16

4.2 Undoing of firing rate adaptation enables invariant population codes 34

4.3 Impact of developmental temperature on neural growth, connectivity, and function 67

5 Discussion 94

5.1 The neurons behind the homeostatic inhibitory feedback loop 94

5.2 Glomerular variability 95

5.3 Background invariance – from ORNs to PNs 95

5.4 Odor representations downstream of the antennal lobe 96

5.5 Conclusions and outlook 97

6 Bibliography 98

7 Acknowledgements 105

8 Appendix 107

8.1 List of Abbreviations 107

8.2 Declaration of Independence 108

8.3 Declaration of Honor 109

Curriculum Vitae 110

1 Abstract

Animals must navigate an ever-changing world in order to survive and reproduce. Plasticity endows sensory systems with the required flexibility to deal with changes on many different timescales and maintain robust outcomes. This is only possible if a balance between plasticity and robustness is achieved. To address this interplay, I studied two instances of plasticity in the olfactory system of *Drosophila melanogaster*: lifelong developmental plasticity and short-term stimulus-driven plasticity (adaptation). In both contexts, I focused on the antennal lobe. In this neuropil that constitutes the first sensory relay of the olfactory system, the combinatorial odor representation that relies on multiple olfactory receptor neuron (ORN) types emerges and is modulated by a network of local neurons that are mainly GABAergic.

The **first manuscript** reviews the current literature on adaptation at the periphery of the olfactory system, setting a starting point for my work. Here, we compare adaptation to a constant background in vision to olfaction. Photoreceptors and ORNs both have background-dependent responses, but they show different strategies for adaptation, endowing the former with contrast sensitivity at the single neuron level but not the latter. Surprisingly, ORN firing rate adaptation is undone in the antennal lobe and ORN presynaptic calcium responses are background invariant.

In the **second manuscript**, which is the main outcome of my work, I set out to investigate the molecular and circuit mechanisms that undo firing rate adaptation at the ORN output synapses and to understand the role of this transformation for odor coding. First, through optogenetic activation of a single ORN type, I found that multi-glomerular activation is not required for background-invariant responses in a single glomerulus. This experiment also confirmed previous observations that background invariance is asymmetric – it is only observed for ON stimuli (increases in concentration compared to the background). Then, I confirmed that ORN synaptic output is required by silencing specific ORN types and measuring presynaptic calcium transients in these ORNs. Since ORNs are cholinergic, this result was confirmed by pharmacologically blocking acetylcholine receptors. Finally, pharmacological blocking of GABA receptors identified a homeostatic feedback circuit that likely involves local neurons and achieves asymmetric background invariance in ORN axon terminal calcium responses. Interestingly, modelling of ORN responses shows that this feedback inhibition results in background-invariant presynaptic ORN responses only if single ORNs adapt differently from photoreceptors, by decreasing their response rather than shifting their sensitivity. When assessing the functional output of the antennal lobe, postsynaptic projection neuron (PN) responses, I found that they are also asymmetric background invariant. By testing a gain-of-function mutation that abolishes calcium-dependent synaptic plasticity in the active zone protein Unc13, I found that background invariance in PNs requires synaptic plasticity. Lastly, modelling of PN responses indicates that these novel functions of olfactory processing in the antennal lobe enable downstream circuits to drive background-robust odor-specific behaviors while tuning odor coding to ON stimuli, which are more behaviorally relevant.

In the **third manuscript**, I investigated how developmental plasticity affects odor coding in the antennal lobe. Changing the developmental temperature has been shown in our lab to substantially alter the wiring of the olfactory system, allowing us to probe developmental plasticity. I found that odor coding in PNs was not altered by the differences in connectivity induced by developmental temperature, suggesting a balance between excitatory and inhibitory pathways that ensures odor coding stability across environmental conditions.

Overall, I have found surprising robustness of odor representations in the antennal lobe, both in the face of different odor backgrounds and of differences in wiring caused by changes in developmental temperature. My work suggests that robustness in this neuropil is actively maintained and implicates local neurons in this process, warranting and providing a framework for further research into this network of functionally and anatomically diverse neurons.

2 Zusammenfassung

Tiere müssen sich in einer immerzu verändernden Umwelt zurechtfinden, um zu überleben und sich fortzupflanzen. Plastizität verleiht den Sinnesorganen die erforderliche Flexibilität, um mit Veränderungen auf vielen verschiedenen Zeitskalen umzugehen und robuste Ergebnisse aufrecht zu erhalten. Dies ist nur möglich, wenn ein Gleichgewicht zwischen Plastizität und Robustheit erreicht wird. Um diese Wechselwirkung zu untersuchen, habe ich zwei Fälle von Plastizität im Geruchssystem von *Drosophila melanogaster* untersucht: lebenslange Entwicklungsplastizität sowohl kurzfristige, durch Reize ausgelöste Plastizität (Adaptation). In beiden Kontexten habe ich mich auf den Antennallobus konzentriert. In diesem Neuropil, der die erste sensorische Relaisstation des Geruchssystems bildet, entsteht eine kombinatorische Geruchsrepräsentation, die auf mehreren Arten von Geruchsrezeptorneuronen (ORN) beruht und durch ein Netzwerk lokaler, überwiegend GABAerger Neuronen moduliert wird.

Das **erste Manuskript** gibt einen Überblick über die aktuelle Literatur zur Adaptierung in der Peripherie des Geruchssystems und bildet den Ausgangspunkt für meine Arbeit. Hier vergleichen wir die Anpassung an einen konstanten Hintergrund im Sehen mit der Anpassung im Geruchssinn. Photorezeptoren und ORNs haben beide hintergrundabhängige Reaktionen, zeigen jedoch unterschiedliche Anpassungsstrategien, wodurch erstere auf der Ebene einzelner Neuronen kontrastempfindlich sind, letztere hingegen nicht. Überraschenderweise wird die Anpassung der ORN-Feuerrate im Antennallobus ungeschehen gemacht, und die präsynaptischen Kalziumreaktionen der ORNs sind hintergrundunabhängig.

Im **zweiten Manuskript**, dass das Hauptergebnis meiner Arbeit darstellt, habe ich mich daran gemacht, die molekularen und schaltkreistechnischen Mechanismen, die die Anpassung der Feuerrate an den ORN-Ausgangssynapsen rückgängig machen zu untersuchen, und die Rolle dieser Transformation für die Geruchskodierung zu verstehen. Zunächst habe ich durch optogenetische Aktivierung eines einzelnen ORN-Typs festgestellt, dass eine multi-glomeruläre Aktivierung für hintergrundunabhängige Reaktionen in einem einzelnen Glomerulus nicht erforderlich ist. Dieses Experiment bestätigte auch frühere Beobachtungen, dass die Hintergrundinvarianz asymmetrisch ist – sie wird nur für ON-Reize (Anstieg der Konzentration im Vergleich zum Hintergrund) beobachtet. Anschließend bestätigte ich, dass synaptische Aktivität der ORN erforderlich ist, indem ich bestimmte ORN-Typen stilllegte und die präsynaptischen Kalziumtransienten in diesen ORNs maß. Da ORNs cholinerg sind, wurde dieses Ergebnis durch die pharmakologische Blockierung von Acetylcholinrezeptoren bestätigt. Schließlich identifizierte die pharmakologische Blockierung von GABA-Rezeptoren einen homöostatischen Rückkopplungskreislauf, der wahrscheinlich lokale Neuronen einbezieht und eine asymmetrische Hintergrundinvarianz in den Calcium-Reaktionen der ORN-Axonenenden erreicht. Interessanterweise zeigt die Modellierung der ORN-Reaktionen, dass diese Rückkopplungshemmung nur dann zu hintergrundinvarianten präsynaptischen ORN-Reaktionen führt, wenn einzelne ORNs sich anders als Photorezeptoren anpassen, indem sie ihre Reaktion verringern, anstatt ihre Empfindlichkeit zu verschieben. Bei der Bewertung des funktionellen Ergebnisses des Antennallobus, Reaktionen der postsynaptischen Projektionsneuronen (PN), stellte ich fest, dass diese ebenfalls asymmetrisch und hintergrundinvariant sind. Durch die Untersuchung einer Funktionsgewinnmutation, die die calciumabhängige synaptische Plastizität im aktiven Zonenprotein Unc13 aufhebt, stellte ich fest, dass die Hintergrundinvarianz in PNs synaptische Plastizität erfordert. Schließlich zeigt die Modellierung der PN-Reaktionen, dass diese neuartigen Funktionen der Geruchsverarbeitung im Antennallobus es den nachgeschalteten Schaltkreisen ermöglichen, hintergrundrobuste geruchsspezifische Verhaltensweisen anzutreiben und gleichzeitig die Geruchskodierung auf ON-Reize abzustimmen, die für das Verhalten relevanter sind.

Im **dritten Manuskript** untersuchte ich, wie sich Entwicklungsplastizität auf die Geruchskodierung im Antennallobus auswirkt. In unserem Labor wurde gezeigt, dass eine Veränderung der Entwicklungstemperatur die Verschaltungen des Geruchssystems erheblich verändert, was uns die

Untersuchung von Entwicklungsplastizität ermöglicht. Ich stellte fest, dass die Geruchskodierung in PNs durch die Entwicklungstemperatur induzierten Unterschiede nicht verändert wurde, was auf ein Gleichgewicht zwischen exzitatorischen und inhibitorischen Bahnen hindeutet, welche die Stabilität der Geruchskodierung unter verschiedenen Umweltbedingungen gewährleisten.

Insgesamt habe ich eine überraschende Robustheit der Geruchsrepräsentationen im Antennallobus festgestellt, sowohl angesichts unterschiedlicher Geruchshintergründe als auch angesichts von Unterschieden in der Verschaltung, die durch Veränderungen der Entwicklungstemperatur verursacht wurden. Meine Arbeit legt nahe, dass die Robustheit in diesem Neuropil aktiv aufrechterhalten wird und lokale Neuronen an diesem Prozess beteiligt sind, was einen Rahmen für weiterfuehrende Forschung zu diesem Netzwerk funktionell und anatomisch vielfältiger Neuronen rechtfertigt und bereitstellt.

3 Introduction

Animals must survive and reproduce in a world that is constantly changing, over both short and long timescales. Temperature can change when one suddenly enters a shadowed area or lives through global warming. Changes can be unexpected like natural disasters, or predictable such as the change in light intensity as night approaches. Sensory systems, which allow animals to perceive their environment, are often robust: they maintain stable function and support behavior despite considerable variations in environmental conditions. But robustness does not mean no change. In fact, plasticity, the brain's ability to change structurally and/or physiologically in response to internal or external factors, often supports robustness. The brain adapts to different contexts through plasticity, during development and adulthood (Turrigiano, 2012; Kolb et al., 2017; Anton and Rössler, 2020; Wu et al., 2020). When such mechanisms fail or are unavailable, animals' behaviors can become maladaptive, with consequences for survival and fitness. As an example, the 'master clock of the brain' in mammals, the suprachiasmatic nucleus (SCN), changes the internal circadian rhythm in response to daily and seasonal changes thanks to its plastic encoding of the light-dark cycle and of day length. But this plasticity makes it possible for excessive artificial blue light at night to deregulate the circadian rhythm, which can lead to negative effects on mental and physical health (Meijer et al., 2010; Wahl et al., 2019). Identifying the mechanisms that allow plasticity in brain function to support behavioral adaptation is therefore key to understanding the principles behind robustness of healthy brains as well as what are the possible causes of unhealthy function.

3.1 Plasticity, adaptability and robustness in olfaction

Olfaction is fundamental for food searching and social and predatory interactions in many species. In the highly plastic olfactory system, information travels forward towards multisensory brain regions through a single synaptic step in the first relay center, making this a great system to investigate neuronal plasticity. Plasticity across different timescales allows the olfactory system to balance flexibility and stability, ensuring robust function in a changing world.

On longer timescales, changes experienced over days or even months during development can have long-term or even lifelong effects on individuals. For example, in mammals, prenatal experience can affect postnatal olfactory phenotypes. This is the case in the European rabbit (*Oryctolagus cuniculus*), where exposure to juniper by the doe (mother rabbit), achieved by feeding her with aromatic juniper berries during pregnancy, increased pup preference to juniper odor after birth (Semke et al., 1995; Hudson and Distel, 1998). The effect of developmental plasticity on the olfactory system has been particularly well studied in eusocial insects, where postembryonic conditions like feeding and temperature are controlled through cooperative care and can be manipulated to obtain different adult phenotypes. Honeybees are a well-known example where the adult phenotype of queen or worker, which involves differences in odor-driven behavior responses to specific pheromones, is dictated by feeding during development (Pettis et al., 1995; Kucharski et al., 2008; Vergoz et al., 2009; Falibene et al., 2016). Together, these studies exemplify how prenatal and early-life experiences and conditions impact the developing olfactory system, with possibly long-lasting consequences that can influence adulthood.

On shorter timescales, stimulus-driven plasticity or adaptation has short-term effects, with neuronal responses to an odor decreasing after repeated or prolonged exposure. This correlates with a decreased perception of the stimulus, which has been shown across animals from humans to

Caenorhabditis elegans (Cain, 1970; Colbert and Bargmann, 1995). In *C. elegans*, AWC neurons respond to benzaldehyde, isoamyl alcohol and butanone. While adaptation to butanone does not cause adaptation to any other of these odorants (no cross-adaptation), adaptation to benzaldehyde induces cross-adaptation to isoamyl alcohol and adaptation to isoamyl alcohol causes cross-adaptation to benzaldehyde. Two different intracellular molecular pathways were found to be responsible for adaptation to benzaldehyde and to isoamyl acetate, but they must converge at some point to enable cross-adaptation. On the other hand, adaptation to butanone requires both pathways, which explains why cross-adaptation with butanone does not occur (Colbert and Bargmann, 1995). Olfactory adaptation has also been investigated in humans through psychophysics by relating objective odor concentrations to how strongly these odors are perceived by human participants – magnitude estimation. To evaluate how adaptation affects human perception, observers were asked to estimate the magnitude of each odor dilution presented, either with or without pre-exposure to the same odor. After adaptation, magnitude estimation curves became steeper: higher concentrations are perceived the same but lower concentrations are perceived as weaker (Cain, 1970). This powerful study illustrates how adaptation can alter our perception and understanding of the world.

The function of adaptation goes beyond the decrease in responsiveness. Several studies demonstrated that sensory neurons adapt to the recent stimulus history to better encode the stimulus statistics (Barlow, 1961; Wark et al., 2007; Weber et al., 2019; Benda, 2021; Brandão et al., 2021; Martelli and Storace, 2021). The neuron is left better able to respond to the more informative features of the stimulus because it devotes less resources to encoding the constant ones. The stimulus features that a system can adapt to can be several depending on the modality, but I will consider only adaptation to the mean of the stimulus unless otherwise mentioned. An example of adaptation to the mean occurs in photoreceptor neurons in the fly visual system. These neurons respond to light intensities that span multiple orders of magnitude because they adapt to the background luminance (Laughlin, 1989; Wark et al., 2007). When they are allowed to adapt to backgrounds of increasing luminance, their response-function **shifts** to higher stimulus intensities while maintaining its shape. This effectively changes the sensitivity of the neuron while maintaining its coding ability (Laughlin and Hardie, 1978; Brandão et al., 2021). Such a mechanism has been observed in photoreceptors of different animals, like the dragonfly and the turtle, but also across sensory modalities, with the example of neurons in the auditory midbrain of the guinea pig (Laughlin and Hardie, 1978; Burkhardt, 1994; Dean et al., 2005; Willmore and King, 2023).

In this dissertation, I investigate the underlying mechanisms and functions of developmental and stimulus-driven plasticity in olfactory processing in the fly brain. *Drosophila melanogaster* is well suited for this endeavor because it has a multitude of genetic driver lines that are well established, including for neurons in the olfactory system; it is relatively easy to breed and care for, having a fast life cycle and being small; it has different published connectomes, which have allowed for thorough knowledge of the olfactory system morphology; and it is an organism where plenty of previous research exists for the olfactory system. To investigate developmental plasticity, we used temperature as a putative environmental factor (Züfle et al., 2025 - manuscript in section 4.3); in this recently published study, I found that odor responses in second-order neurons in the olfactory system are invariant to major circuit changes that were induced by different developmental temperatures. However, most of my work in the past years focused on understanding stimulus-driven plasticity in the olfactory system, which I will develop henceforth.

3.2 Adaptation in olfactory receptor neurons

Stimulus-driven plasticity, or adaptation, is observed in olfactory receptor neurons (ORNs), the neurons at the periphery of the olfactory system (Kurahashi and Menini, 1997; Reisert and Matthews, 1999; Nagel and Wilson, 2011; Martelli and Fiala, 2019). As part of my doctorate, I co-authored a review paper where data from photoreceptors (fly and dragonfly) and ORNs (fruit fly and frog) are directly compared (Brandão et al., 2021 – manuscript in section 4.1; figure 2 - data reanalyzed from Laughlin and Hardie, 1978; Reisert and Matthews, 1999; Martelli et al., 2013). While photoreceptors shift their responses after adaptation, this is not the case for ORNs. For these neurons, the response is instead **reduced** after adaptation: they respond to the same intensities of the stimulus but their responses are lower than in the non-adapted condition. This is true for both the fruit fly and the frog data analyzed, indicating that it is a shared feature between vertebrates and invertebrates. This left us questioning whether the different types of adaptation observed in the two sensory systems underly different functions.

To understand the function of adaptation, it's important to consider Barlow's efficient coding hypothesis (named by him as the 'redundancy-reducing hypothesis'), which posits that neuronal circuits use a coding strategy that allows their limited capacity to transmit information to be optimally utilized (Barlow, 1961; Wark et al., 2007). This means that a neuron will devote fewer resources (or none) to encoding a feature of the stimulus that is frequent while devoting more resources to less common features (Barlow, 1961). This hypothesis has since created a theoretical framework in which we can understand adaptation as a mechanism enabling efficient coding in sensory systems. Photoreceptors are an example of Barlow's efficient coding hypothesis since they adapt their response curve to the mean background luminance. Their adaptation to the background also ensures that they are contrast sensitive, following the Weber's law (Fechner, 1966; Laughlin, 1989). Proposed by E. H. Weber but formalized and named by G. Fechner, this law states that perception through most sensory modalities can be understood by a *just noticeable difference* (JND) that depends on the stimulus background intensity (Fechner, 1966). For example, you can easily tell if you are holding two books of similar size instead of one, but a coin on top of a book is difficult to tell apart from the book alone. Weber's law suggests that distinguishing the second book but not the additional coin can be explained by the JND: the weight of the book is higher than the JND for the book weight (the background intensity), but the coin is lighter, therefore not being perceived. From this we can understand that when we have a certain background intensity (in our example, the book weight), it is the contrast between the additional item and the book that matters for perception and not the absolute weight of the second item. Adaptation in photoreceptors is therefore one of the mechanisms that guarantees that vision is luminance constant – objects appear the same in different luminance conditions (e.g. bright day light vs dusk) (Laughlin and Hardie, 1978; Ketkar et al., 2023; Gür et al., 2024).

Contrast coding in the olfactory system could be beneficial for odor source localization, allowing animals to find sustenance and mates, and avoid danger. In a natural environment, this can be a very complex task, with odors often being transported by turbulent airflows in plumes (Riffell et al., 2008; Cardé, 2021). However, in the absence of airflow and under purely diffusive conditions, an animal only needs to follow the increasing odor gradient to reach the odor source. This strategy, called chemotaxis, is used even by unicellular organisms such as bacteria**:** *Escherichia coli* accumulate near attractants such as amino acids due to their gradient-sensing capability (Sourjik and Wingreen, 2012; Luo, 2015). Without such a gradient, bacteria exhibit two types of motion – **runs** where they mainly move in one direction and **tumbles** where they change their direction of movement randomly. However, in the

presence of an attractant gradient, tumble frequency is decreased when the bacterium is swimming up the gradient (towards the attractant) (Luo, 2015). Through adaptation, the cell is making temporal comparisons of the concentration of the attractant and suppressing the onset of the next tumble if the change in concentration is positive (Sourjik and Wingreen, 2012). ORNs could use a similar strategy, encoding contrast through adaptation, which would enable animals to find the odor source. However, while analyzing ORN firing rate adaptation, we found that they adapt by lowering their responses rather than shifting their dynamic range, as would be expected (Brandão et al., 2021 – manuscript in section 4.1). This type of adaptation does **not** support contrast encoding in single ORNs. How is contrast encoded in the olfactory system then? And what is the function of firing rate adaptation in ORNs? To answer these questions, we first need to better understand the mechanisms underlying response adaptation in ORNs and how their activity is processed in downstream neurons of the olfactory system.

3.3 Mechanisms for response and adaptation in olfactory receptor neurons

Odors are sensed by receptors localized in the dendrites of olfactory receptor neurons (ORNs). In mammals, ORN somata and dendrites localize to the olfactory epithelium inside the nasal cavity, whereas in fruit flies they are in the third segment of the antenna and in the maxillary palps (see Figure 1) (Vosshall and Stocker, 2007; Su et al., 2009; Joseph and Carlson, 2015). The surface of the fruit fly's olfactory organs is covered by small hair-like structures called sensilla, where the dendrites of up to 4 ORNs are located (Vosshall and Stocker, 2007; Su et al., 2009; Joseph and Carlson, 2015). ORN activity in the periphery can be measured *in vivo* with single sensillum recordings (SSRs), where a sharp pipette is inserted into a sensillum without any damage to the ORN (Clyne et al., 1997). This technique offers a significant advantage when working with insects over vertebrates, since measuring single ORN activity *in vivo* is not possible in the latter. Responses of neurons in the same sensillum can be distinguished in SSR recordings by the action potential shape/amplitude and by using receptor-specific ligands (Nagel and Wilson, 2011; Brandão et al., 2021). ORN firing rate response dynamics are dependent on the dynamics of the odor delivery (which are constrained by physicochemical properties) and are intensity invariant when odor concentrations are within their dynamic range; this is the case even if ORNs are adapted to a background before being presented to pulses of the same odor (Martelli et al., 2013). These identical dynamics exclude a small time delay (from 0 to 18ms) that ORNs implement when responding to different odors (Martelli et al., 2013).

In mammals, the transduction mechanism that generates action potentials in ORNs is well understood (Firestein, 2001). Odorants bind odorant receptors (Ors), which are G-protein coupled receptors that activate a pathway leading to production of cAMP (cyclic adenosine monophosphate) by the adenyl cyclase ACIII (Pace et al., 1985; Sklar et al., 1986; Jones and Reed, 1989; Boekhoff et al., 1990; Breer et al., 1990; Buck and Axel, 1991). cAMP then binds cyclic-nucleotide gated (CNG) channels, allowing the entrance of calcium and sodium cations into the neuron (Nakamura and Gold, 1987; Brunet et al., 1996). Ca^{2+}-gated Cl^- channels open due to the entrance of calcium, resulting in an efflux of chloride anions that amplify the neuron response (Kleene and Gesteland, 1991; Reuter et al., 1998; Boccaccio and Menini, 2007). Calcium is necessary for ORN transient dynamics and adaptation in mammals (Zufall et al., 1991; Kurahashi and Menini, 1997). Modulation of the CNG channel and ACIII by Ca^{2+}-calmodulin were previously held as the major mechanisms for adaptation (Kramer and Siegelbaum, 1992; Chen and Yau, 1994; Liu et al., 1994; Leinders-Zufall et al., 1999; Zufall and Leinders-Zufall, 2000; Sinnarajah et al., 2001). However, later research showed that these mechanisms have smaller roles than

previously thought or may serve only to regulate response termination (Song et al., 2008; Reisert and Zhao, 2011).

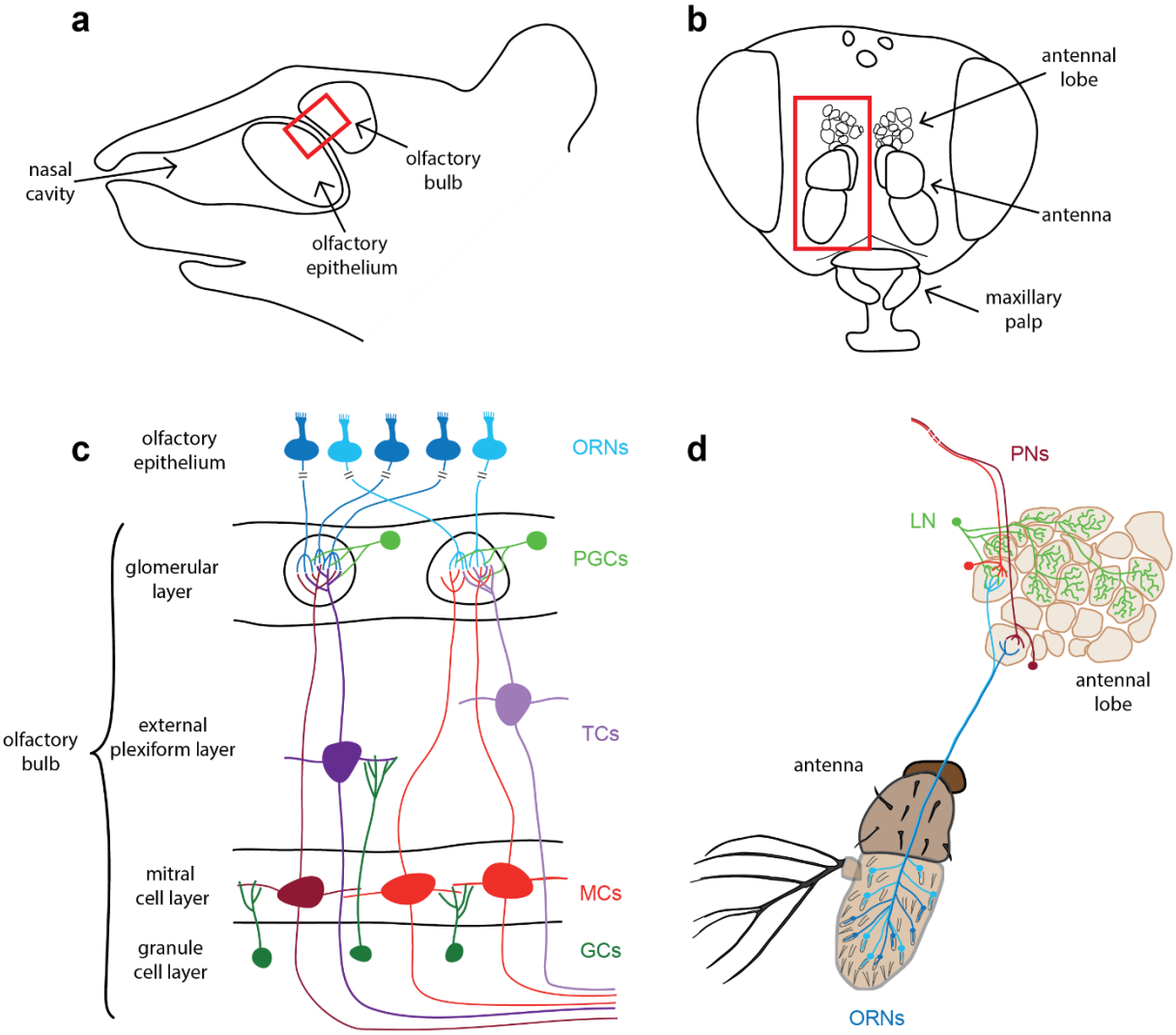

Figure 1. The mammalian and the insect olfactory systems. Overview of the mouse (**a**) and the fruit fly (**b**) olfactory systems; areas highlighted in red are shown in better detail in **c)** and **d)**, respectively. **c)** Schematics for the mouse olfactory system and olfactory bulb circuitry. **d)** Schematics for the fruit fly olfactory system and antennal lobe circuitry. GCs, granule cells; LN, local neuron; MCs, mitral cells; ORNs, olfactory receptor neurons; PGCs, periglomerular cells; PNs, projection neurons; TCs, tufted cells.

In invertebrates, ORNs sense volatile compounds through different types of chemosensory receptors belonging to three families: odorant receptors (Ors), ionotropic receptors (Irs) and gustatory receptors (Grs) (Joseph and Carlson, 2015). Most ORNs express only Ors and most of these ORNs express only one Or gene, which confers odorant specificity and selectivity, along with the odorant-receptor co-receptor (Orco) (Hallem et al., 2004; Joseph and Carlson, 2015). These two receptors form a heterodimer that functions as an ion channel: when the odorant binds this complex, the channel opens, leading to membrane depolarization and action potential generation (Sato et al., 2008; Wicher et al., 2008; Joseph and Carlson, 2015).

The molecular processes underlying ORN firing rate adaptation in invertebrates are also not well understood, but different modulatory mechanisms have been observed in ORN dendrites and have been proposed as possible explanations. One example in *Drosophila* involves inositol triphosphate (IP3), which could lead to the release of calcium from internal stores through the activation of its receptor (Deshpande et al., 2000). A role for calcium is further supported by the finding that flies expressing a mutant Trp (transient receptor potential) channel show normal naïve odor responses but no response adaptation after pre-exposure to the odor (Störtkuhl et al., 1999). Another example involves Orco dephosphorylation, which drives ORN firing rate adaptation specifically when using long odor exposures, in the range of minutes to hours (Guo et al., 2017). Despite little being known about adaptation, the pathway responsible for sensitization in ORNs has been somewhat characterized. Sensitization and adaptation can be conceived as functional opposites: while adaptation decreases neuronal responses to moderate or strong stimuli, sensitization increases neuronal responses to weak stimuli. During a sensitization protocol, the initial subthreshold odor stimulus leads to cAMP production despite not eliciting spike generation (Miazzi et al., 2016; Wicher, 2018). Orco proteins form non-selective cyclic nucleotide-activated cation channels that open when cAMP binds, initiating calcium influx (Wicher et al., 2008). Calcium further activates Orco, for example through phosphorylation by protein kinase c (Sargsyan et al., 2011). Such feedback loops are posited to leave the Or-Orco ion channels in a sensitized state that opens the next time there is odor binding (Wicher, 2018). Taking together what is known both about adaptation and sensitization, the phosphorylation state of Orco emerges as an important locus for ORN response modulation, with Orco dephosphorylation driving adaptation and Orco phosphorylation eliciting sensitization.

After exploring the underpinnings of ORN response initiation and plasticity, we must understand how these early odor responses are further processed in the brain. However, we first require a better understanding of the structure and organization of the olfactory system, which will be provided in the next section.

3.4 Organization of the olfactory system

ORNs at the periphery of the olfactory system send their axons to glomeruli, which are discrete neuropil structures in the first olfactory processing unit in the brain: the olfactory bulb in vertebrates or the antennal lobe in invertebrates. ORNs expressing the same receptor type innervate the same glomerulus, thereby defining its identity (Mombaerts et al., 1996; Couto et al., 2005; Fishilevich and Vosshall, 2005; Wilson and Mainen, 2006). But each receptor does not bind just one odorant: most receptors are able to bind to a variety of odorants, usually with different sensitivities to each one. Moreover, different odorants can, and commonly do, bind to different receptors. Identity and concentration information are then represented in the combinatorial activation of different glomeruli in the antennal lobe (AL) or the olfactory bulb (Hallem and Carlson, 2006).

ORNs give synaptic inputs to mitral/tufted cells in the olfactory bulb and projection neurons in the antennal lobe (see Figure 1) (Firestein, 2001; Marin et al., 2002; Chou et al., 2010). In both cases, these output neurons send their axons to higher multisensory brain regions, such as the olfactory cortex and the amygdala in vertebrates and the mushroom body and lateral horn in insects (Zald and Pardo, 1997; Marin et al., 2002; Jefferis et al., 2007; Lin et al., 2007; Su et al., 2009). In insects, the lateral horn has been mainly associated with innate behavior while the mushroom body is necessary for learning (Heimbeck et al., 2001; Heisenberg, 2003).

In both mammals and insects, a network of axonless, often GABAergic, local neurons (LNs) interconnect the different glomeruli and the output from the first olfactory center is the result of all the transformations that take place there (Firestein, 2001; Marin et al., 2002; Olsen and Wilson, 2008; Chou et al., 2010). What are these transformations? To answer this question, I will focus on the *Drosophila melanogaster* olfactory system.

3.5 Antennal lobe computations

Projection neurons (PNs) are the neuronal output from the antennal lobe (AL). Their responses are more reliable and faster than their cognate ORN responses because the ORN-PN synapse is strong: each synaptic vesicle released has a high likelihood of activating the corresponding PN (Bhandawat et al., 2007; Kazama and Wilson, 2008). This synapse exhibits short-term presynaptic depression, likely due to vesicle depletion, but also depression on slow timescales of 10-20s (Kazama and Wilson, 2008; Martelli and Fiala, 2019). Considering that ORN firing rate responses are transient and that the ORN-PN synapse is depressing, one would expect PN responses to be more transient than they are. This discrepancy is explained by two different mechanisms: 1) PN responses have two components with different kinetics, a fast and a slow one, with the slow component being more stable over time and less affected by synaptic depression and 2) transient dynamic presynaptic inhibition diminishes the impact of synaptic depression to sustained stimuli, ensuring that PN responses are stable, while also keeping PN responses to short pulses brief (Nagel et al., 2015). The interaction between these mechanisms ensures that PNs can adequately respond to stimuli that change over a wide range of frequencies, supporting broadband transmission at the periphery of the olfactory system (Nagel et al., 2015).

Interestingly, PNs and their cognate ORNS commonly respond to different odors (Bhandawat et al., 2007). When they respond to the same odors, the order of the strongest responses is usually different between ORNs and PNs synapsing in the same glomerulus (Bhandawat et al., 2007). Even for ORN types that are narrowly tuned to specific odorants, their cognate PN responses may be more broadly tuned – that is the case for glomerulus VA6 but not for glomerulus DA1 (Schlief and Wilson, 2007). Despite these drastic changes in ORN to PN odor selectivity, PN responses can still be explained by a highly non-linear transformation of their direct ORN inputs, which tends to redistribute responses so that they are uniformly distributed across the PN firing rate range: weak ORN responses are strongly amplified while strong ORN responses are less affected (Bhandawat et al., 2007; Olsen et al., 2010). The profile of the ORN-PN transformation is similar between glomeruli with some exceptions (Bhandawat et al., 2007; Olsen et al., 2010). For just one glomerulus, DM1, the transformation was less steep – weaker ORN signals were not as strongly amplified as in other glomeruli; for this case, applying GABA receptor antagonists made the ORN-PN transformation similar to other glomeruli (Olsen et al., 2010). The same blocking of GABA receptors had no effect on one of the other glomeruli tested that had a more common steep ORN-PN transformation, VM7, suggesting that this ORN-PN transformation of a private odor representation is intraglomerular for most glomeruli (Olsen et al., 2010).

An important computation that LNs implement in the AL is a form of gain control of glomerular responses called *divisive normalization*. This mechanism was initially discovered by understanding how a public odor (odor that activated many glomeruli) affects responses to a private odor (odor that activates only one glomerulus at the concentration used) (Olsen et al., 2010). Increasing concentrations of the public odor reduced responses to the respective private odor in two different glomeruli – VM7 and DL5; the effect was stronger when low concentrations of the private odorant were used and was

blocked by GABA receptor antagonists, indicating that it relies on inhibitory LNs (Olsen et al., 2010). As the concentration of the public odor was increased, the ORN responses were scaled down concordantly to input gain control, confirming that inhibition of the ORN-PN synapse occurs at presynapses through GABA-B receptors; this was corroborated in a contemporary study by knocking down GABA-B receptors in ORNs (Olsen and Wilson, 2008; Root et al., 2008; Olsen et al., 2010). This mechanism was found to prevent PN saturation compared to a model where there is response gain control instead of input gain control, and to decorrelate glomeruli and equalize PN responses when compared to a model without any lateral inhibition (Olsen et al., 2010). This input gain control potentially improves concentration-invariant odor discrimination in higher brain regions and is considered to be a form of divisive normalization, since the scaling is proportional to the overall ORN activation in the entire AL (Olsen and Wilson, 2008; Olsen et al., 2010). This important role of LNs supports the need to further investigate these cells and their physiological and anatomical properties, as well as what other roles they might play in the complex network that is the AL.

When discussing LNs as a group, one might start to think they are a homogeneous and identical group of cells. One would then be quite surprised to find that they are instead an incredibly heterogeneous category of neurons, both at the physiological and morphological level. Starting with their physiological differences, individual LNs have specific odor responses, even though subgroups that are more similar within do exist (Wilson and Laurent, 2005; Chou et al., 2010). A study analyzing 45 LNs found their responses vary along two axes: ON-OFF and fast-slow (Nagel and Wilson, 2016). ON-OFF refers to whether they respond to the onset or the offset of the stimulus, respectively, or a combination of the two (Nagel and Wilson, 2016). Principal component analysis of LN responses showed that the first two principal components, that captured the majority of the diversity of the responses, corresponded to the response of an ON cell and an OFF cell, with all LNs laying between these two extremes (Nagel and Wilson, 2016). Fast-slow refers to their response latency: fast LNs are better able to follow quickly changing stimuli while slow cells are only able to respond to longer pulses with longer interpulse durations (Nagel and Wilson, 2016).

But morphology also differs greatly between LNs. Indeed, thanks to recent advances in connectomics that yielded the 'hemibrain' large-scale electron microscopy (EM) dataset, LNs have been categorized into patchy, broad, regional and sparse according to their morphology and glomerular pattern of innervation (Scheffer et al., 2020; Schlegel et al., 2021). Most of the output synapses from LNs come from patchy and broad LNs (Schlegel et al., 2021; Barth-Maron et al., 2023). Patchy LNs are unique because they seem to be the only nonspiking LNs in the AL: the ones tested so far do not generate action potentials but respond instead with graded potentials (Barth-Maron et al., 2023; Schenk and Gaudry, 2023). For each of the three subsets of patchy LNs, the entire population completely tiles the AL but each LN arborizes only in a few specific glomeruli in discrete tufts that are separated by long processes, which isolate them in terms of voltage and calcium propagation (Chou et al., 2010; Barth-Maron et al., 2023). These morphological and physiological characteristics result in functional compartmentalization, which should enable patchy LNs to perform intraglomerular inhibition. This has been confirmed for one of the subsets of patchy LNs (likely LN2P_c), which was found to enact intraglomerular inhibition specifically postsynaptically in PNs (Barth-Maron et al., 2023). Full LNs were also studied in more detail; they are a subtype of broad LNs that possess very dense arborizations covering the entire AL except for one glomerulus (VL1) (Barth-Maron et al., 2023). Full LNs were found to mediate global presynaptic inhibition at ORN axon terminals, identifying them as neurons that

perform the *divisive normalization* computation described before (Barth-Maron et al., 2023). So far, not much is known about the role of these LN types and inhibition in the context of adaptation.

Overall, computations in the AL can be summarized as three independent mechanisms (Barth-Maron et al., 2023). The first one is independent of LNs and intraglomerular, consisting of synaptic depression at the ORN-PN synapses; the second one is broad presynaptic inhibition performing divisive normalization and the third one is intraglomerular postsynaptic inhibition. But what is the input to the AL that goes through these computations? We have seen that ORN firing rate responses are transient and that they adapt to the mean concentration of a prolonged odor stimulus, so it would be fair to conclude that this is the input to the AL. However, when ORN responses are measured at the axon terminals in the AL, through calcium imaging, the responses of the same ORNs look surprisingly different: they are tonic in response to a sustained stimulus and they do not adapt to it (Nagel and Wilson, 2011; Martelli et al., 2013; Martelli and Fiala, 2019). These observations suggest that ORN dynamics and stimulus-dependent adaptation are undone at the AL level. Why, then, do ORNs even adapt at the periphery, if this adaptation is simply undone at the axon terminals? And what characteristics do PNs, the output of the AL, preserve and transmit to higher brain regions?

3.6 Aims of the dissertation and summary of the findings

In the next section, I compile the three manuscripts that I contributed to during my PhD.

The first manuscript is a review on the current knowledge (before my work) about ORN response properties and adaptation. Together with my supervisor, we went through a comparative analysis of peripheral sensory adaptation in vision and olfaction to point out key differences in how receptors adapt to background stimuli (luminance or odors). This manuscript sets the motivations for my experimental work.

The second manuscript is the main outcome of my work. Here I focused on understanding how peripheral firing rate adaptation of the ORNs is processed within the main olfactory neuropil, the antennal lobe. My experiments focused on identifying molecular and circuit mechanisms that undo firing rate adaptation at the ORN output synapses and on understating the role of this transformation for odor coding. The main finding of this work is that odor representations are invariant to the presence of a background odor and that this invariance requires presynaptic feedback inhibition and synaptic plasticity. This property of olfactory processing is key for downstream circuits to drive odor-specific behaviors.

Finally, in the third manuscript, I investigated how developmental temperature affects odor coding. My work here is part of a collaboration with colleagues in the lab who have shown that changing temperature during pupation substantially alters the wiring of the olfactory system. My contribution showed that odor coding is actually robust to changes in connectivity induced by developmental temperature, suggesting that the circuit developmental program is designed to balance excitatory and inhibitory pathways to ensure odor coding stability across environmental conditions.

4 Manuscripts

4.1 Adaptive temporal processing of odor stimuli

This manuscript is published in Cell and Tissue Research (October 2020) and is available under the DOI: https://doi.org/10.1007/s00441-020-03400-9 (Brandão et al., 2021).

I contributed to the preparation of the original draft and of the figures, and editing.

Cell and Tissue Research (2021) 383:125–141
https://doi.org/10.1007/s00441-020-03400-9

REVIEW

Adaptive temporal processing of odor stimuli

Sofia C. Brandão[1] · Marion Silies[1] · Carlotta Martelli[1]

Received: 16 October 2020 / Accepted: 14 December 2020 / Published online: 6 January 2021

Abstract
The olfactory system translates chemical signals into neuronal signals that inform behavioral decisions of the animal. Odors are cues for source identity, but if monitored long enough, they can also be used to localize the source. Odor representations should therefore be robust to changing conditions and flexible in order to drive an appropriate behavior. In this review, we aim at discussing the main computations that allow robust and flexible encoding of odor information in the olfactory neural pathway.

Keywords Olfactory system · Stimulus dynamics · Sensory adaptation

Introduction

Detecting changes in the world is the main challenge for any sensory system. Signals in the form of light, pressure, temperature, or chemicals are rarely static entities for an observer. Either because sensory signals are dynamic, such as cars moving on the street or odors carried by wind, or because of the observer's movement, there is no stimulus that can be described as static. The external world acquires meaning by connecting causes and effects across different timescales. As a consequence, insight on the function of a sensory system relies on the understanding of how it processes changing stimuli (temporal processing) and how it changes the way it processes stimuli based on their history (adaptation or stimulus-driven plasticity). In this review, we aim at discussing the current understanding of temporal processing and stimulus-driven plasticity in insect olfaction. We focus mostly on peripheral encoding and provide an outlook on how odor stimuli are processed in higher brain regions. We will mostly discuss the *Drosophila* olfactory system, as this is where we have the best mechanistic and functional insight, but also compare with other animal models when relevant, to properly understand brain function.

The olfactory system aids two main behavioral tasks: odor source recognition and localization. Odors rarely exist in isolation and the ability to localize an odor source requires the ability to recognize it across a wide range of stimulus conditions. Recent work in model systems like *Drosophila* and mice has begun to quantify in detail the behavioral responses to odors in different conditions (Álvarez-Salvado et al. 2018; Demir et al. 2020; Radvansky and Dombeck 2018; Tadres and Louis2020). Understanding which decision the animal takes in response to a specific stimulus and context is fundamental to infer the underlying neural computations. This leads to the investigation of the neural circuits and molecular mechanisms that implement or support these computations.

The main neural circuit in the insect olfactory system is the antennal lobe (AL), the equivalent of the vertebrate's olfactory bulb (OB) (Wilson and Mainen 2006). The principles underlying the architecture of the AL and OB are very similar. They both have a glomerular structure resulting from the axonal projections of olfactory receptor neurons (ORNs) and the dendritic arborizations of projection neurons (PNs) (Fig. 1). In the fly, the ORNs are located on two main peripheral organs, the antennae and maxillary palps (Joseph and Carlson 2015). Each ORN type expresses a single or few chemosensory receptors and sends its axon to a single glomerulus of the AL (Fig. 1) (Couto et al. 2005; Fishilevich and Vosshall 2005; Marin et al. 2002). A large class of PNs is uniglomerular and takes input from a single ORN type (Stocker et al. 1990). The glomeruli are therefore parallel functional units whose chemical sensitivity depends on the receptor gene expressed in the ORNs (Hallem and Carlson 2006). These functional units are coupled through

✉ Carlotta Martelli
cmartell@uni-mainz.de

[1] Institute of Developmental Biology and Neurobiology, Johannes Gutenberg University, Mainz, Germany

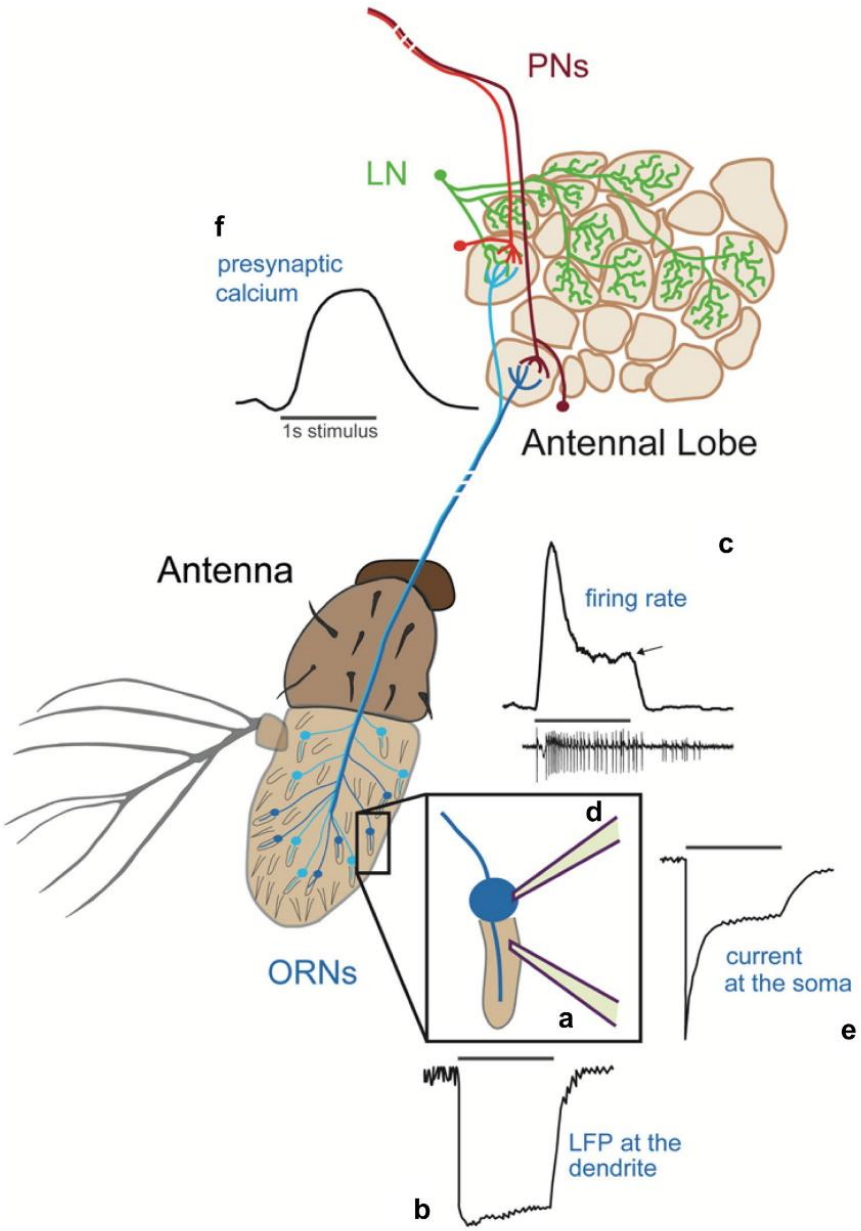

Fig. 1 Temporal aspects of the odor response within a single neuron. ORNs (blue) extend their dendrites in hair-like structures called sensilla. Single sensillum recordings (**a**) are carried out in vivo from the intact antenna and allow the quantification of the LFP (**b**) and the spiking activity of the neuron (**c**) (Clyne et al. 1997). In a sliced antenna preparation, it is possible to access the cell body for patch clamp (**d**) (Cao et al. 2016). This technique allows the quantification of somatic and dendritic currents (up to a certain distance from the recording site) (**e**). ORNs expressing the same OR send their axons to a single glomerulus in the antennal lobe, where they make synaptic connections with local neurons (LNs, green) and uniglomerular projection neurons (PNs, red). 2-photon calcium imaging allows the quantification of the presynaptic activity (**f**) reported by the calcium indicator GCaMP genetically expressed in specific ORNs (Riemensperger et al. 2012). All the curves are schematic representations of the neuron response to a 1s odor puff reported by the specified technique. See main text for more detail

a diverse family of local neurons (LNs), most of which are inhibitory (Chou et al. 2010; Liou et al. 2018). Therefore, odor stimuli are first encoded in the activity of single ORNs and this peripheral representation is then integrated and processed centrally in the AL.

What kind of computations should the olfactory system support in order to aid odor source localization? As we will see in the first section, odor concentration changes in time and space, depending on the environmental conditions. The statistics of the stimulus set constraints on which behavioral strategy and neural computation will work best under different conditions. For example, the problem of localizing the source of an odor that diffuses, forming a smooth gradient, has a simple optimal solution: moving up to the highest concentration gradient (chemotaxis) (Gaudry et al. 2012). Therefore, the odor gradient should be computed within the sensory pathway. Does the olfactory system perform such computation?

Is this computation implemented in peripheral sensory neurons? Or downstream in the AL?

Sensory systems adapt to stimulus features that remain constant over time, such as mean intensity or variance. The function of adaptation is not to simply decrease responsiveness to a stimulus feature, but rather to maintain a robust sensory representation in different environmental conditions. In vision, for example, adaptation aids contrast invariant response in different luminance conditions (Clark and Demb 2016; Ketkar et al. 2020; Laughlin 1989). Similarly, adaptation in olfaction could support the contrast sensitivity necessary for chemotaxis. But, to what extent we can stretch the analogy between different sensory modalities depends on differences in the type of stimuli and the organization of the corresponding neural circuitries. Both in vision and in olfaction, stimuli are encoded by parallel functional units of receptor neurons or their postsynaptic circuitry. A visual scene is spatially mapped into a retinotopic representation, in which neighboring cells in the visual system encode information from neighboring points in visual space. Correspondingly, in olfaction, a smell is mapped into the combinatorial activation of the ORNs, with similar odors activating similar combinations (Haddad et al. 2008; Malnic et al. 1999). However, while the retina is composed of computational units, photoreceptors, that are identical in terms of the stimuli they detect (number of photons of a given wavelength), ORNs sense stimuli that are chemically different. Downstream of the sensory periphery, the identity of an odor must be reconstructed by pooling information across all the ORNs. So, when it comes to the integration of these distributed inputs, mechanisms for encoding information about changing stimuli could largely diverge in olfaction and vision. In olfaction, adaptive changes in the stimulus representation should retain chemical specificity at least up to the AL, which holds a representation of odor identity. Understanding how adaptation occurs across parallel functional units is therefore key to identify stimulus features that are robustly transmitted to the brain (i.e., intensity, identity, contrast, etc.).

The olfactory system has another peculiarity: the AL constitutes the only sensory processing layer before odor information is integrated with other sensory inputs in higher brain areas, the mushroom body (MB) and the lateral horn (LH) in insects (Jefferis et al. 2007; Lin et al. 2007; Stocker et al. 1997). These brain areas, although serving different functions, must process olfactory information in a stimulus-dependent manner to associate it to other sensory inputs. In order to support context and experience dependent behavioral responses to olfactory stimuli, these brain areas must retain an adaptive and flexible representation of the stimulus.

In this review, we will discuss which neural computations might aid odor source localization by keeping this task robust, chemically specific, and flexible. First, we will talk about odor stimulus properties and their relevance for behavior. Second, we will describe peripheral computations focusing on what stimulus features activate the ORNs and how the ORNs adapt to static characteristics of the stimulus. Third, we will highlight the major computations that occur at the first olfactory processing center. Finally, we will discuss the form of temporal processing and stimulus driven plasticity in higher brain areas involved in multisensory integration.

The dynamics of odor stimuli and what matters for behavior

Describing the stimuli present in the environment is the first step for understanding which information is available to the animal and inferring what a sensory system is designed to detect. In vision, a quantitative understanding of the statistics of natural scenes has allowed major insight in the function of the visual pathway (Dyakova and Nordström 2017). A quantitative description of the stimulus is certainly what makes the study of the olfactory system unsettling when compared with other sensory modalities. Identifying the specific molecules and relative abundance present in an environment can be accomplished via the analysis of the chemical content of a gas sample. However, obtaining temporal and spatial resolution of a chemical stimulus is an even more complicated issue (for a recent review, see Pannunzi and Nowotny 2019). All mass-based approaches, from the molecular specific GS-MS (gas-chromatography mass-spectroscopy) to the more widely used fast PID (photoionization detector), rely on sample collection and analysis. Therefore, these methods perturb the stimulus, such that the better we sample, the farther from the real stimulus we get. However, these approaches are still useful in laboratory conditions where the chemical composition of a smell can be simplified down to a single component and samples are available in nearly unlimited amounts.

Importantly, not only the absolute concentration, but also the time-dependency of the concentration is odor specific (Andersson et al. 2012; Martelli et al. 2013). Odor-dependent differences in stimulus dynamics can be attributed to two independent processes: liquid source evaporation and surface interaction (Gorur-Shandilya et al. 2019; Pannunzi and Nowotny 2019). These odor-specific properties then couple with the fluid dynamics of the odor delivery system. Even when odors are delivered in a continuous air stream in controlled lab conditions, the output odor concentration will depend on the fluid dynamics of the specific delivery method—which can attenuate or enhance odor-specific differences in the stimulus (Gorur-Shandilya et al. 2019). As a result of these observations, odor stimuli must be measured for every experiment and experimental setup in order to draw conclusions

about temporal processing in olfaction. Different dynamics in the stimulus cause measurable differences in the temporal response of the ORNs (Martelli et al. 2013; Su et al. 2011), which necessarily provide additional odor-specific information to higher brain regions. For example, it has been shown that flies can discriminate odors sensed by a single ORN type, likely using temporal information (DasGupta and Waddell 2008). In this study, flies had to discriminate pairs of odors with very different volatility, a parameter that correlates well with the dynamics of the odor stimuli (Martelli et al. 2013). This suggests that temporal differences used for odor learning and discrimination might be already intrinsic to the stimuli themselves, rather than arising from physiological processes at the periphery. Mixtures of inhibitory and excitatory stimuli with different dynamics can elicit mixture-specific temporal patterns of ORN activation (Su et al. 2011), suggesting a possible role for odor-dependent dynamics in the perception of mixtures. The behavioral consequences of odor-specific dynamics in lab assays and in natural conditions remain a relatively new area of research that requires further investigation.

When it comes to quantifying the odor stimulus in more realistic and behaviorally-relevant conditions (e.g., in 2D and 3D assays), measuring odor stimuli by sampling in space and time is not the best solution, unless the stimulus is well reproducible (Álvarez-Salvado et al. 2018). Away from the source and from surfaces, odor stimuli can be modelled as scalar quantities (concentrations) superimposed on a vector field (air speed). Therefore, a possible approach is to neglect odor-specific effects (by using mono-molecular high volatility inert compounds) and to use optical methods for quantifying the spatiotemporal distribution of tracer molecules, such as acetone (Connor et al. 2018) or smoke (Demir et al. 2020). These approaches allow direct spatiotemporal quantification of the stimulus used for behavioral analysis. But what did we learn about the stimuli themselves? As shown by earlier field studies (Cardé and Willis 2008; Murlis and Jones 1981; Murlis et al. 2000; Riffell et al. 2008) and predicted by physical models (Celani et al. 2014), odor signals in turbulent flow conditions are intermittent due to chaotic changes in the speed and direction of wind. This means that the odor concentration measured at a given position downstream of a fixed source will fluctuate abruptly as plumes come by. The statistics of the plumes depend on air speed and geometrical constraints dictated by the environment. Importantly, only those stimuli that exceed the sensitivity threshold of the olfactory system are relevant to behavior. This imposes a biological cut-off on the stimulus statistics, which is equivalently hard to estimate, given the variety of chemicals and the repertoire of sensors available in each animal. In general, average odor concentration decreases and plume intermittency increases with distance from the source (Celani et al. 2014). These different conditions likely induce different levels of adaptation in the olfactory pathway. Although we do not know the true statistics of specific natural stimuli, we expect both a certain degree of flexibility in how odor information is used and a robust encoding of stimulus features at different distances from the source.

When animals localize an odor source, they must deal with and take advantage of whatever information is available. Pure odor-driven behavior is only achieved in the absence of wind and visual cues and, therefore, in conditions where the odor distribution is solely determined by diffusion. In this case, the animal must climb a rather smooth concentration gradient, similarly to what bacteria experience during chemotaxis (Sourjik and Wingreen 2012). In most cases, however, odors do not only diffuse passively, but are also transported by the wind. Wind adds two factors into the problem of odor source localization: (1) it modifies the statistics of odor concentration, which is no longer smoothly changing, but rather flickering, and (2) it engages a second sensory modality: mechano-sensation. In close-to-laminar conditions, when fluid particles move with little mixing, the odor concentration is stable over time and wind direction, detected by the mechano-sensory system, provides a reliable cue for source localization. The detection of an odor will thus induce a surge upwind (Álvarez-Salvado et al. 2018). In flight, surging behavior is also aided by the visual system (Van Breugel and Dickinson 2014). In between the two scenarios of pure chemotaxis vs pure odor-driven upwind surging, a nearly infinite range of conditions exists, for which localization of an odor source can involve a variety of strategies that rely on the integration of olfaction, mechano-sensation and vision (Baker et al. 2018). It could be a general approach of the animal to make choices that maximize the gain of information about the source location (Vergassola et al. 2007). Surely, there is no odor source localization without the olfactory system, but it remains unclear whether and in which range of conditions wind detection is necessary in addition to being useful. Turning upwind at an odor encounter is not an optimal strategy if the turbulence is too high and wind direction uninformative (Demir et al. 2020). Similarly, it is not optimal to try to estimate the mean stimulus intensity when the rate of plume encounter is low (Boie et al. 2018; Victor et al. 2019). Instead, behavioral decisions require a trade-off between odor sampling accuracy and response speed.

But what information about the stimulus is encoded in the olfactory system? We will start from discussing which stimulus features are encoded in the response of ORNs.

The dynamics of olfactory receptor neuron response

The first step of odor sensing occurs when the odor molecules bind to a chemosensory receptor. ORNs in flies express one or few members of one of five families of

chemical sensors (Joseph and Carlson 2015). Here, we focus on ORNs that express members of the odorant receptor (OR) family (Clyne et al. 1999; Gao and Chess 1999; Vosshall et al. 1999). ORs respond to fruit and plants odors, which constitute cues for food sources (Hallem and Carlson 2006). In insects, odors activate a heterodimer of the OR and the OR co-receptor (orco), a receptor complex that functions as an ion channel (Sato et al. 2008; Wicher et al. 2008). Most ORNs express a single OR gene, which confers odor sensitivity and selectivity (Hallem et al. 2004). Odor binding opens the channel inducing membrane depolarization and the ensuing generation of action potentials. ORN responses in *Drosophila* have been quantified using single sensillum recordings (SSR) and patch clamp recordings.

In SSR, a sharp pipette is placed into the sensillum at the level of the dendrite and used to record ORN activity in vivo, extracellularly from the intact neuron (Clyne et al. 1997)(Fig. 1a). Most sensilla in *Drosophila* house only two ORNs, which express specific receptors in stereotyped combinations and fire action potential of different shapes. In addition to firing rates, SSR recordings allow quantifying the sensillum local field potential (LFP) and, using receptor-specific ligands, it is possible to attribute the LFP to a single neuron (Nagel and Wilson 2011). The LFP should be representative of transduction events that drive membrane depolarization at the dendrite (Vermeulen and Rospars 2001). As initially reported in moths (Kaissling et al. 1986), the LFP has more tonic dynamics and adapts less than the firing rate (Fig. 1b, c). Qualitatively, similar firing dynamics have been observed in cockroaches (Lemon and Getz 1997) and locusts (Raman et al. 2010), but have been studied in great detail in *Drosophila*. The fly's ORN responds to a short stimulus pulse ($0 \rightarrow C$, from zero odor to concentration C) with a transient increase in firing rate, which then decreases to an adapted value (Fig. 1c, arrow). At odor offset ($C \rightarrow 0$), the firing rate transiently reaches zero and then recovers to spontaneous activity. There is enough similarity in ON and OFF firing dynamics that linear-nonlinear models can be used to fit ORN firing response (Martelli et al. 2013; Nagel and Wilson 2011). The ORN response can be well predicted by convoluting the stimulus with a biphasic linear filter coupled to a rectifying non-linearity (Martelli et al. 2013; Nagel and Wilson 2011). The filters extracted from the response to bimodal flickering stimuli (where at each time point the concentration is either 0 or C) are similar to those obtained with fluctuating stimuli with Gaussian distributed amplitudes around a mean concentration C (Gorur-Shandilya et al. 2017). The presence of a negative lobe in these filters indicates that the ORN can compute temporal differences in concentration. The linear filter has a width of about 200 ms (with small variations due to stimulus statistics), suggesting that this is the typical timescale on which an ORN computes changes in the stimulus. However, this estimate could be an upper bound due to the intrinsic dynamics of the stimulus used. Importantly, ORNs do not calculate a perfect derivative, as the positive and negative lobes of the filter do not sum up to zero. Consistently, on short timescales, the ORN firing rate does not adapt back to basal activity after stimulus onset. ORN firing rate rather adapts proportionally to peak response and with the same degree of adaptation across concentrations and adapted states (Martelli et al. 2013). This is true in spite of transduction kinetics being slower than in non-adapted conditions (Nagel and Wilson 2011). The slower transduction is indeed compensated by faster spike generation (Gorur-Shandilya et al. 2017). When the effect of stimulus kinetics is deconvolved from the ORN response, similar dynamics are observed for different odorants and receptor combinations (Gorur-Shandilya et al. 2017; Martelli et al. 2013). Analogous conclusions were drawn from measurements of calcium responses in the dendrites of larval ORNs (Si et al. 2019). Here, ORN dynamics have slower timescales than those measured in SSR, not only due to the kinetics of the calcium reporter, but also because dendritic calcium might contain a slower component involved in adaptation (discussed below).

There are few exceptions to these rules. First, when stimuli reach saturating concentrations, dynamics can fail to follow the stimulus ON and OFF (Martelli, unpublished). Moreover, there are reports of *Drosophila* (Montague et al. 2011) and mosquito (Turner et al. 2011) ORNs with sustained responses to specific odorants delivered at non-saturating concentrations. A short puff of these odorants elicits minute-long activation of specific ORNs, impairing responses to subsequent stimuli. This phenomenon is possibly due to slow unbinding kinetics of the odor molecule or slow deactivation of the receptor and can have important behavioral consequences by masking response to other stimuli.

Similar to observation in moths (Kaissling et al. 1986), the dynamics of the sensillum LFP in flies is much less transient than the firing rate and can be fitted with monophasic linear filters (Gorur-Shandilya et al. 2017; Nagel and Wilson 2011). This difference between the LFP and firing rate suggested that ORN response dynamics could, at least partially, be determined by mechanisms involved in action potential generation. Knockdown of the Na^+ channel α-subunit $DmNa_v$ makes ORN dynamics more transient (Nagel and Wilson 2011), suggesting that the ratio of Na + /K + conductance is a determinant of the kinetics.

In contrast to the tonic LFP signals, receptor currents measured in patch clamp recordings in antennal slices show transient and strongly adapting kinetics in response to an odor puff (Cao et al. 2016)(Fig. 1d, e). These transient receptor currents depend on calcium influx. In absence of extracellular calcium, the peak current amplitude is

also increased, arguing in favor of an immediate feedback of calcium on channel inactivation. We do not know whether the receptor complex and/or other channels are being inactivated, but it seems clear that an adaptive process is visible in the receptor current and not in LFP measurements. Identifying which mechanisms determine ORN dynamics and adaption is important because specific mechanisms impose different computational constraints for stimulus encoding. However, a direct comparison between LFP and current is not straightforward. First of all, the preparation (in vivo intact antenna vs sliced antenna) and the odor delivery methods (gas vs liquid phase) are very different. Second, the LFP is measured at the dendrite, while currents are measured patching the soma at the base of the sensillum; therefore, it is possible that these techniques capture different electrical events. Importantly, different ionic gradients might be present at the dendrites, which bathe in the sensillum lymph, and at the soma, which is surrounded by auxiliary cells (Vermeulen and Rospars 2001). It will be important to compare firing rate dynamics obtained with these techniques to understand how the measured transduction dynamics depend on the stimulus and the physiological conditions or the recording site.

Contrary to what was found for ORNs expressing ORs, ORNs that express ionotropic receptors (IRs) show sustained and non-adaptive currents (Cao et al. 2016). IRs are a more ancient family of chemosensory channels that in *Drosophila* are expressed in dedicated sensilla (coeloconic) (Rytz et al. 2013). Functionally, they are more narrowly tuned and less sensitive than ORs (Silbering et al. 2011; Yao et al. 2005). In SSR, IR-dependent firing rate dynamics adapt less than ORs to consecutive odor pulses (Getahun et al. 2012). However, in contrast to the tonic transduction current, ORNs expressing IRs show relatively phasic spiking responses (Benton et al. 2009) and ectopic expression of IRs in an ORN that normally hosts ORs is sufficient to recapitulate the firing patterns measured in the endogenous neuron (Abuin et al. 2011). This suggests that the cellular context in which these different receptors are expressed is similar and determines to some degree the conversion of the transduction current into firing events. A more detailed comparison of the firing dynamics of IR- and OR-expressing neurons will be useful to understand to what degree their response kinetics and adaptation properties differ and what the relevant steps are that shape firing rate dynamics.

The fast and transient response of ORNs facilitates the quick detection of changes in stimulus concentration. The timing of odor detection has been shown to be very precise across ORNs of the same type distributed on the antenna (Egea-Weiss et al. 2018). Moreover, the speed of odor processing is similarly fast across insect species (Szyszka et al. 2014), suggesting a fundamental function in behavior, for example when insects navigate complex odor plumes. The timing of an odor response is important not only for the quick reaction to a stimulus, but also for stimulus identity encoding. Indeed, ORNs respond with different delays to different odors (Martelli et al. 2013) and concentrations (Egea-Weiss et al. 2018) and this information can be used for the quick recognition of an odor cue (Szyszka et al. 2011). A "primacy coding" scheme has been proposed in vertebrates as a mechanism to encode odor identity in the temporally precise activation of the most sensitive ORNs (Wilson et al. 2017). This mechanism supports a representation of odor that is concentration invariant, since the sequence of activated ORNs is the same across odor concentrations.

ORN adaptation and its functional consequences

Unicellular organisms like bacteria perform chemotaxis by comparing odor concentrations in space. To do so, they move around and calculate the temporal difference of the ligand concentration sampled at subsequent positions and bias their locomotion towards where the concentration increases (Sourjik and Wingreen 2012). This strategy also works well for more complex organisms in windless environments, with the advantage that they can rely on multiple sensors such as two antennae or two nostrils (Duistermars et al. 2009; Louis et al. 2008; Rajan et al. 2006) and they can move their head for active sampling (Gomez-Marin et al. 2011, Alex et al. 2010). Bilateral comparison clearly requires precise temporal computations downstream of the sensors, but here we will focus on computations downstream of a single pathway.

Flies can perform chemotaxis with a single ORN type (Louis et al. 2008), suggesting that differences in concentration can be calculated along a single sensory pathway. Calculating changes in the input is one of the basic computations a single neuron or a single synapse can perform (Brunel et al. 2014). To achieve responses across a wide range of stimuli and under different adapted states, changes are ideally calculated relative to the intensity of the background stimulus, the definition of stimulus contrast ($\Delta C/C_0$). Sensitivity to relative changes in the stimulus is the main computation that mediates bacterial chemotaxis (Sourjik and Berg 2002). For neurons that respond to stimuli on a logarithmic scale, for example following a Hill function, being contrast sensitive corresponds to shifting the response function to match the background intensity. This shift in logarithmic scale implies a decrease in response gain inversely proportional to the background (Weber-Fechner law). Neurons in the visual pathway can shift their response around the mean luminance such that they can maintain sensitivity to variation in light intensity. For example, insect photoreceptors respond to light intensities covering

around three orders of magnitude (Fig. 2a, black dots from (Laughlin and Hardie 1978)). Adaptation to the background shifts this response range along the stimulus intensity axis for at least three-log units (Fig. 2a, colored dots).

A shift in sensitivity is often assumed and postulated as a fundamental computation necessary for odor navigation (Kadakia and Emonet 2019; Victor et al. 2019). Indeed, also ORNs exhibit a different response function when adapted to different background odor intensities (Fig. 2b). However, the decrease in ORN activity cannot be strictly interpreted as a shift. There are three important differences when comparing odor adaptation to light adaptation. First, when adapted to a background concentration, the saturated firing rate is significantly reduced as compared with non-adapted conditions, indicating a decreased coding capacity. Second, ORNs saturate at the same concentrations as in non-adapted conditions. Third, the response function becomes steeper, as also shown in moths (Kaissling et al. 1986). Thus, while photoreceptors effectively shift their dynamic range to match the background stimulation, ORNs decrease their response without shifting it, ending up with a reduced coding capacity. Another property of the ORN response in adapted conditions is the asymmetric coding of increases and decreases in concentration (ΔC vs $-\Delta C$). We mentioned that on short time-scales ORNs adapt their firing rate proportionally to peak response. However, when the stimulus is presented for longer times (> 10 s), ORN firing rate further decreases to a level closer to baseline activity (Fig. 2b, arrows). As a consequence, in background-adapted conditions, even a small decrease in odor concentration can easily drive the firing rate to zero. Therefore, any decrease in concentration is encoded as a zero, while an increase is encoded depending on its amplitude. In conclusion, in adapted conditions, ORNs respond to changes in concentration, but do not strictly encode stimulus contrast (Cafaro 2016; Kim et al. 2011), and respond asymmetrically to ON and OFF stimuli.

For a comparison, we show the results of similar experiments obtained in earlier studies in frog ORNs (Reisert and Matthews, 1999). Background adaptation reduces both currents and firing rate in response to an odor stimulus, without shifting the concentration at which the neuron reaches saturation (Fig. 2c). Notably, no spikes are fired in response to stimuli presented on a background of intensity within the dynamic range of the blank-adapted ORN. These data have been interpreted as a decrease in ORN sensitivity, because effectively, the ORN cannot respond to low concentrations anymore. It also certainly does not gain coding capacity at higher stimulus intensities, as would happen with a shift of the response function.

So far, we considered pulse-shaped stimuli delivered on a clean air stream or superimposed on a fixed background concentration, conceptually similar to flashes of light in dark or light adapted conditions. However, the neuron response function might be different when tested with different stimulus statistics. Gorur-Shandilya et al. have shown that in response to small fluctuations around a background stimulus, ORN gain decreases proportionally to the inverse of the adapting stimulus, consistent with the Weber-Fechner law (Gorur-Shandilya et al. 2017). The result means that there is a precise relationship between the background concentration and the change that is necessary to elicit an equally-sized response. This holds true for small fluctuation, about sixfold change in amplitude, as reported by PID measurements. But as we have seen, the result cannot be extended to large and quick changes in the stimulus, as those generated by odor pulses superimposed on a fixed background (Fig. 2). This is most likely because large variations drive the neurons response in a more nonlinear regime and out of the mean-adapted condition.

These nonlinearities are partially due to properties of the receptor kinetics itself, as proposed by models (Gorur-Shandilya et al. 2017). Nonetheless, it is conceivable that the ORN response adapts to other statistical features than the mean. One study reported that ORNs adapt their response gain to the variance of a fluctuating stimulus with Gaussian amplitude distribution (Gorur-Shandilya et al. 2017), although another study did not observe any variance adaptation (Kim et al. 2011). An important point to keep in mind is that it is basically impossible to deliver white noise stimuli in olfaction, as changing the concentration requires a finite amount of time that depends also on ΔC. Therefore, Gaussian stimuli with the same mean and variance can vary substantially in correlation time. In cockroaches, ORNs respond with different gain to sinusoidal stimuli of different frequency (same mean and amplitude) (Burgstaller and Tichy 2012) due to the interplay between stimulus and adaptation timescales. Moreover, in moths, the same linear-nonlinear model for the ORN response cannot equally well predict the response to temporally structured stimuli with different statistics (Jacob et al. 2017) and differences in the distribution of blanks and whiffs lead to distinct response functions in ORNs (Levakova et al. 2018). These results suggest that different mechanisms are engaged in the response to stimuli with different correlation timescales. More systematic investigation of how stimulus autocorrelation affects ORN gain control could bring insights on the multiple mechanisms that shape ORN adaptation in *Drosophila*.

If we map these observations back to their behavioral relevance, it seems that in the presence of smooth gradients with no or small fluctuations, ORNs can readily encode relative changes in concentration (both

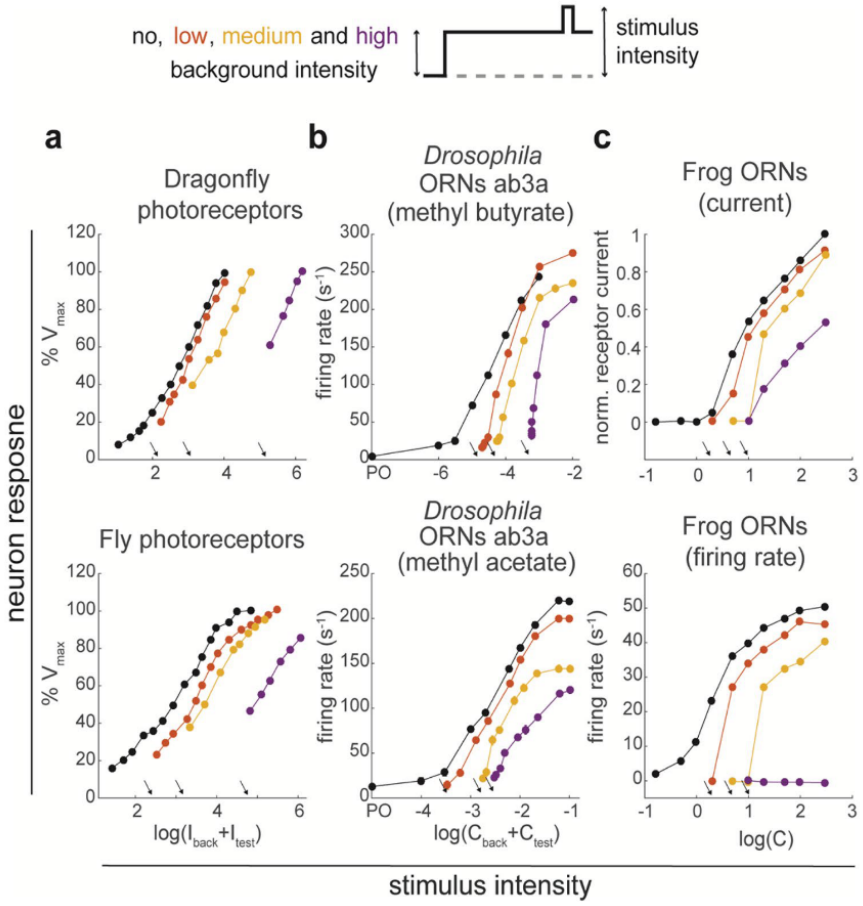

Fig. 2 Comparing the effect of background stimulus intensity on the response of light- and odor-sensitive neurons. (**a**) Response of photoreceptors to light stimuli of different intensity in dark-adapted conditions (black) spans three-log units of light intensity. In the presence of an adapting background light (intensity indicated by the arrows), photoreceptor sensitivity shifts up to more than three-log units (from black to purple). Adaptation to the background stimulus increases the basal potential (first data point of each curve) and pushes response saturation to higher light intensities, keeping the response dynamic range centered around the mean stimulus. Data are from Laughlin and Hardie (1978) reproduced with permission of S. Laughlin. (**b**) Response of *Drosophila* ORN ab3A to two odorants at different concentrations. Odor puffs are presented isolated (black) or on a background of the same odorant at concentrations indicated by the arrow. Data are same as in Fig. 4 of Martelli et al. (2013), but plotted as a function of the total stimulus concentration ($C_{back} + C_{test}$) for comparison with the data of the photoreceptors. Adaptation to the background only slightly increases the basal firing rate (first data point of each curve). The response reaches saturation at lower firing rates and at the same concentration as in no-background conditions. (**c**) Response of frog ORNs: receptor current (top) and firing rate (bottom) from (Reisert and Matthews 1999), reproduced with permission of J. Reisert. Adaptation to the background decrease receptor current and firing rate. The ORN dynamic range does not simply shift to the right, and, for the highest background, the neuron stops firing spikes

ON and OFF) which can be used downstream of the antenna to support chemotaxis. However, in more turbulent conditions, the nature of odor plumes will result in large fluctuations in concentration ($0 \rightarrow C \rightarrow 0$ or $C_0 \rightarrow C_1 \rightarrow C_0$). In this case, mean and variance adaptation likely have no time to occur or develop less than in the presence of Gaussian stimuli or possibly on different timescales. Unless saturated, adapted ORNs can still respond fast to increases and decreases of concentration. However, even a long exposure to a stable background does not seem to shift ORN sensitivity, rather the ORN response amplitude and, therefore, its coding capacity are greatly reduced. More insight in what adaptation does or does not do could be brought about by identification of the molecular mechanisms. This will be discussed in the next paragraph.

Candidate mechanisms of ORN adaptation

We know surprisingly little about the molecular mechanisms that determine ORN response dynamics and adaptation. Although the phasic part of the firing rate response could be linked to mechanisms of spike generation (Nagel and Wilson 2011), adaptation to the mean of the stimulus seems to occur already in the LFP and therefore at the transduction site of the ORN response (Gorur-Shandilya et al. 2017). This is consistent with the adaptive current measurements in patch clamp recordings (Cao et al. 2016). On the contrary, the fact that the ORN response saturation occurs at the same concentrations across adapted conditions (Fig. 2b) suggests that adaptation does not directly affect the receptor activation kinetics, although this has been proposed as a likely adaptive step. In addition, the response mediated by a specific OR can be decreased by activation of a second OR ectopically expressed in the same neuron (Nagel and Wilson 2011). This implies that the activity of the receptor itself is not necessary for adaptation. However, it does not exclude a modulation of the receptor or of the coreceptor Orco. More experiments are needed in order to exclude one or the other mechanism.

Patch clamp recordings demonstrated a role of extracellular calcium in shaping the dynamics of the transduction current mediated by OR activation (Cao et al. 2016). The source(s) of the calcium and the target(s) of the calcium feedback remain unknown. Is calcium that is flowing in through the receptors sufficient to drive adaptation or are there other channels involved? Does this feedback loop directly affect receptor activation or an amplification step? Contrary to evidence in *Drosophila*, earlier studies in moths showed that extracellular calcium is not necessary for a response, but that calcium released intracellularly mediates response termination (Pézier et al. 2007). In *Drosophila*, inositol triphosphate (IP_3) has been proposed to mediate adaptation, possibly by activation of the IP_3 receptor and the release of calcium from internal stores (Deshpande et al. 2000). Similar conclusions have been reached by imaging calcium transients in the antennal lobe (Murmu et al. 2011), but these candidate mechanisms need to be confirmed by more detailed and controlled experiments.

ORN odor responses in the fly are dependent on the phosphorylation state of Orco, which is in turn determined by ORN activity (Guo et al. 2017). However, this modulation occurs over long timescales (several minutes) and there is no direct evidence that this mechanism may affect the ORN response dynamics described above. Several other modulatory metabotropic pathways are present in ORNs (Wicher 2018), but they have not been directly linked to stimulus-induced adaptation on the timescales or with the functional role described above.

As it remains unclear where adaptation exactly happens, two types of computational models have been proposed to explain ORN adaptive response. Spike frequency adaptation (SFA) is a common mechanism for neuronal adaptation (Benda and Herz 2003). Although the specific currents involved might differ across neurons, the general mechanism is a slow hyperpolarizing conductance that is activated upon spike generation. Computational studies have proposed SFA as the main adaptation mechanism in ORNs (Farkhooi et al. 2013; Nawrot 2012; Rapp and Nawrot 2020). This inhibitory feedback could in principle involve calcium influx and would be able to reproduce the linear scaling between adapted and peak firing rate (Liu and Wang 2001), a prominent feature of the ORN response (Martelli et al. 2013). However, a direct comparison of these models to experimental data has not been attempted. Another set of models has instead considered adaptation of the transduction current, which implies the feedback of a second messenger (presumably calcium) on the receptor activity (Gorur-Shandilya et al. 2017; Kadakia and Emonet 2019; Lazar and Yeh 2020; Nagel and Wilson 2011). These models can reproduce a number of features of the ORN response to dynamic stimuli, but the molecular basis will need to be validated experimentally.

In conclusion, a role for calcium in shaping the dynamics of ORNs is plausible, but further studies are necessary to identify its source and molecular targets. Computational models can help in this process. To better understand what ORN dynamics and adaptation are good for, we should next consider (1) their role in odor coding and (2) the information processing steps downstream of ORNs.

Temporal processing and adaptation in the first olfactory processing center

The limited capability of single ORNs to adapt their sensitivity is likely not a limitation for the olfactory system. Odors are encoded in the combinatorial activity of a large population of ORNs, each responding with different sensitivity to the specific odor (Hallem et al. 2004). When the odor concentration increases, one ORN might get saturated, but another ORN, expressing an OR with lower affinity to the odor, will be activated. For example, the *Drosophila* larva uses multiple sensors with different sensitivity to the same odor in order to maintain a robust behavioral response over a large range of concentrations (Asahina et al. 2009; Kreher et al. 2008). But how is odor information preserved in the combinatorial activity when the single ORN adapt? And which information is preserved? Consider two ORNs with different sensitivity to the same odorant (Fig. 3a). Here, a background stimulus could elicit adaptation in the more

sensitive ORN and therefore a change in its response function, but would leave the response of a less sensitive ORN unaffected (Fig. 3c, d). As a result, peripheral adaptation could change the combinatorial representation of a test stimulus superimposed on the background, possibly confounding the encoding of odor identity (Fig. 3a, b). So, how can we make sense of what an adaptive change in sensitivity implies for the combinatorial code?

This question can be answered by looking at olfactory responses downstream of the antenna, where the axons of ORNs expressing the same receptor form dense synaptic structures called glomeruli (Fig. 1). Within a glomerulus, ORNs connect to PNs and LNs. The network of GABAergic LNs performs a normalization of the incoming ORN odor representation that prevents PN response saturation by adjusting the gain of synaptic transmission (Olsen and Wilson 2008; Olsen et al. 2010; Root et al. 2008; Silbering and Galizia 2007; Silbering et al. 2008). This transformation is mostly considered an instantaneous computation that involves quick inhibitory feedback from the LNs. However, odor representations in PNs are dynamic and adaptive. In the locust, complex spatiotemporal responses measured in PNs are the result of temporally structured spiking patterns of the ORNs converging on a highly plastic neural network within the AL (Raman et al. 2010). How do dynamic and adaptive ORN representations drive AL output?

Electrophysiological studies in flies have shown that the synapses between ORNs and PNs are strong and depressing (Kazama and Wilson 2008). Short-term depression is a mechanism by which a synapse can compute changes in the

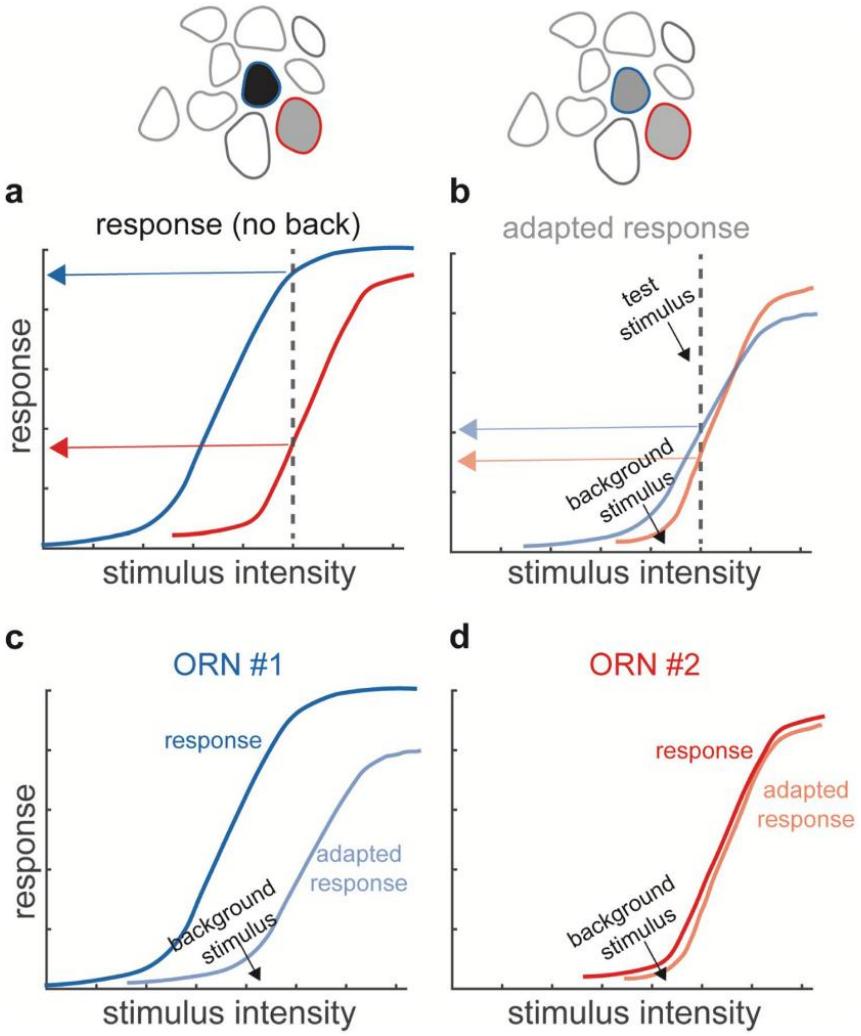

Fig. 3 Adaptation changes the combinatorial representation. **a** Response of two ORNs to stimuli of increasing intensities. Red and blue arrows indicate the response of two ORNs to a given stimulus intensity (dotted line). **b** In the presence of a background the odor representation in the two ORNs (red and blue arrows) differs from the non-adapted response (**a**). **c**, **d** A background stimulus, indicated by the black arrow, changes the response function of ORN1. ORN2 is not sensitive to the background stimulus and its response function is unaffected by the background stimulus

presynaptic neuron activity (Abbott et al. 1997). Short-term depression at ORN-PN synapses likely results from vesicle depletion (Kazama and Wilson 2008) and works as a band-pass filter for the transmission of information from ORNs to PNs. Electrophysiological measurements from PNs indeed showed that their response peaks earlier than that of ORNs (Bhandawat et al. 2007) as if they were computing changes in the ORN firing patterns (Kim et al. 2015). Consistent with these observations, PN activity can be fitted by biphasic linear filters (Geffen et al. 2009). Similar conclusions have been reached in studies that compared ORN and PN response to pheromones in moths (Rospars et al. 2014). It remains unclear whether spike frequency adaptation plays an additional role in shaping PN responses, in addition to synaptic depression, as proposed by computational models (Farkhooi et al. 2013).

But how does a phasic firing pattern, like the one from the ORNs, get through such depressing synapses? Differential encoding of the stimulus in the ORN input and synaptic depression at the ORN output constitute two consecutive filtering steps. Computational models show that these two filtering steps would result in very transient PN responses (Nagel et al. 2015). On the contrary, in the fly, prolonged stimulation elicits sustained and stable PN responses. A few additional mechanisms might explain this discrepancy. First, a slow acetylcholine-driven component in the PN response current allows integration of the input over longer timescales making the response more sustained (Nagel et al. 2015). Moreover, transient lateral inhibitory inputs sharpen and stabilize synaptic activity, tuning the effect of incoming firing patterns (Nagel et al. 2015).

To better investigate presynaptic regulation, a recent study combined SSR with imaging of the presynaptic calcium dynamics (Martelli and Fiala 2019). Calcium transients are usually interpreted as a read-out of firing activity. Consistent with this assumption, the amplitude of ORN firing rate measured from the sensillum and the calcium response measured from the presynapses of the same ORN in the AL are strongly correlated in response to short odor pulses delivered in isolation. However, adaptation to the background did not decrease the calcium responses measured at the axon terminals, in spite of an adaptation-dependent decrease in firing rate. Moreover, calcium signals remained sustained (for up to two minutes of odor stimulation), while firing rate was transient (Fig. 1c–f). These non-adaptive dynamics in the presynaptic calcium signal do not seem to rely on inhibitory lateral inputs and point at a role of cell-intrinsic regulation of calcium transients. Additional experiments are needed to understand the mechanistic bases of the calcium regulation and how it is modulated by lateral inputs. From a functional point of view, presynaptic calcium seems to be able to reconstruct the non-adapted ORN response, independently of the strength of the background. This way, the odor representation is preserved at the population level in adapted conditions and does not change over repeated or sustained stimulations (Martelli and Fiala 2019). A direct comparison between firing rate and presynaptic calcium is difficult in vertebrates, because it is hard to reach the olfactory epithelium in a live preparation. However, there are indications of similar differences between peripheral firing adaptation and ORN calcium activity in the olfactory bulb. Indeed, ORN response is suppressed for odor stimuli presented at frequencies comparable with the respiration rate (Ghatpande and Reisert 2011; Zufall and Leinders-Zufall 2000). In contrast, calcium transients in ORN axon terminals measured in vivo report more sustained ORN responses (Carey et al. 2009; Lecoq et al. 2009; Pírez and Wachowiak 2008; Storace and Cohen 2019; Verhagen et al. 2007).

These observations would fit in a scenario where adaptation occurs (or reoccurs) at the level of the antennal lobe, as a coordinated change across all glomeruli. Calcium imaging from *Drosophila* PNs indeed shows that the odor representations at the population level are adapted to the stimulus statistics and encode stimulus contrast, preserving information about the stimulus identity (Martelli and Fiala 2019). The quantification of synaptic release showed that a slow component of the PN response dynamics originates presynaptically, through depletion of vesicle release and independently of the calcium dynamics (Martelli and Fiala 2019). This slow component is consistent with models of vesicle recycling that involve two pools of vesicles (Hallermann et al. 2010).

Adaptive processes through the AL almost certainly involve LNs. LNs are an extremely diverse population of neurons which differ both anatomically and functionally (Chou et al. 2010; Liou et al. 2018; Nagel and Wilson 2016; Seki et al. 2010). They are not very selective to odor identity, but they show different preference to features of the stimulus (ON vs OFF) depending on the input they receive. Moreover, their temporal dynamics are extremely diverse depending on intrinsic cellular properties (Nagel and Wilson 2016). This means that the effective amount of inhibition a glomerulus receives will depend on the type of LN that innervates it in combination with the stimulus dynamics. Inputs from a fast LN will drive strong transient inhibition when the stimulus strength steps up or down, while slow LNs will drive more tonic inhibition through the entire stimulus presentation. Furthermore, a considerable subset of LNs has patchy morphology connecting only subsets of glomeruli (Chou et al. 2010) and not all glomeruli are equally sensitive to inhibition (Hong and Wilson 2015). Additionally, some commonly used LN driver lines seem to be dispensable for an odor response to isolated pulses (Strube-Bloss et al. 2017), indicating that they might have a function in other stimulus conditions. Although adaptation has not been directly studied in LNs, we expect that the rich dynamics and tuning of inhibitory inputs play a role in

adapting the PN odor representation to the statistics of the stimulus. Lateral inhibition in the AL mediates a divisive normalization of the input from ORNs, which rescales PN activity based on the overall activation of the AL (Olsen and Wilson 2008; Olsen et al. 2010). What happens to this transformation when stimuli are sustained or repeated remains an open question. Work in moths shows that ORN adaptation drives a shift in frequency of odor-induced oscillations in the AL, suggesting a role of adaptation in engaging lateral inhibition to synchronize the PNs population dynamics (Ito et al. 2009). Moreover, early studies in the locust have shown that plasticity in the AL driven by repeated stimulus presentations decreases PN activity, but increases firing precision and population synchrony (Stopfer and Laurent 1999). This is independent of ORN adaptation, occurs at different time scales, and could be mediated by tuning of the inhibitory synapses (Bazhenov et al. 2005).

AL plasticity also occurs on longer timescales. Hour- and days-long exposure to odors induces reversible changes in the activity of specific glomeruli and reduces behavioral response selectively to these odors (Das et al. 2011; Devaud et al. 2001; Sachse et al. 2007; Sadanandappa et al. 2013; Sudhakaran et al. 2012). These forms of long- and short-term habituation have been attributed to the selective potentiation of recurrent GABAergic inhibition specifically onto PNs (reviewed in (Ramaswami 2014)).

Overall, these studies suggest that different subsets of LNs have different functions and operate on a large range of timescales. Connectomics data will provide useful information to investigate the computational function of LN subsets (Bates et al. 2020; Berck et al. 2016; Horne et al. 2018). Targeted behavioral experiments should finally aim to disentangle the different functions that lateral inhibition seems to mediate adaptive and robust encoding of stimulus features, modulation of odor preference, and context integration.

Stimulus history modulates odor representations in higher brain regions

Downstream of the AL, PNs form synapses onto the Kenyon cells of the mushroom body (MB) and lateral horn neurons (LHNs). How do odor-driven dynamics and plasticity in PNs affect the representation of odor information in these downstream neurons? LHNs have been shown to be faster and more accurate in responding to odors compared with their presynaptic PNs (Jeanne and Wilson 2015). This is due to a dynamic spike threshold that is activity dependent and enables the detection of simultaneously incoming spikes. It remains to be investigated how these physiological properties adapt to sustained or repeated stimulation. LHNs have been recently characterized in terms of their anatomical properties and odor response spectrum (Frechter et al. 2019; Jeanne et al. 2018). This neuron population is incredibly diverse suggesting that it supports different functions. Current models suggest that the LH mediates innate behavior and olfactory navigation (Schultzhaus et al. 2017). However, further studies should be aimed at understanding which specific LH neurons are involved in navigation and which computations and stimulus features are used in the LH to help the fly localize an odor source.

Stimulus-driven plasticity in the olfactory system might have multiple roles. So far, we have discussed how this plasticity can support robust function by keeping an invariant representation of stimulus features of possible behavioral relevance. However, when looking at neural computations downstream of the AL and their behavioral implications, we must distinguish between what the fly can do and what the fly wants to do. On the one hand, stimulus-driven plasticity could support robust encoding of stimulus features for goal-directed odor tracking. A recent theoretical study showed that adaptation in the olfactory pathway supports sparse odor representations in the MB, facilitating the quick recall of memories necessary to drive animals during navigation (Rapp and Nawrot 2020). On the other hand, stimulus-driven plasticity could support flexible representations that allow the fly to change its goals. In flies, the short-term history of the chemical composition of an odor scene can change the animal behavioral response to an odor (Badel et al. 2016). A model of preference normalization based on olfactory context suggests a plastic role in the circuit downstream of the AL in integrating PN output (Badel et al. 2016). Whether this type of normalization happens in the LH or in the MB is unclear. In their behavioral assay, Badel et al. did not associate odors to a reinforcement or to a behavioral outcome, rather the odor preference seems to rescale based on the valence of the previously experienced chemical context. This phenomenon indicates a form of stimulus-driven short-term plasticity which could in principle involve either the MB or the LH. That stimulus context shapes MB output has been shown in several studies (Bräcker et al. 2013; Lewis et al. 2015), but whether context integration is adaptive and on what timescales past stimuli are integrated remains to be clarified.

Stimulus-driven adaptation is a mechanism that enhances the encoding of novel features of a stimulus. On short timescales, novelty can be an increase or a decrease in concentration, but on longer timescales, novelty can depend on how familiar the animal is with the stimulus. At least one mushroom body output neuron in the fly encodes the novelty of an odor stimulus (Hattori et al. 2017) and requires odor-driven activity in dopaminergic neurons. While sensory representations must be stable to reliably report stimulus information, the brain must remain flexible to what that information means for the animal. Stimulus-driven plasticity in brain areas that support learning has been previously reported in

rats (Best and Wilson 2004) and more recently in zebrafish (Jacobson et al. 2018). Changes in the odor representation in higher order areas are sometimes referred to as adaptation, habituation or plasticity. The common aspect is that they are driven by stimulus history, which in turn indicates that the underlying neural substrates must contain information about stimulus history and filter sensory information based on stimulus history. These changes in the coding space could either lead to changes in behavior (flexibility) or support behavioral invariance (robustness). Which of the two scenarios occurs depends on the specific local and downstream circuit.

Remarks and conclusions

At the sensory periphery, the encoding of the olfactory stimuli consists of two main steps: the activation of individual ORNs in specific combinations and the coordinated integration of this combinatorial input within the AL. Here, we have discussed in detail the temporal aspects of these encoding steps, with a main focus on their adaptive features. However, our understanding of this encoding process is still lacking essential insights.

First of all, it would be beneficial to understand which molecular mechanisms mediate adaptation of the ORN response. Although limited compared with other sensory modalities, the ORN response function changes depending on stimulus history, which means that based on stimulus history, the ORN selects which information should be transmitted downstream. Mechanisms of olfactory adaptation are better understood in vertebrates, but the kind of computation they mediate has been extensively debated (Reisert and Zhao 2011). Therefore, across organisms, a clear function for ORN adaption is still missing.

A missing tile in understanding the role of adaptation in olfaction is certainly the link between molecular mechanisms, neural function and behavioral output. The tools to investigate these links are one strength of model systems like *Drosophila*, but in the specific context of stimulus-driven adaptation, little has been done. Whether a certain neural computation, e.g. stimulus differentiation, plays a functional role in behavior, such as climbing odor gradients, needs to be investigated experimentally. Having more mechanistic insights on adaptation will make it easier to link computation to function.

Similarly, it will be important to study behaviorally relevant stimuli using electrophysiology and imaging, since basic design principles of the olfactory system might be hidden by using simplified stimulation protocols (like single puffs). There is a trade-off between generating naturalistic and reproducible stimuli in the lab, but new approaches are being developed to control and measure the stimuli delivered.

One conclusion we would like to draw here is that in order to understand adaptation in olfaction, one must look downstream of the receptor neurons. The combinatorial aspect of odor coding requires integration of information across parallel channels. This central integration is what makes the olfactory system different from a chemical sensor, like a single cell. The AL network is likely doing more than a global divisive normalization. The diversity of LNs alone speaks for multiple functions, selective integration of incoming stimuli, and temporal processing on different timescales. The mechanisms of stimulus induced plasticity in this network and their role in olfactory navigation deserve further investigation.

Finally, odor perception involves also long-term state-dependent modulation. How the internal state affects peripheral odor representations has been analyzed so far only in terms of response amplitude to isolated odor pulses (Ko et al. 2015; Martelli et al. 2017). Is hunger only shaping the valence of an olfactory perception? Or is a hungry fly better at localizing an odor because of enhanced peripheral processing? Currently, there are no answers to these questions. However, one interesting possibility is that the internal or behavioral state may directly modulate odor processing in the AL, similarly to how the behavioral state shapes visual processing (Maimon 2011).

Current theories of adaptive behavior suggest a role for top-down modulation of sensory perception (Młynarski and Hermundstad 2018). This means that not only behavioral states, like resting or walking, but also behavioral output could potentially affect fundamental sensory computations. After an evaluation of the smell has been made, different strategies might be used to localize an odor source (Baker et al. 2018; Gaudry et al. 2012). Therefore, behavioral output might feedback onto odor processing in order to adjust or improve the search strategy.

New tools for stimulus quantification and behavioral analysis are being developed and implemented to study how animals use olfaction to move around aimfully. These approaches will allow the field to address long-standing fundamental questions concerning the identification of neural computations that mediate animal decision-making in the presence of odor cues.

Acknowledgements We are grateful to M. Ketkar, L. Leandro Batista, A. Methner, and D. Storace for feedback on the manuscript; to T. Emonet, J. Reisert, S. Ryglewski, D. Storace, and C-Y. Su for helpful discussions; and to S. Laughlin and J. Reisert for permission on using previously published data.

Funding Open Access funding enabled and organized by Projekt DEAL. MS has received funding from the European Research Council (ERC) under the European Union's Horizon 2020 research and

innovation programme (grant agreement No. 716512). Work in the Martelli lab is supported by the Deutsche Forschungsgemeinschaft (DFG) through grant MA 7804/2-1.

Compliance with ethical standards

Conflict of interest The authors declare that there is no conflict of interest.

References

Abbott LF, Varela JA, Sen K, Nelson SB (1997) Synaptic depression and cortical gain control. Science 80(275):220–224

Abuin L, Bargeton B, Ulbrich MH, Isacoff EY, Kellenberger S, Benton R (2011) Functional Architecture of Olfactory Ionotropic Glutamate Receptors. Neuron 69:44–60

Alex G-M, Duistermars B, Frye MA, Louis M (2010) Mechanisms of odor-tracking: multiple sensors for enhanced perception and behavior. Front Cell Neurosci 4:6

Álvarez-Salvado E, Licata AM, Connor EG, McHugh MK, King B, Stavropoulos N, Victor JD, Crimaldi JP, Nagel KI (2018) Elementary sensory-motor transformations underlying olfactory navigation in walking fruit-flies. Elife 7:e37815

Andersson MN, Schlyter F, Hill SR, Dekker T (2012) What reaches the antenna? How to calibrate odor flux and ligand-receptor affinities. Chem Senses 37:403–420

Asahina K, Louis M, Piccinotti S, Vosshall LB (2009) A circuit supporting concentration-invariant odor perception in Drosophila. J Biol 8:9

Badel L, Ohta K, Tsuchimoto Y, Kazama H (2016) Decoding of context-dependent olfactory behavior in Drosophila. Neuron 91:155–167

Baker KL, Dickinson M, Findley TM, Gire DH, Louis M, Suver MP, Verhagen JV, Nagel KI, Smear MC (2018) Algorithms for olfactory search across species. J Neurosci 38:9383–9389

Bates AS, Schlegel P, Roberts RJV, Drummond N, Tamimi IFM, Turnbull R, Zhao X, Marin EC, Popovici PD, Dhawan S et al (2020) Complete connectomic reconstruction of olfactory projection neurons in the fly brain. Curr Biol

Bazhenov M, Stopfer M, Sejnowski TJ, Laurent G (2005) Fast odor learning improves reliability of odor responses in the locust antennal lobe Neuron

Benda J, Herz AVM (2003) A universal model for spike-frequency adaptation. Neural Comput 15:2523–2564

Benton R, Vannice KS, Carolina G-D, Vosshall LB (2009) Variant ionotropic glutamate receptors as chemosensory receptors in Drosophila. Cell 136:149–162

Berck ME, Khandelwal A, Claus L, Luis H-N, Si G, Tabone CJ, Li F, Truman JW, Fetter RD, Louis M et al (2016) The wiring diagram of a glomerular olfactory system. Elife 5:e14859

Best AR, Wilson DA (2004) Coordinate synaptic mechanisms contributing to olfactory cortical adaptation. J Neurosci

Bhandawat V, Olsen SR, Gouwens NW, Schlief ML, Wilson RI (2007) Sensory processing in the Drosophila antennal lobe increases reliability and separability of ensemble odor representations. Nat Neurosci 10:1474–1482

Boie SD, Connor EG, McHugh M, Nagel KI, Ermentrout GB, Crimaldi JP, Victor JD (2018) Information-theoretic analysis of realistic odor plumes: what cues are useful for determining location? PLoS Comput Biol 14:e1006275

Bräcker LB, Siju KP, Varela N, Aso Y, Zhang M, Hein I, Vasconcelos M, Kadow IC (2013) Essential role of the mushroom body in context-dependent CO2 avoidance in Drosophila. Curr Biol 23:1228–1234

Van Breugel F, Dickinson MH (2014) Plume-tracking behavior of flying drosophila emerges from a set of distinct sensory-motor reflexes. Curr Biol 24:274–286

Brunel N, Hakim V, Richardson MJE (2014) Single neuron dynamics and computation. Curr Opin Neurobiol

Burgstaller M, Tichy H (2012) Adaptation as a mechanism for gain control in cockroach ON and OFF olfactory receptor neurons. Eur J Neurosci

Cafaro J (2016) Multiple sites of adaptation lead to contrast encoding in the Drosophila olfactory system. Physiol Rep 4:e12762

Cao L-H, Jing B-Y, Yang D, Zeng X, Shen Y, Tu Y, Luo D-G (2016) Distinct signaling of Drosophila chemoreceptors in olfactory sensory neurons. Proc Natl Acad Sci U S A 113:117906951774860

Cardé RT, Willis MA (2008) Navigational strategies used by insects to find distant, wind-borne sources of odor. J Chem Ecol 34:854–866

Carey RM, Verhagen JV, Wesson DW, Pírez N, Wachowiak M (2009) Temporal structure of receptor neuron input to the olfactory bulb imaged in behaving rats. J Neurophysiol

Celani A, Villermaux E, Vergassola M (2014) Odor landscapes in turbulent environments. Phys Rev X 12:62

Chou Y-H, Spletter ML, Yaksi E, Leong JCS, Wilson RI, Luo L (2010) Diversity and wiring variability of olfactory local interneurons in the Drosophila antennal lobe. Nat Publ Gr 13:439–449

Clark DA, Demb JB (2016) Parallel computations in insect and mammalian visual motion processing. Curr Biol 26:R1062–R1072

Clyne P, Grant A, O'Connell R, Carlson, JR (1997) Odorant response of individual sensilla on the Drosophila antenna. In Invertebrate Neuroscience, (Springer), 127–135

Clyne PJ, Warr CG, Freeman MR, Lessing D, Kim J, Carlson JR (1999) A novel family of divergent seven-transmembrane proteins: candidate odorant receptors in Drosophila. Neuron 22:327–338

Connor EG, Mchugh MK, Crimaldi JP (2018) Quantification of airborne odor plumes using planar laser-induced fluorescence. Exp Fluids 59:137–138

Couto A, Alenius M, Dickson BJ (2005) Molecular, anatomical, and functional organization of the Drosophila olfactory system. Curr Biol 15:1535–1547

Das S, Sadanandappa MK, Dervan A, Larkin A, Lee J, Sudhakaran IP, Priya R, Heidari R, Holohan EE, Pimentel A et al (2011) Plasticity of local GABAergic interneurons drives olfactory habituation. Proc Natl Acad Sci U S A 108:E646–E654

DasGupta S, Waddell S (2008) Learned odor discrimination in Drosophila without combinatorial odor maps in the antennal lobe. Curr Biol 18:1668–1674

Demir M, Kadakia N, Anderson HD, Clark DA, Emonet T (2020) Walking Drosophila navigate complex plumes using stochastic decisions biased by the timing of odor encounters. Elife

Deshpande M, Venkatesh K, Rodrigues V, Hasan G (2000) The inositol 1,4,5-trisphosphate receptor is required for maintenance of olfactory adaptation in Drosophila antennae. J Neurobiol 43:282–288
Devaud JM, Acebes A, Ferrús A (2001) Odor exposure causes central adaptation and morphological changes in selected olfactory glomeruli in Drosophila. J Neurosci 21:6274–6282
Duistermars BJ, Chow DM, Frye MA (2009) Flies require bilateral sensory input to track odor gradients in flight. Curr Biol 19:1301–1307
Dyakova O, Nordström K (2017) Image statistics and their processing in insect vision. Curr Opin Insect Sci
Egea-Weiss A, Renner A, Kleineidam CJ, Szyszka P (2018) High precision of spike timing across olfactory receptor neurons allows rapid odor coding in Drosophila. IScience 4:76–83
Farkhooi F, Froese A, Muller E, Menzel R, Nawrot MP (2013) Cellular adaptation facilitates sparse and reliable coding in sensory pathways. PLoS Comput Biol 9:e1003251
Fishilevich E, Vosshall LB (2005) Genetic and functional subdivision of the Drosophila antennal lobe. Curr, Biol
Frechter S, Bates AS, Tootoonian S, Dolan MJ, Manton J, Jamasb AR, Kohl J, Bock D, Jefferis G (2019) Functional and anatomical specificity in a higher olfactory centre. Elife
Gao Q, Chess A (1999) Identification of candidate Drosophila olfactory receptors from genomic DNA sequence. Genomics 60:31–39
Gaudry Q, Nagel KI, Wilson RI (2012) Smelling on the fly: sensory cues and strategies for olfactory navigation in Drosophila. Curr Opin Neurobiol 22:216–222
Geffen MN, Broome BM, Laurent G, Meister M (2009) Neural encoding of rapidly fluctuating odors. Neuron 61:570–586
Getahun MN, Wicher D, Hansson BS, Olsson SB (2012) Temporal response dynamics of Drosophila olfactory sensory neurons depends on receptor type and response polarity. Front Cell Neurosci 6:1–11
Ghatpande AS, Reisert J (2011) Olfactory receptor neuron responses coding for rapid odour sampling. J Physiol 589:2261–2273
Gomez-Marin A, Stephens GJ, Louis M (2011) Active sampling and decision making in Drosophila chemotaxis. Nat Commun 2:441
Gorur-Shandilya S, Demir M, Long J, Clark DA, Emonet T (2017) Olfactory receptor neurons use gain control and complementary kinetics to encode intermittent odorant stimuli. Elife 6:e27670
Gorur-Shandilya S, Martelli C, Demir M, Emonet T (2019) Controlling and measuring dynamic odorant stimuli in the laboratory. J Exp Biol
Guo H, Kunwar K, Smith D (2017) Odorant Receptor Sensitivity Modulation in Drosophila. J Neurosci 37:9465–9473
Haddad R, Lapid H, Harel D, Sobel N (2008) Measuring smells. Curr Opin Neurobiol 18:438–444
Hallem EA, Carlson JR (2006) Coding of odors by a receptor repertoire. Cell 125:143–160
Hallem EA, Ho MG, Carlson JR (2004) The molecular basis of odor coding in the Drosophila antenna. Cell 117:965–979
Hallermann S, Heckmann M, Kittel RJ (2010) Mechanisms of short-term plasticity at neuromuscular active zones of Drosophila. HFSP J 4:72–84
Hattori D, Aso Y, Swartz KJ, Rubin GM, Abbott LF, Axel R (2017) Representations of novelty and familiarity in a mushroom body compartment. Cell 169:956-969.e17
Hong EJ, Wilson RI (2015) Simultaneous encoding of odors by channels with diverse sensitivity to inhibition. Neuron 85:1–18
Horne JA, Langille C, McLin S, Wiederman M, Lu Z, Xu CS, Plaza SM, Scheffer LK, Hess HF, Meinertzhagen IA (2018) A resource for the Drosophila antennal lobe provided by the connectome of glomerulus VA1v. Elife 7
Ito I, Bazhenov M, Ong R, Raman B, Stopfer M (2009) Frequency transitions in odor-evoked neural oscillations. Neuron 64:692–706
Jacob V, Monsempes C, Rospars J-P, Masson J-B, Lucas P (2017) Olfactory coding in the turbulent realm. PLoS Comput Biol 13:e1005870
Jacobson GA, Rupprecht P, Friedrich RW (2018) Experience-dependent plasticity of odor representations in the telencephalon of zebrafish. Curr, Biol
Jeanne JM, Wilson RI (2015) Convergence, divergence, and reconvergence in a feedforward network improves neural speed and accuracy. Neuron 88:1014–1026
Jeanne JM, Fişek M, Wilson RI (2018) The organization of projections from olfactory glomeruli onto higher-order neurons. Neuron
Jefferis GSXE, Potter CJ, Chan AM, Marin EC, Rohlfing T, Maurer CR, Luo L (2007) Comprehensive maps of Drosophila higher olfactory centers: spatially segregated fruit and pheromone representation. Cell 128:1187–1203
Joseph RM, Carlson JR (2015) Drosophila chemoreceptors: a molecular interface between the chemical world and the brain. Trends Genet 31:683–695
Kadakia N, Emonet T (2019) Front-end Weber-Fechner gain control enhances the fidelity of combinatorial odor coding. Elife
Kaissling KE, Strausfeld ZC, Ruo ER (1986) Adaptation processes in insect olfactory receptors. Ann N Y Acad Sci 510:104–112
Kazama H, Wilson RI (2008) Homeostatic matching and nonlinear amplification at identified central synapses. Neuron 58:401–413
Ketkar MD, Sporar K, Gür B, Ramos-Traslosheros G, Seifert M, Silies M (2020) Luminance information is required for the accurate estimation of contrast in rapidly changing visual contexts. Curr Biol 30:657-669.e4
Kim AJ, Lazar AA, Slutskiy YB (2011) System identification of Drosophila olfactory sensory neurons. J. Comput, Neurosci
Kim AJ, Lazar AA, Slutskiy YB, Calabrese RL (2015) Projection neurons in Drosophila antennal lobes signal the acceleration of odor concentrations. Elife 4:e06651
Ko KI, Root CM, Lindsay SA, Zaninovich OA, Shepherd AK, Wasserman SA, Kim SM, Wang JW (2015) Starvation promotes concerted modulation of appetitive olfactory behavior via parallel neuromodulatory circuits. Elife 4:e08298
Kreher SA, Mathew D, Kim J, Carlson JR (2008) Translation of sensory input into behavioral output via an olfactory system. Neuron 59:110–124
Laughlin SB (1989) The role of sensory adaptation in the retina. J Exp Biol 146:39–62
Laughlin SB, Hardie RC (1978) Common strategies for light adaptation in the peripheral visual systems of fly and dragonfly. J Comp Physiol □ A
Lazar AA, Yeh CH (2020) A molecular odorant transduction model and the complexity of spatio-temporal encoding in the Drosophila antenna. PLoS Comput Biol
Lecoq J, Tiret P, Charpak S (2009) Peripheral adaptation codes for high odor concentration in glomeruli. J Neurosci
Lemon W, Getz W (1997) Temporal resolution of general odor pulses by olfactory sensory neurons in American cockroaches. J Exp Biol 200:1809–1819
Levakova M, Kostal L, Monsempès C, Jacob V, Lucas P (2018) Moth olfactory receptor neurons adjust their encoding efficiency to temporal statistics of pheromone fluctuations. PLoS Comput Biol 14:e1006586
Lewis LPC, Siju KP, Aso Y, Friedrich AB, Bulteel AJB, Rubin GM, Kadow IC (2015) A higher brain circuit for immediate integration of conflicting sensory information in Drosophila. Curr Biol 25:2203–2214
Lin H-H, Lai J, Chin A-L, Chen Y-C, Chiang A-S (2007) A map of olfactory representation in the Drosophila mushroom body. Cell 128:1205–1217

Liou NF, Lin SH, Chen YJ, Tsai KT, Yang CJ, Lin TY, Wu TH, Lin HJ, Chen YT, Gohl DM et al (2018) Diverse populations of local interneurons integrate into the Drosophila adult olfactory circuit. Nat Commun

Liu YH, Wang XJ (2001) Spike-frequency adaptation of a generalized leaky integrate-and-fire model neuron. J Comput Neurosci 10:25–45

Louis M, Huber T, Benton R, Sakmar TP, Vosshall LB (2008) Bilateral olfactory sensory input enhances chemotaxis behavior. Nat Neurosci

Maimon G (2011) Modulation of visual physiology by behavioral state in monkeys, mice, and flies. Curr Opin Neurobiol

Malnic B, Hirono J, Sato T, Buck LB (1999) Combinatorial receptor codes for odors. Cell 96:713–723

Marin EC, Jefferis GSXE, Komiyama T, Zhu H, Luo L (2002) Representation of the glomerular olfactory map in the Drosophila brain. Cell 109:243–255

Martelli C, Fiala A (2019) Slow presynaptic mechanisms that mediate adaptation in the olfactory pathway of Drosophila. Elife 8

Martelli C, Carlson JR, Emonet T (2013) Intensity invariant dynamics and odor-specific latencies in olfactory receptor neuron response. J Neurosci 33:6285–6297

Martelli C, Pech U, Kobbenbring S, Pauls D, Bahl B, Sommer MV, Pooryasin A, Barth J, Arias CWP, Vassiliou C et al (2017) SIFamide translates hunger signals into appetitive and feeding behavior in Drosophila. Cell Rep 20

Młynarski WF, Hermundstad AM (2018) Adaptive coding for dynamic sensory inference. Elife

Montague SA, Mathew D, Carlson JR (2011) Similar odorants elicit different behavioral and physiological responses. Some Supersustained Jneurosci Org 31:7891–7899

Murlis J, Jones C (1981) Fine-scale structure of odour plumes in relation to insect orientation to distant pheromone and other attractant sources. Physiol Entomol 6:71–86

Murlis J, Willis MA, Cardé RT (2000) Spatial and temporal structures of pheromone plumes in fields and forests. Physiol Entomol 25:211–222

Murmu MS, Stinnakre J, Réal E, Martin JR (2011) Calcium-stores mediate adaptation in axon terminals of olfactory receptor neurons in Drosophila. BMC Neurosci

Nagel KI, Wilson RI (2011) Biophysical mechanisms underlying olfactory receptor neuron dynamics. Nat Neurosci 14:208–216

Nagel KI, Wilson RI (2016) Mechanisms underlying population response dynamics in inhibitory interneurons of the Drosophila antennal lobe. J Neurosci 36:4325–4338

Nagel KI, Hong EJ, Wilson RI (2015) Synaptic and circuit mechanisms promoting broadband transmission of olfactory stimulus dynamics. Nat Publ Gr 18:56–65

Nawrot M (2012) Dynamics of sensory processing in the dual olfactory pathway of the honeybee. Apidologie 43:269–291

Olsen SR, Wilson RI (2008) Lateral presynaptic inhibition mediates gain control in an olfactory circuit. Nature 452:956–960

Olsen SR, Bhandawat V, Wilson RI (2010) Divisive normalization in olfactory population codes. Neuron 66:287–299

Pannunzi M, Nowotny T (2019) Odor stimuli: not just chemical identity. Front, Physiol

Pézier A, Acquistapace A, Renou M, Rospars J-P, Lucas P (2007) Ca2+ stabilizes the membrane potential of moth olfactory receptor neurons at rest and is essential for their fast repolarization. Chem Senses 32:305–317

Pírez N, Wachowiak M (2008) In vivo modulation of sensory input to the olfactory bulb by tonic and activity-dependent presynaptic inhibition of receptor neurons. J Neurosci

Radvansky BA, Dombeck DA (2018) An olfactory virtual reality system for mice. Nat, Commun

Rajan R, Clement JP, Bhalla US (2006) Rats smell in stereo. Science (80-.)

Raman B, Joseph J, Tang J, Stopfer M (2010) Temporally diverse firing patterns in olfactory receptor neurons underlie spatiotemporal neural codes for odors. J Neurosci 30:1994–2006

Ramaswami M (2014) Network plasticity in adaptive filtering and behavioral habituation. Neuron 82:1216–1229

Rapp H, Nawrot MP (2020) A spiking neural program for sensorimotor control during foraging in flying insects. Proc Natl Acad Sci USA

Reisert J, Matthews HR (1999) Adaptation of the odour-induced response in frog olfactory receptor cells. J Physiol

Reisert J, Zhao H (2011) Response kinetics of olfactory receptor neurons and the implications in olfactory coding. J Gen Physiol 138:303–310

Riemensperger T, Pech U, Dipt S, Fiala A (2012) Optical calcium imaging in the nervous system of Drosophila melanogaster. Biochim Biophys Acta 1820:1169–1178

Riffell JA, Abrell L, Hildebrand JG (2008) Physical processes and real-time chemical measurement of the insect olfactory environment. J Chem Ecol 34:837–853

Root CM, Masuyama K, Green DS, Enell LE, Nässel DR, Lee C-H, Wang JW (2008) A presynaptic gain control mechanism fine-tunes olfactory behavior. Neuron 59:311–321

Rospars J-P, Grémiaux A, Jarriault D, Chaffiol A, Monsempes C, Deisig N, Anton S, Lucas P, Martinez D (2014) Heterogeneity and convergence of olfactory first-order neurons account for the high speed and sensitivity of second-order neurons. PLoS Comput Biol 10:e1003975

Rytz R, Croset V, Benton R (2013) Ionotropic receptors (IRs): chemosensory ionotropic glutamate receptors in Drosophila and beyond. Insect Biochem Mol Biol 43:888–897

Sachse S, Rueckert E, Keller A, Okada R, Tanaka NK, Ito K, Vosshall LB (2007) Activity-dependent plasticity in an olfactory circuit: neuron. Neuron 56:838–850

Sadanandappa MK, Redondo BB, Michels B, Rodrigues V, Gerber B, Buchner KVE, Ramaswami M (2013) Synapsin function in GABA-ergic interneurons is required for short-term olfactory habituation. J Neurosci 33:16576–16585

Sato K, Pellegrino M, Nakagawa T, Nakagawa T, Vosshall LB, Touhara K (2008) Insect olfactory receptors are heteromeric ligand-gated ion channels. Nature 452:1002–1006

Schultzhaus JN, Saleem S, Iftikhar H, Carney GE (2017) The role of the Drosophila lateral horn in olfactory information processing and behavioral response. J Insect Physiol 98:29–37

Seki Y, Rybak J, Wicher D, Sachse S, Hansson BS (2010) Physiological and morphological characterization of local interneurons in the Drosophila antennal lobe. J Neurophysiol 104:1007–1019

Si G, Kanwal JK, Hu Y, Tabone CJ, Baron J, Berck M, Vignoud G, Samuel ADT (2019) Structured odorant response patterns across a complete olfactory receptor neuron population. Neuron

Silbering AF, Galizia GC (2007) Processing of odor mixtures in the Drosophila antennal lobe reveals both global inhibition and glomerulus-specific interactions. J Neurosci 27:11966–11977

Silbering AF, Okada R, Ito K, Galizia GC (2008) Olfactory information processing in the Drosophila antennal lobe: anything goes? J Neurosci 28:13075–13087

Silbering AF, Rytz R, Grosjean Y, Abuin L, Ramdya P, Jefferis GSXE, Benton R (2011) Complementary function and integrated wiring of the evolutionarily distinct Drosophila olfactory subsystems. J Neurosci 31:13357–13375

Sourjik V, Berg HC (2002) Receptor sensitivity in bacterial chemotaxis. Proc Natl Acad Sci U S A 99:123–127

Sourjik V, Wingreen NS (2012) Responding to chemical gradients: bacterial chemotaxis. Curr Opin Cell Biol 24:262–268

Stocker RF, Lienhard MC, Borst A, Fischbach KF (1990) Neuronal architecture of the antennal lobe in Drosophila melanogaster. Cell Tissue Res 262:9–34

Stocker RF, Heimbeck G, Gendre N, deBelle J (1997) Neuroblast ablation in Drosophila P[GAL4] lines reveals origins of olfactory interneurons. J Neurobiol 32:443–456

Stopfer M, Laurent G (1999) Short-term memory in olfactory network dynamics. Nature 402:664–668

Storace DA, Cohen LB (2019) The olfactory bulb contributes to the adaptation of odor responses: the input-output transformation. BioRxiv 829531

Strube-Bloss MF, Grabe V, Hansson BS, Sachse S (2017) Calcium imaging revealed no modulatory effect on odor-evoked responses of the Drosophila antennal lobe by two populations of inhibitory local interneurons. Sci Rep 7:595

Su C-Y, Martelli C, Emonet T, Carlson JR (2011) Temporal coding of odor mixtures in an olfactory receptor neuron. Proc Natl Acad Sci U S A 108:5075–5080

Sudhakaran IP, Holohan EE, Osman S, Rodrigues V, K, V., and Ramaswami, M. (2012) Plasticity of recurrent inhibition in the Drosophila antennal lobe. J Neurosci 32:7225–7231

Szyszka P, Demmler C, Oemisch M, Sommer L, Biergans S, Birnbach B, Silbering AF, Galizia CG (2011) Mind the gap: olfactory trace conditioning in honeybees. J Neurosci 31:7229–7239

Szyszka P, Gerkin RC, Galizia CG, Smith BH (2014) High-speed odor transduction and pulse tracking by insect olfactory receptor neurons. Proc Natl Acad Sci USA 111:16925–16930

Tadres D, Louis M (2020) PiVR: An affordable and versatile closed-loop platform to study unrestrained sensorimotor behavior. PLoS Biol

Turner SL, Li N, Guda T, Githure J, Cardé RT, Ray A (2011) Ultra-prolonged activation of CO2-sensing neurons disorients mosquitoes. Nature 474:87–91

Vergassola M, Villermaux E, Shraiman BI (2007) 'Infotaxis' as a strategy for searching without gradients. Nature 445:406–409

Verhagen JV, Wesson DW, Netoff TI, White JA, Wachowiak M (2007) Sniffing controls an adaptive filter of sensory input to the olfactory bulb. Nat Neurosci 10:631–639

Vermeulen A, Rospars J-P (2001) Membrane potential and its electrode-recorded counterpart in an electrical model of an olfactory sensillum. Eur Biophys J 29:587–596

Victor JD, Boie SD, Connor EG, Crimaldi JP, Ermentrout GB, Nagel KI (2019) Olfactory navigation and the receptor nonlinearity. J Neurosci 39:3713–3727

Vosshall LB, Amrein H, Morozov PS, Rzhetsky A, Axel R (1999) A spatial map of olfactory receptor expression in the Drosophila antenna. Cell

Wicher D (2018) Tuning insect odorant receptors. Front Cell Neurosci

Wicher D, Schäfer R, Bauernfeind R, Stensmyr MC, Heller R, Heinemann SH, Hansson BS (2008) Drosophila odorant receptors are both ligand-gated and cyclic-nucleotide-activated cation channels. Nature 452:1007–1011

Wilson RI, Mainen ZF (2006) Early events in olfactory processing. Annu Rev Neurosci 29:163–201

Wilson CD, Serrano GO, koulakov, A.A., and rinberg, D. (2017) A primacy code for odor identity. Nat Commun 8:135

Yao AC, Ignell R, Carlson JR (2005) Chemosensory coding by neurons in the coeloconic sensilla of the Drosophila antenna. J Neurosci 25:8359–8367

Zufall F, Leinders-Zufall T (2000) The cellular and molecular basis of odor adaptation. Chem Senses 25:473–481

4.2 Undoing of firing rate adaptation enables invariant population codes

This manuscript is published on bioRxiv (latest version on August 2025) and is available under the DOI: https://doi.org/10.1101/2024.09.26.614457 (Brandão et al., 2025).

I contributed to conceptualization and design of the study. I performed all the experiments and subsequent visualization of the data except for glomeruli DM3 and DM6 in figure S2. The stimulation and analysis code was developed by Carlotta Martelli before I started working on this project, and I edited it for the different experiments as required. I helped to review and edit the manuscript.

Undoing of firing rate adaptation enables invariant population codes

Brandão S.C. [1†], Ramirez L. [1†], Züfle P. [1], Walter A.M. [2], Silies M. [1], Martelli C. [1‡]

[1]Institute of Developmental Biology and Neurobiology, Johannes Gutenberg University, Mainz, Germany
[2]Department of Neuroscience, Faculty of Health and Medical Sciences, University of Copenhagen, Denmark
[†] These authors contributed equally to this work.
[‡] Corresponding author: cmartell@uni-mainz.de

Summary

Neural adaptation supports coding efficiency by tuning responses to prevailing stimulus statistics. However, when information is represented by neural populations, adaptation of individual units could degrade behaviorally relevant signals. Here we investigate how the fly olfactory system implements adaptation in Olfactory Receptor Neurons (ORNs) and the consequences for combinatorial coding in downstream circuits. We show that adaptation of ORN firing rate is compensated at the axon terminal, where calcium transients remain background-invariant through inhibitory presynaptic feedback. Background invariance requires an adaptation strategy that shifts ORN response amplitude rather than sensitivity, diverging from efficient coding principles in single neurons. This property supports contrast encoding in ORN populations necessary for background compensation across the glomeruli. Downstream, the modulation of presynaptic Unc13 proteins maintains postsynaptic projection neurons responses to ON stimuli background invariant. We identify a new coding strategy where olfactory neuronal populations encode asymmetrically contrast information by implementing circuit computations that compensate peripheral firing rate adaptation.

Introduction

Neural adaptation is an essential strategy of sensory systems that allows the encoding of stimuli over a range of intensities exceeding the limits of the individual sensory cell[1]. To do so, neurons tune their stimulus-response function to the relevant statistics of the stimulus[2]. For instance, efficient coding theories at the single-neuron level predict that a shift in neuron sensitivity that matches the mean stimulus optimizes the encoding of relevant information within the neuron's dynamic range[3]. Such shifts in sensitivity have been observed in several sensory systems, from audition to vision, in artificial and natural conditions[4–6]. However, much less is known about the role of adaptation in odor coding. The olfactory system is by design endowed with a large array of sensory receptors with different affinities to the same odorant[7,8]. When the stimulus intensity (concentration) increases, the more sensitive receptors saturate while new ones with lower affinity are recruited. Therefore, the system as a whole is rarely out of its broad dynamic range. While the benefits of adaptation in single neurons have been widely discussed[9,10], the benefits of single neuron adaptation for population coding require a deeper understanding. Studies in the visual cortex suggest that neuronal adaptation can improve coding accuracy at the population level in a stimulus-dependent manner[11]. Here we investigate the function and potential benefits of adaptation in populations of olfactory neurons.

In both vertebrates and invertebrates, the firing rate of Olfactory Receptor Neurons (ORNs) decreases upon persistent stimulation[12–18], inducing a change in their response curve. Yet, the coding function of this adaptive change remains unclear. On one hand, a decrease in ORN response could lead to a decrease in perception of the odor stimulus. However, the relationship between ORN adaptation and decreased stimulus perception is so far correlative[19] since a decreased behavioural response to persistent odour stimuli could derive from plasticity (e.g. habituation[20–22]) in higher brain areas rather than from decreased receptor sensitivity. On the other hand, adaptation of the sensory neurons could play a role in odor-driven navigation. Behavioral studies in *Drosophila* suggest that flies can implement a chemotactic strategy for odour-guided searching behaviour[23,24]. In single cell organisms, such as bacteria, chemotaxis relies on receptor adaptation for contrast computations[25]. Such contrast

computations could in principle also occur in the ORNs[26,27], although the contrast sensitivity of these neurons across a physiological range of concentrations is marginal[28,29]. Importantly, contrast computation in single ORNs prior to the encoding of odor identity across the ORN population could interfere with information transmission in downstream circuits.

To understand the role of peripheral ORN adaptation it is necessary to analyze odor coding principles in downstream pathways. ORNs expressing the same chemosensory receptor send axons to the same olfactory glomerulus, where they connect to projection neurons (PNs) in insects and mitral/tuft cells (M/T cells) in vertebrates[30]. Synaptic depression in these first order connections[31] and lateral inhibition[32] mediated by local neurons (LNs) modulate odor representations in the insect antennal lobe[33] (AL) and in the vertebrate olfactory bulb[34]. However, a role of these two circuit mechanisms in adaptation has not been investigated so far.

Here we combine computational and experimental approaches in *Drosophila* to understand how ORN adaptive properties shape odor representations in populations of second-order olfactory neurons, the PNs. We start with a computational analysis to show that the odor information encoded in populations of ORNs depends on adaptation properties of single neurons. Specifically, an adaptive change in response amplitude, rather than in response sensitivity, supports the encoding of both contrast and intensity in a population of ORNs. We show that adaptation by a change in response amplitude is required to drive the proper amount of feedback inhibition in the ORN presynapses to maintain calcium responses invariant to background stimuli, undoing the effect of firing rate adaptation. This invariance is specific for ON stimuli (increase in concentrations compared to the background) creating an asymmetry between ON and OFF odor representations. Such asymmetric invariance persists in postsynaptic PNs and is disrupted by mutation of a modulatory domain of Unc13, suggesting a role of presynaptic plasticity in achieving the response invariance. We propose that adaptation in ORN firing rates enhances the separation of ON and OFF stimuli in the downstream population of PNs, while allowing a background-invariant representation of odor identity for ON stimuli which requires the encoding of contrast information in ORN populations.

Results

Single neuron adaptation shapes odor information coding in ORN populations.

Adaptation has often been described in both peripheral and central sensory neurons as a mechanism that tunes neuron sensitivity to the stimulus statistics. For example, adaptation to an increasing background luminance leads to a shift in the response curve of fly photoreceptors towards higher luminances[35]. This shift is consistent with the efficient coding hypothesis[10] and implies that the neuron encodes contrast rather than absolute luminance. ORNs in both insects and vertebrates do not seem to follow the same adaptive strategy as visual neurons since they do not exhibit a shift in sensitivity (in the stimulus domain), but rather a decreased response (in the activity domain) after adaptation to an odor background (reviewed in [29]). An important difference between vision and olfaction is that stimulus sensitivity across ORNs is highly heterogeneous due to the expression of large odorant receptor repertoires, leading to an early combinatorial encoding of odor information by the ORN population[7,8] (**Fig. 1a**). To understand how single neuron adaptation shapes odor coding at the population level, we simulated the response of a population of ORNs under three different strategies for background adaptation (**Fig. 1b**): I) sensitivity-shift (core mechanism in contrast-sensitive visual neurons), II) amplitude-compression and III) amplitude-shift, the latter two being plausible based on measurements in ORNs[14,29]. For each scenario, we simulated the population response to increasing concentrations of a single odor presented in isolation or after adaptation to a background of the same odor. For all three cases, we described the population responses in a low-dimensional manifold focusing on its capability to encode either stimulus intensity or contrast (relative to the background). If single ORNs adapt by shifting their sensitivity (**Fig. 1c**), the population responses lie on a one-dimensional manifold where the stimulus intensity strongly correlates with the first principal component, which explains most of the response variance across all backgrounds (**Fig. 1d**). Background adaptation leads to similar representations of iso-intensity stimuli (**Fig. 1d,** black dots). Conversely, the encoding of contrast information in this population is ambiguous, as the same contrast can be represented by very different representations (**Fig. 1e**, black dots). Therefore, an adaptive strategy that allows the encoding of contrast in single neurons leads to population responses

that retain mostly information about intensity. On the contrary, in a population of neurons that adapt their response amplitude by a compression or a shift, odor representations lay on a 2-dimensional manifold (**Fig. 1f, i**), allowing the parallel encoding of both intensity and contrast information (**Fig. 1g-h and j-k,** black dots). These results generalize across different update rules for the parameters (see Methods).

Altogether, we find that adaptation strategies at the single neuron level determine how odor information is represented by the population. Importantly, a strategy that is commonly used in other sensory systems (strategy I) performs poorly at encoding stimulus features such as contrast at the population level when compared to adaptive strategies that modify response amplitude (strategies II and III). This counter-intuitive result has a simple explanation. When adaptation induces a shift in sensitivity, the total amount of activity generated by the ORN population is the same across background conditions. Instead, when adaptation leads to a change in response amplitude (a compression or shift), the total activity in neural space decreases with background intensity. This shifts the representational space, creating a dimension to encode contrast as combination of background and stimulus intensity. In the following we ask whether and how this coding scheme is passed to or used by downstream neurons.

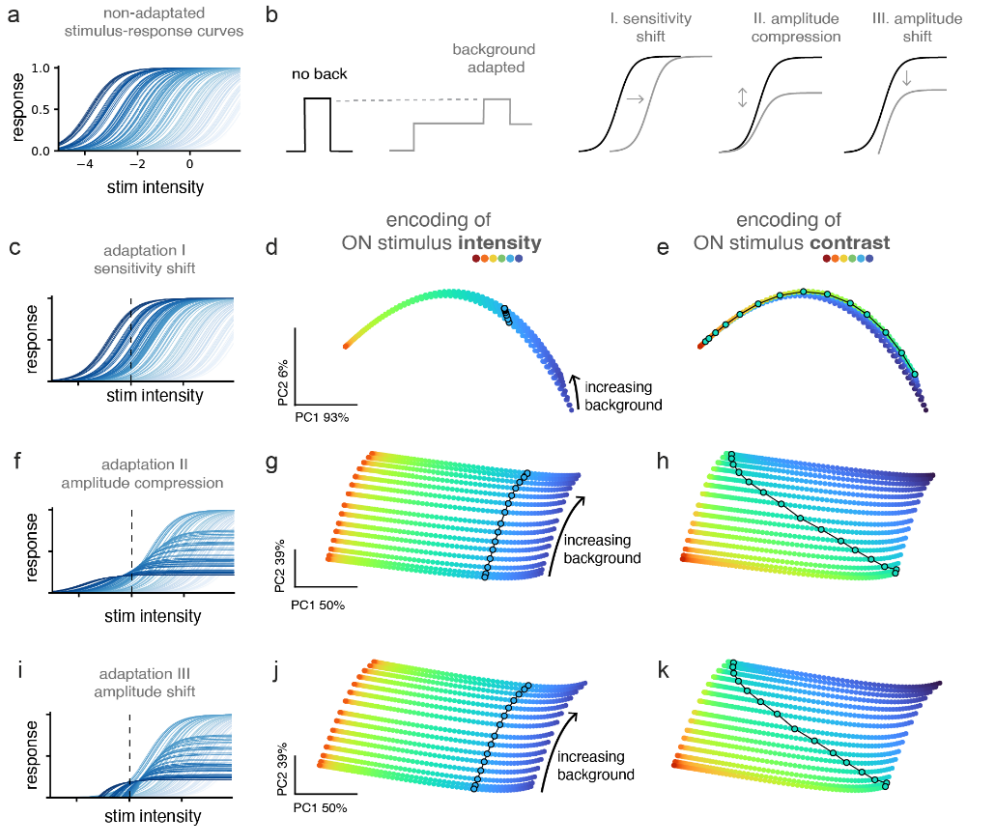

Figure 1. Encoding of intensity and contrast in neuron populations with different adaptive properties. a) Simulated stimulus response curves for a population of ORNs with different stimulus sensitivities (stimulus in log scale). **b)** Three types of background-induced adaptation for individual neurons, implemented as a change in a specific parameter for each adaptation case (see Methods). **c)** Response curves of the same neurons as in a) after adaptation to a background stimulus indicated by the dotted line. Adaptation to the background induces a shift of the response sensitivity towards higher stimulus intensities. **d)** 2D-manifold of the population responses to stimuli of different intensity (color coded) in different background adapted conditions. Black circles highlight an iso-intensity response curve across all backgrounds. **e)** Same data as in **d)** but color coded by stimulus contrast. Black circles highlight an iso-contrast response curve across all backgrounds. **f-g-h)** as in **c-d-e)** for a population of neurons that adapt by a compression in amplitude. **i-j-k)** as in **c-d-e)** for a population of neurons that adapt by shifting their response amplitude.

ORNs transform adapted firing rate responses to ON odor stimuli into background-invariant calcium representations.

To understand the computational role of ORN firing rate adaptation, it is essential to examine how these signals are processed in the olfactory glomeruli, where ORNs project their axons (**Fig. 2a**). We have previously characterized the response dynamics of ORNs[14,36], which we briefly summarize here. ORNs exhibit phasic firing rate responses to an increase in odor concentrations, with activity peaking shortly after stimulus onset and subsequently relaxing to an adapted steady-state. In the adapted state the neuron's response to subsequent odor stimuli is weaker (**Fig. 2b**, data from[36]). This form of background-dependent adaptation, typical of sensory neurons, is observed at the dendritic terminals within the antenna (**Fig. 2a, b**). The dendritic firing activity drives calcium transients in the axon terminals of ORNs within specific glomeruli of the antennal lobe (**Fig. 2a**). We have previously shown that these presynaptic calcium signals exhibit sustained, rather than phasic, dynamics (**Fig. 2c**) and, importantly, that their amplitude remains invariant to background odor levels despite adaptation of the firing rate (**Fig. 2c** and more data in[36]). Therefore, when odor stimuli are presented in isolation, presynaptic calcium transients, assayed by fluorescence indicators, depend linearly on firing rate, but this relationship is altered by background adaptation (**Fig. 2d**, data adapted from[36]). These findings led us to hypothesize that presynaptic calcium dynamics and therefore synaptic release are regulated in an activity-dependent manner.

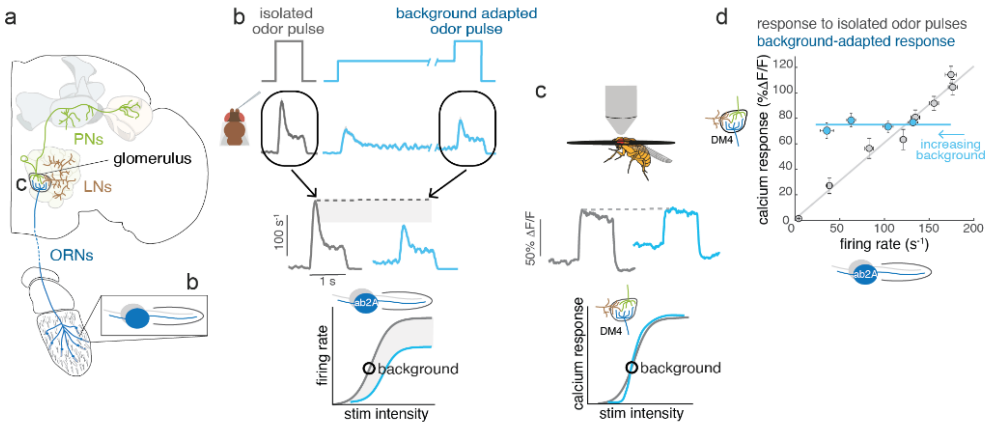

Figure 2. The undoing of firing rate adaptation at central synapses. a) Schematics of the olfactory pathway. Olfactory Receptor Neurons (ORN) located in the antenna extend their axons to a specific glomerulus in the antennal lobe and make synapses onto Local Neurons (LNs) and uniglomerular Projection Neurons (PNs). PNs' axons innervate the Lateral Horn and the calix of the Mushroom Body. The labels (b and c) indicate the location of recordings of the corresponding panels. **b)** *Top:* Schematics of the stimulus protocol and firing rate response of the ab2A ORNs in control and background adapted conditions (data adapted from[36]). *Bottom:* schematics of the ORNs firing response in control and background-adapted conditions. The circle indicates the intensity of the background stimulus. **c)** *Top:* ORN calcium responses induced by an odor puff in control and adapted conditions measures from the ab2A ORN axon terminals in the corresponding glomerulus DM4. *Bottom:* schematics of the ORN calcium response curve showing background-invariant responses. **d)** Mean firing rate and mean calcium responses for odor puffs of different intensity tested in adapted (blue) and non-adapted (gray) conditions (data from[36]). The lines are linear regressions. Error bars indicate SE.

Activation of a single glomerulus is sufficient for background-invariant ORN presynaptic activity.

Odor stimuli can recruit more than one ORN type, raising the question of whether the background invariance of ORN presynaptic responses depends on multi-glomerular activation. We used an optogenetic approach to restrict activity to a single ORN type (expressing the odorant receptor Or42b) targeting the glomerulus DM1 (**Fig. 3a**). Using a combination of background and test stimuli, we show that, as with odors, ON stimuli elicited the same response irrespective of background, while OFF stimuli always lead to drops in calcium below the non-adapted response (**Fig. 3b, c**). We refer to this encoding

property of the olfactory system as "asymmetric background invariance". We further measured firing rates from the ab1 sensillum that contains the Or42b-ORNs to verify that the firing rate responses are actually adapted to the stimulus background (**Fig. 3d**). Optogenetic activation leads to lower firing rates and a smaller dynamic range compared to odor stimuli (response saturates at around 40 Hz rather than the usual 250 Hz). Yet, as with odors, background adaptation leads to a striking change of the dose-response curve for both ON and OFF stimuli (**Fig. 3d**). We conclude that presynaptic calcium is regulated such that both uni-glomerular (**Fig. 3**) and multi-glomerular (**Fig. 2**) odor representations are normalized to achieve asymmetric background invariance.

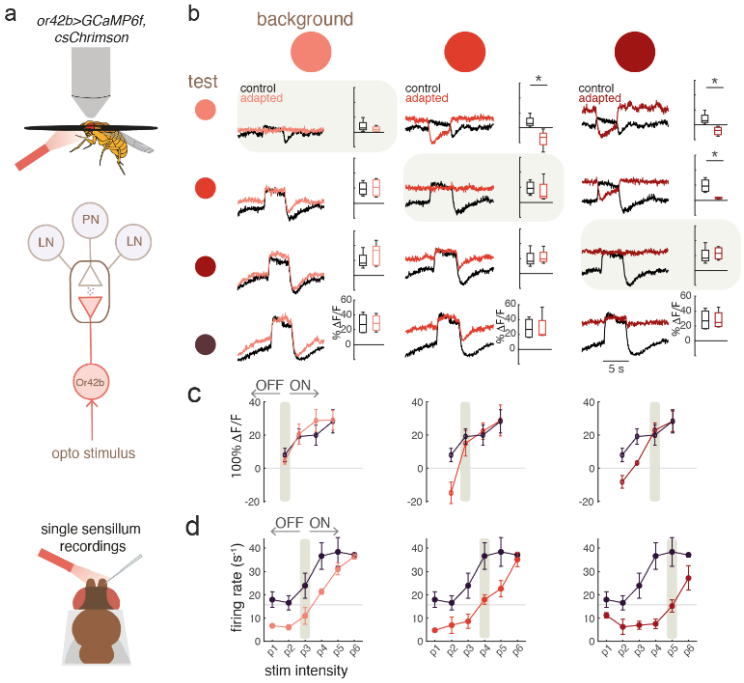

Figure 3. Asymmetric background-invariance in ORN upon optogenetic activation. a) Schematics of the experimental protocol. **b)** Mean calcium responses from ORN axon terminals in the glomerulus DM1 in control (black, no background) and adapted (shades of red) conditions. Columns represent different background intensities, rows different intensities of the test stimulus. Test intensities are: 0.01, 0.03, 0.055, 0.08 µW/mm^2 (from light to dark red). The plots on the diagonal (gray quadrants), corresponds to the same intensity of the test and background stimuli. Quadrants above this diagonal, are OFF stimuli and quadrants below are ON stimuli. Boxplots show median, quartiles and min/max values of the response averaged in 3 sec after stimulus onset (N=4-5, *p<0.05). **c)** Mean response plotted as a function of the test stimulus intensity; error bars indicate SE. **d)** Same as **c)** but for firing rate responses (N=3). A similar range of stimuli was used for the electrophysiology (p1-p6 = 0.06, 0.1, 0.2, 0.4, 0.7, 0.92 µW/mm^2). Gray boxes indicate the intensity of the background stimulus.

Homeostatic feedback regulates ORN presynaptic calcium responses.

Next, we investigated the potential mechanisms that compensate the firing rate adaptation and achieve ON background invariance. Specifically, we asked whether ORN presynaptic calcium is regulated in a cell-intrinsic manner or through a circuit computation. To distinguish between these two cases, we expressed the temperature-sensitive dynamin mutant shibire^{ts} in Or42b-ORNs to block neurotransmitter release and measured odor responses at the same presynapses (**Fig. 4a**). To capture slower adaptive processes, we presented the test odor 8 consecutive times (**Fig. 4b**). As expected, flies of the control genotype showed tonic and background-invariant responses (**Fig. 4c**). In contrast, blocking synaptic release led to more transient and background dependent responses (**Fig. 4d-f**), reminiscent of firing rate adaptation (**Fig. 2a, b**). Similar results were obtained for the glomerulus DL1 (**Fig. S41a-d**). Therefore, ORN presynaptic calcium depends on other circuit components to compensate the change in firing rate induced by background adaptation. Importantly, lateral inputs from other glomeruli, activated by this

odor but unaffected by the manipulation (e.g. from DM4), are not sufficient to compensate adaptation of the DM1-ORNs. Together with the optogenetic manipulations previously discussed, this data provides further evidence for an intra-glomeruli mechanism.

ORN synapses release acetylcholine in the AL. Pharmacological block of acetylcholine receptors (AChRs) also led to transient and background-dependent responses (**Fig. 4g-j**) for different combinations of test and background stimuli (DL1, **Fig. S2a-c**), further indicating that the regulation of the presynaptic calcium is not a cell-intrinsic property and requires a synaptic feedback loop. ORNs make most of their synapses with PNs and LNs. Genetically silencing PN output had no effect on presynaptic calcium in ORNs, excluding an output gain control mechanism (**Fig. S41e-f**). LNs form a diverse population of inhibitory neurons mediating different types of gain control in the AL[33,37], but their role in the context of background adaptation remains unexplored. Pharmacological block of GABA

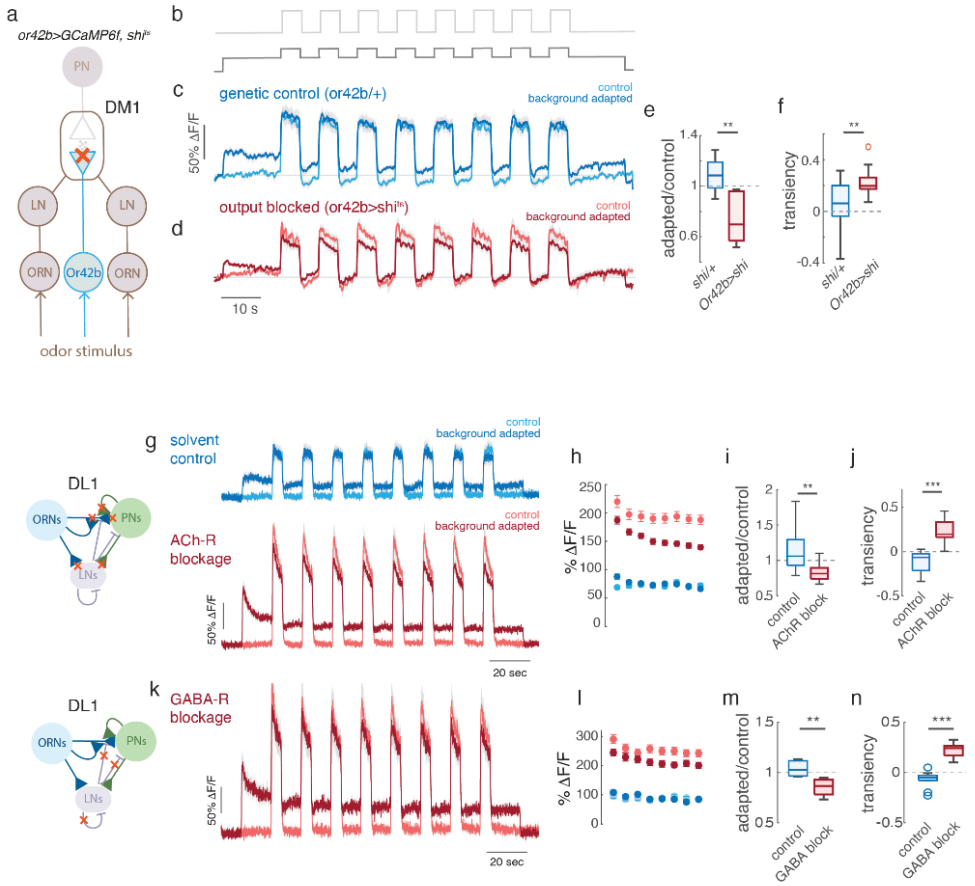

Figure 4. An input gain control mechanism maintains ORN presynaptic calcium background-invariant. a) Genetic blockage of neurotransmitter release from Or42b-ORNs. **b)** Stimulation protocol in control (light gray) and background adapted conditions (dark gray). **c)** Calcium response of the DM1 glomerulus in genetic control flies showing background-invariant responses and **d)** calcium response in flies with blocked ORN synapses showing background-dependent responses to methyl acetate (liquid dilution of 10^{-4}, background airflow dilution C5 and pulse C6, see **Table S3**). **e)** Relative adaptation measure as the response ratio in adapted and control conditions. **f)** Response transiency measured as the relative change in response at stimulus onset and offset (transiency=1-f_{offset}/f_{onset}) N=7, 8. **g)** Calcium responses from the DL1 glomerulus before and after drug application. Pure 2-butanone was used in airflow dilutions of C7 for the background and C8 for the pulse. For the blockage of AChR 100 µM atropine + 20 µM tubocurarine + 200 nM imidacloprid was used, N=10. **h)** Mean response to the single pulses, error bars indicate SE. **i-j)** As in **e-f). k-n)** as **g-j)** for GABA-R blockage: 25 µM CGP54626 + 5 µM picrotoxin, N=5. Thick lines indicate mean and shaded areas indicate SE. Box plots indicate median, quartiles, min/max values and outliers. **p<0.01, ***p<0.001, Kruskal-Wallis.

receptors led to similar effects as blocking of AChRs (**Fig. 4m-p, and Fig. S2a**), suggesting that GABAergic LNs play a major role in tuning background adaptation in this glomerulus.
We observed similar or partial effects in other glomeruli (DM3, DM6 in **Fig. S2b**), but not in all (DL5, **Fig. S2**). Some of this variability might be attributed to differences in drug penetration. However, DL5 recordings were obtained from the same preparation, on the same focal plane and with the same stimuli as for DL1, minimizing potential differences in drug access. The background-invariant response of DL5 ORNs is unaffected by the blockage of either AChRs or GABA receptors (**Fig. S2a,b**). Additionally, these neurons display an unusual slow increase in baseline calcium across stimulus repetitions, forming a ramp resistant to drug application. This makes us postulate the existence of a cell-intrinsic mechanisms for the regulation of pre-synaptic calcium in DL5.
Overall, our data indicate that, in many glomeruli, inhibitory inputs on the ORN presynapses are necessary to mediate a form of input gain control that counteracts firing rate adaptation, making responses to ON stimuli background invariant. Some glomeruli might implement a redundant or alternative strategy relying on cell-intrinsic homeostatic control of presynaptic calcium.

An amplitude-shift adaptation mechanism is required to achieve background invariance through inhibitory feedback.

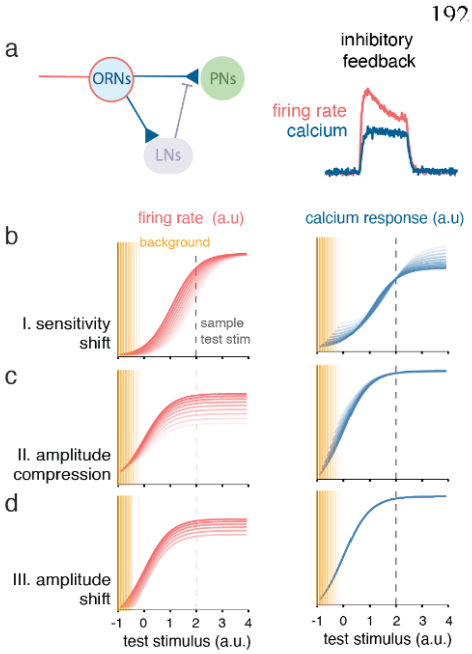

Figure 5. Adaptation mechanisms for background-invariant response. a) We consider an inhibitory presynaptic feedback loop with ORN firing rate as input and ORN axonal calcium as output (see Methods and Eqs. (3-8)). **b-c-d)** Simulated firing rate (red) and calcium response (blue) for the three different adaptive functions in Eq. (8): sensitivity-shift, amplitude-compression, amplitude-shift. Different color intensities correspond to different simulated background stimuli indicated by the orange lines. Dotted lines indicate a representative test stimulus.

We next asked how inhibitory feedback from the LNs can lead to invariant calcium dynamics across different background conditions. To address this question, we implemented a dynamic model of the ORN presynaptic calcium response where ORN firing rates provide the excitatory inputs while LN drive the inhibitory feedback (**Fig. 5a** and Methods). We show that to achieve response invariance across all background conditions, single ORNs must implement an adaptation mechanism of their firing rate that acts as a differential operator in the response domain (**Eq. 7** in Methods). Strikingly, this mechanism corresponds to the amplitude-shift adaptation mechanism that we showed to preserve both intensity and contrast information at the population level (**Fig. 1i-k**). To further understand the role of firing rate adaptation for background invariance of calcium responses, we modeled ORN calcium responses for the three different adaptation mechanisms in **Fig. 1b** (**Eq. 8** in the Methods). The sensitivity-shift mechanism ensures an invariant calcium response in a test-dependent manner, for which information about both the test and background stimuli are required. As a consequence, calcium responses after adaptation to different backgrounds are invariant only for a specified test stimulus (**Fig. 5b,** dashed line). Similarly, the amplitude-compression mechanism leads to a test-dependent response that ensures invariance only for stimuli much higher than the background (**Fig. 5c**). As formally predicted (**Eq. 7** in Methods), only the amplitude-shift adaptation mechanism ensures invariant calcium responses for all backgrounds and test stimuli (**Fig. 5d**). This current-based dynamical model captures both the firing rate and calcium dynamics but does not explicitly include the divisive normalization implemented by LNs[33]. To better understand the interaction between divisive normalization and background adaptation, we also implemented a stationary model of divisive normalization with an inhibitory input provided by adaptive

LN neurons (see Supplementary Material). We show that also in this case background invariance is guaranteed only for an adaptation mechanism that is amplitude dependent - in this case a combination of both shift and compression (**Fig. S3a**).
Altogether, we demonstrated that inhibitory feedback can mediate ON background invariance only if the input firing rate adapts by an amplitude dependent mechanism, highlighting a new computational role of adaptation that deviates from efficient coding predictions at the single-neuron level.

Olfactory projection neurons inherit a background-invariant representation of ON odor stimuli

To understand the relevance of these axonal computations in ORNs, we investigated whether background adaptation is preserved in the postsynaptic neurons. ORNs make most of their synapses on uniglomerular PNs. ORN-PN synapses undergo depression on both fast[31] and slow[36] timescales. We reasoned that even a tonic activation of depressing synapses would result into phasic and adaptive responses in postsynaptic neurons. Indeed, contrary to ORNs, PNs calcium dynamics are phasic (as also shown in [36]), but surprisingly their responses to odors are independent of background adaptation, as in the ORN axons (**Fig. 6a**).
To validate the generality of this observation, we explored a range of ON and OFF stimuli, i.e. odor pulses higher or lower than the adapting background stimulus (**Fig. 6a, b**). PN responses to ON stimuli had similar amplitudes independently of background adaptation (**Fig. 6a, Fig. S4a**), also for high background concentrations (**Fig. S4b**). In contrast, OFF stimuli, even of small amplitude, always produced large decreases in calcium (**Fig. 6b, Fig. S4b, c**). To capture the transition between ON and OFF responses irrespective of experimental noise in the generation of the stimuli, we quantified relative adaptation as a function of contrast. We use response *contrast* (defined as the relative difference between the response to the control pulse and the response to the background) as a proxy for stimulus contrast and define *relative adaptation* as the relative difference in the response to the pulse between control and adapted conditions (**Fig. S4c**). Zero contrast means that the tested stimulus equals the background, and zero adaptation means that PNs respond in a background-invariant manner. By binning the single trials based on contrast value, one can capture the sharp transition between ON and OFF stimuli (**Fig. 6c**), which demonstrates background-invariance only for ON stimuli in the PN dendrites. Responses to OFF stimuli instead fall much below the non-adapted response also for very small contrast values. Therefore the asymmetric background invariance of ORN axonal calcium is preserved in PNs.
These observations contrast with a previous study that described background adaptation in PNs firing rates[38]. This could be attributed to a more precise control of test and background stimuli in our experimental setup (**Fig. S4f, g**). However, it could be also due to the different measures of neural activity: calcium versus voltage. PNs' subthreshold potentials and firing rates follow a linear relationship[38], therefore, to support our observations, we performed optical voltage recordings from their dendrites. Using the voltage sensor ASAP2s[39], we show that PN dendrites depolarize similarly (**Fig. 6d**, DM1) or even slightly more (rather than less, **Fig. S4d, e**, DM2 and VM7d) when odor stimuli are presented on a background (ON stimuli). Consistently with calcium measurements, OFF responses are not background invariant (**Fig. 6d**). Finally, we asked whether these properties are preserved in the PNs output. Calcium imaging from the axonal innervations of PNs in the LH shows phasic and background invariant odor responses (**Fig. 6e**) further supporting the relevance of these dynamics for information transmission.
We conclude that both PNs' dendritic and axonal activities encode a background-invariant representation of ON odor stimuli overcoming the background adaptation of ORN firing rates[13,14] and the depression of ORN-PN synapses[31,36].

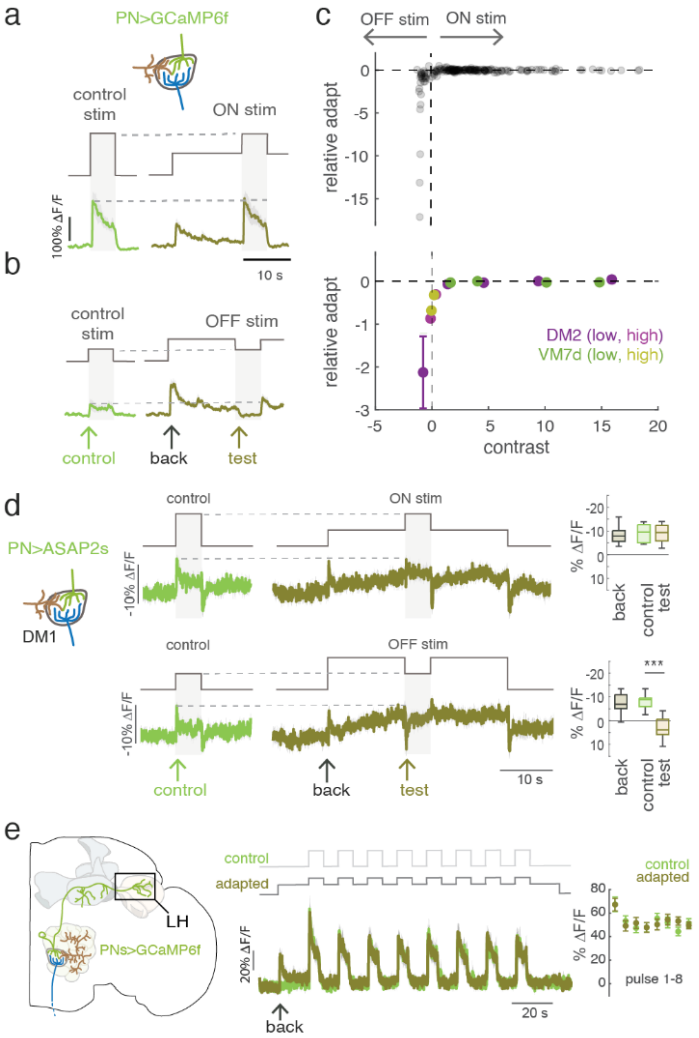

Figure 6. Asymmetric background-invariance of PN responses. a, b) Schematics of the stimulus protocol and calcium responses of PNs withing glomerulus DM2 for two examples of ON and OFF stimuli. Colored lines indicate the mean ΔF/F, shaded area SE, N=9-11. The arrows indicate the control ($F_{control}$, green), background (F_{back}, black) and test responses (F_{test}, olive) used to define the contrast stimulus and relative adaptation. **c)** *Top:* Relative adaptation as a function of contrast for each single trial, including two independent datasets recorded from two different glomeruli. Relative adaptation is defined as $(F_{test}-F_{control})/F_{control}$. Since stimulus concentrations are too low to be measured, we use response contrast as a proxy for stimulus contrast $(F_{test}-F_{back})/F_{back}$ under the assumption that the response is monotonic. *Bottom*: relative adaptation averaged in bins of contrast; color coded by glomerulus type. *Low* and *high* indicate two different datasets where different ranges of background concentration where used (N=9-11, see also **Fig. S4**). **d)** Control and background adapted responses measure in DM1 using the voltage sensor ASAP2s. Thick lines indicate the mean ΔF/F and the shaded areas SE. Liquid dilution of methyl acetate is 10^{-2}, flow dilutions are B6C9 for ON stimuli and B9C6 for OFF stimuli, N=10. Boxplots represent median, quartiles, min/max values and outliers **e)** Calcium responses measured from the PNs axons in the LH, N=6. Odor stimuli were chosen to excite a single glomerulus (DM4, B5C5 with 10^{-4} and 10^{-6} liquid dilutions).

PN's background invariance requires modulation of ORN synaptic release.

Next, we asked how the depressing ORN-PN synapses could preserve background invariance. One key difference between presynaptic ORN and postsynaptic PN calcium is their dynamics: tonic in ORNs and phasic in PNs. We reasoned that tonic levels of presynaptic calcium – induced by the sustained

background - might be associated with enhanced engagement of the neurotransmitter release machinery (**Fig. 7a**). Conserved Unc13 proteins mediate several types of presynaptic plasticity (e.g. short-term facilitation and fast and long-term potentiation)[40–47]. The two Unc13 splice variants, Unc13A and Unc13B, are differentially organized at the ORN-PN synapses and mediate different postsynaptic currents [48]. Unc13-dependent plasticity has been linked to three domains that can be modulated directly or indirectly by calcium: the Ca^{2+}/calmodulin binding CaM domain (only present in Unc13A), the C1 domain binding diacylglycerol (whose metabolism is Ca^{2+}-dependent), and the C2B domain, that binds phosphoinositides in a Ca^{2+}-dependent manner[40,49]. The C1 and C2B domain were shown to exert autoinhibition on the vesicle priming reaction, which makes vesicles responsive to action potentials[50]. Activation of the Unc13-C1 domain enhances action-potential induced transmitter release and diminishes multiple forms of presynaptic plasticity (i.e. short-term facilitation, post-tetanic potentiation, and homeostatic potentiation)[47,51–53]. A single amino acid exchange (H→K) in the C1 domain reconstitutes this enhanced potentiation and blocks synaptic plasticity (short term facilitation and potentiation) [47,52,54]. We used the Unc13-$C1^{HK}$ mutation to test if ORN presynaptic plasticity is required to achieve background invariance. We used three stimulus conditions combining two concentrations of the background and test stimulus which, in control flies, led to background-invariant responses in both DL5 ORNs and PNs (**Fig. 7b, c**). It should be noted that in this glomerulus the background compensation is initially overestimated, and background invariance is achieved only at the second odor pulse. Such invariance was lost in Unc13-$C1^{HK}$ mutants for two of the three stimulus conditions tested (**Fig. 7d**). We did not see major effects of the C1 domain mutation for the high contrast condition, which indicates that the calcium modulation probably involves more than one mechanism. Comparing control and mutant flies across three different glomeruli (including DL1 and DM4), we observed significant effects of the mutation on relative adaptation for most stimulus conditions tested (**Fig. 7e**). Unlike expected from a loss of function of Unc13 in ORNs[48], the C1 gain-of-function mutation had no significant effects on the controls and specifically affected only the response to background adapted stimuli (**Fig. 7f**). This indicates that only activity-dependent modulation of the domain is disrupted, while synaptic transmission itself is not impaired or attenuated in this context, consisted with enhanced, but non-plastic synaptic transmission at the larval NMJ[47].

Overall, we conclude that modulation of Unc13 proteins is necessary to keep PN postsynaptic response background invariant and stable over time. This pathway might act redundantly or synergistically with other calcium-dependent modulations of presynaptic function.

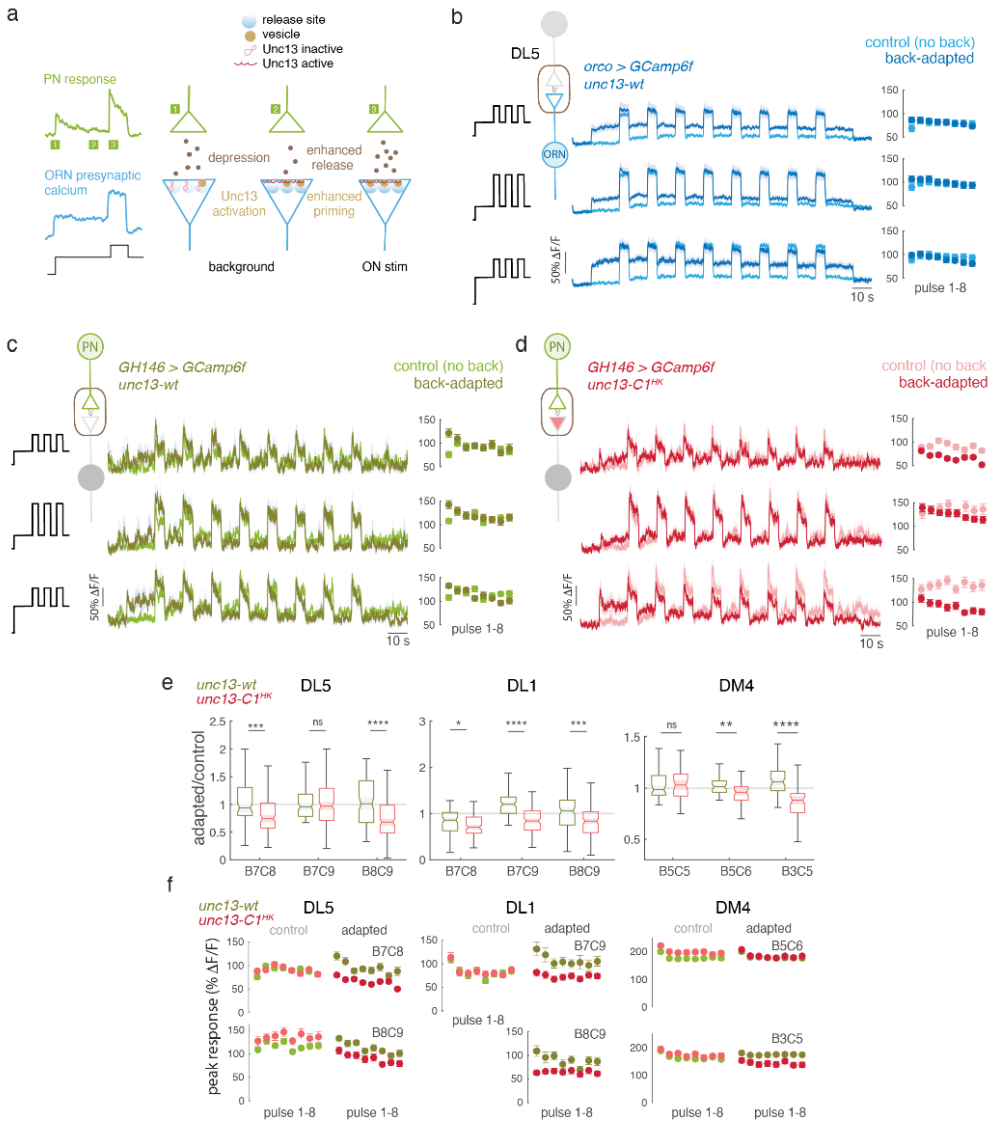

Figure 7. Unc13-C1 domain is required for background-invariant PN response. a) Schematics of hypothesis. **b)** Mean calcium response from ORN axon terminal to 8 odor pulses in control and adapted conditions for three combinations of background and test stimuli. Shaded areas indicate SE. Right, quantification of the mean response to each odor pulse. **c,d)** same as **b)** for PNs in control and Unc13-C1^{HK} mutant flies (WT N=6-7, mutant N=7-11). **e)** Background adapted response divided by the control for each stimulus condition tested in three different glomeruli. For DL5 and DL1, pure 2-butanone was used for background and pulse. For DM4, we used methyl acetate with liquid dilution of 10^{-6},10^{-4} (B5C5 and B5C6) and 10^{-4},10^{-4} (B3C5). Bar plots are generated from all flies measured and all 8 puffs in each trial (DL1: control N= 6-7, mutant N=7-11, DM4: control N= 6-8, mutant N=6-7). Bar plots indicate median, notch, quartiles, max and min. BXCX indicates the flow rate for background (B) and test (C) stimuli, see Table S3. **f)** Mean peak response for control and Unc13-C1^{HK} mutant flies for 8 consecutives odor puffs in control adapted conditions. Error bars indicate SE.

A population code with asymmetric background invariance

Having identified the mechanisms that ensure background invariance in PNs, we ask how odor information is represented in the background-invariant population responses of PNs compared to the background-dependent population rates of ORNs. We model ORNs based on their peripheral firing dynamics using the amplitude-shift model of adaptation (as in **Fig. 1i)** with the update rule that ensures

background invariance (**Fig. 5d** and **Eq. 8** in Methods). We model individual PNs as background invariant and using gaussian noise to recapitulate their sharp response transition between ON and OFF stimuli (**Fig. 6c**) which we attribute to low signal-to-noise in their input (**Fig. S5** and Methods). As shown in **Fig. 1** for ON stimuli, a population of ORNs encodes both intensity and contrast information, but the odor representations shrink close to zero contrast leading to a continuous transition to OFF stimuli (**Fig. 8a, b**). On the contrary, the response space of the PN population exhibits a discontinuity that separates ON and OFF stimuli across different backgrounds while preserving a background-invariant representation of ON stimuli (**Fig 8c**).

Since the background-invariant responses of PNs do not encode contrast explicitly at the population level, there is a remaining question of why ORN populations should encode this feature. We have shown both experimentally (**Fig. 3**) and computationally (**Fig. 5**) that firing rate compensation can be performed in a glomerulus-intrinsic manner. However, when multiple glomeruli are active, background invariance must be achieved in a coordinated way across the AL. We ask whether this task could be achieved by multiglomerular LNs that would be able to read out both intensity and contrast information from ORN activity (**Fig. 1**). LNs mediate a form of normalization that relaxes the non-linearity of the ORN-PN transformation[32,33]. This normalization is mostly presynaptic[33,55] and relies on a measure of overall activity across receptor types. We studied the effects of such normalization by including an interglomerular LN to the local ORN-PN circuit (**Fig. 8d** and Methods). Adding this interglomerular normalization factor enhances the encoding of low contrast stimuli in ORNs (**Fig. 8e**). We show analytically that with this normative input at the presynapses, ON background invariance of the PNs response can only be achieved by the amplitude-shift mechanism if multiglomerular LNs encode contrast information, in agreement with our hypothesis (Methods). Remarkably, in the absence of background stimuli, the encoding of contrast equals the encoding of intensity consistently with reported

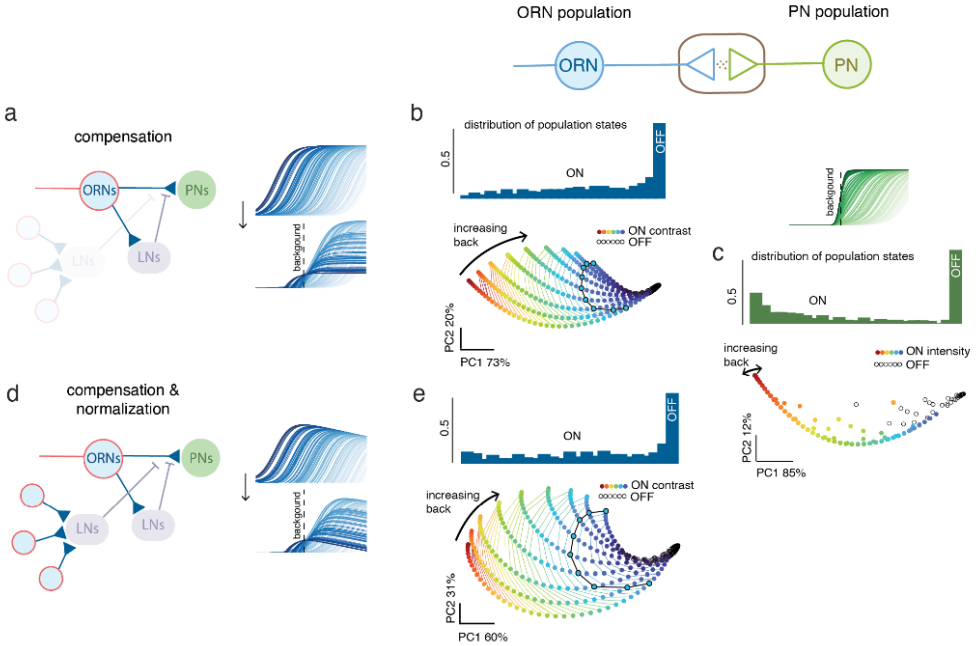

Figure 8. Combinatorial representation of ON and OFF stimuli in ORN and PN populations: a) Schematics of the circuit model that implements synaptic compensation of firing rate adaptation. *Right*: firing response curves for a population of ORNs with different stimulus sensitivities in control (*top*) and background adapted conditions (*bottom*). **b)** 2D-manifold of the population response to stimuli of different ON (color coded) and OFF (black) contrast in different background adapted conditions. The histogram represents the distribution of population states calculated on the first principal component. **c)** Same as **b)** for PNs, but responses are color-coded by stimulus intensity. PNs ON background-invariance was modeled as described in **Fig. S4**. **d)** Schematics of the circuit model that implements both synaptic compensation and interglomerular normalization. *Right*: response curves for a population of ORNs with different stimulus sensitivities in control (top) and background adapted conditions (bottom). **e)** Same as **b)** but responses of single neurons are normalized by a term proportional to stimulus contrast.

normative function of the LNs[33]. Using a divisive rather than a linear model of lateral inhibition leads to similar results (Supplementary Material, **Appendix 1** and **Fig. S3**).
Overall, we propose that the AL implements a circuit computation that extracts contrast information encoded in ORNs to enhance the discriminability between ON and OFF stimuli in postsynaptic PNs while preserving information of odor identity for ON stimuli.

Discussion

Odors are detected by single sensory neurons that work combinatorially to represent complex natural stimuli at the population level. Despite the key role of adaptation for information coding in both single neurons and neuronal populations, the adaptive properties of the olfactory system downstream of the receptors have been largely overlooked. In this work, we investigated adaptation as a coding strategy of single ORNs that shapes the encoding capabilities of olfactory neural populations. By combining experiments and computational models, we identified a novel property of the olfactory pathway that we defined as asymmetric background invariance. We show that the adapted firing responses of single ORNs are compensated to achieve an asymmetric representation of ON and OFF contrast stimuli, where ON responses are background invariant while OFF responses collapse in the representation space of the downstream populations, the PNs. Mechanistically background invariance requires a feedback compensation induced by ORN synaptic release and involves a GABAergic inhibitory pathway that modulates ORN presynapses. We propose that this feedback compensation facilitates vesicle release through interaction with the Unc13-C1 domain, which stabilizes the background invariance of the PNs. The PN population therefore preserves ON stimulus identity necessary for downstream computations.

The role of adaptation at the single neuron and population level.

Efficient coding principles provide an explanation for how single sensory neurons adapt their response function to changes in stimulus statistics over behaviorally[2,9,10] or evolutionary[56–58] relevant time scales. Similar principles have been used to understand how the response function of neurons in a population should adjust to tile the stimulus space in a flexible manner[59]. This is of particular importance to understand coding principles in the olfactory system, which uses a repertoire of receptors to detect and discriminate odors within neuronal populations. Receptor repertoires are tuned, through evolutionary times, to the ecology of the animal[60], leading to efficient sensory codes in the ecologically relevant stimulus space[61]. A similar adaptive strategy also applies on shorter timescales. For instance, the expression levels of the receptors are plastic in mammals, providing a mechanism to optimize the composition of a receptor repertoire to changes in the environment[62].
Similar adaptive changes in the coding capability of a receptor repertoire could in principle occur also on shorter time scales, but there is limited evidence of such a strategy in the olfactory system[28]. In this work, we provided evidence that the fly olfactory system does not adapt the odor representation to the background. Rather, it implements mechanisms that keep odor representations robust with respect to changes in the background. While efficient coding theories of single neurons predict the conventional sensitivity-shift strategy widely observed in the visual system, both ORNs and PNs do not follow this principle. ORNs adapt by modifying their response amplitude (and not their sensitivity), which ensures the compensation necessary to achieve ON background invariance in downstream neurons, the PNs. Therefore, even though a persistent stimulus (the background) induces synaptic depression and a corresponding decrease in postsynaptic activity[36], it also primes the synapses to respond to ON stimuli as strongly as in the absence of background. The mechanisms underlying adaptation involve inhibitory feedback potentially provided by LNs. Both dynamic and stationary models for ORN adaptation through inhibitory feedback confirm the role of an amplitude-based adaptation that can come as a single amplitude shift or as a combination of both amplitude-shift and -compression.
Our findings raise the question of why ORNs would adapt at all if the goal was to encode absolute stimulus intensities. We argue that firing rate adaptation is beneficial to the asymmetric encoding of ON and OFF stimuli, where only ON stimuli preserve stimulus identity, while OFF stimuli collapse into a low-response state. Such asymmetry would not be possible if the ORNs simply encoded stimulus intensity. From a more speculative perspective, another potential benefit of adapting firing rate and then compensating it downstream could be a lower total energetic cost of sending information through the brain with no loss. However, further work is necessary to assess whether the synaptic computations that

compensate firing rate adaptation are indeed less energetically costly than implementing a non-adaptive spiking code.

The role of asymmetric odor encoding downstream of PNs.

PNs send odor information to both the LH and MB, contributing to higher order computations. Odor representations in the Kenyon cells (KCs) of the MB are used to form associative memories based on the co-occurrence of an odor and a reinforcement[63]. For memory retrieval, it is critical that the same KCs are activated by the conditioned stimulus in training and test phase and therefore it is critical that the odor is represented independently of possible backgrounds. Altogether, memory retrieval provides a potential function for background-invariant encoding in PNs. Consistently with this hypothesis, a recent study showed that locusts learn in a background-invariant manner[64], suggesting that the MB has access to a background-invariant representation of odors.

Odor cues are used not only to evaluate, but also to explore the environment. Animals use odor gradients[65,66], plume statistics[67,68] and odor motion[69] to direct their behavior in complex olfactory environments. These computations require the detection of gradients and contrast in an odor-specific manner. It is plausible that such computations do not occur in the AL, where odor representations are formed, but in downstream neurons that can read out a population response from the AL to then compute stimulus-specific information on contrast. The LH provides the cellular complexity[70,71] to perform odor-specific computations in parallel[72], including the encoding of contrast[73]. We suggest that the encoding of background-invariant ON responses through the compensation of ORNs adaptation is essential for downstream stimulus-specific computations that drive key behaviors in flies. These computational requirements do not generalize to OFF stimuli, which have a very different relevance for the fly behavior compared to ON stimuli, leading to an explorative search rather than an oriented behavior [65,74].

Cell intrinsic and circuit mechanisms that maintain ON stimulus invariance.

Asymmetric background invariance is the most robust observation we made across all our measurements in both ORNs axons and PNs dendrites. However, we also encountered differences across glomeruli. Firstly, ORN calcium dynamics range from being slightly phasic (DM1), completely flat (DL1), to slightly ramping up (DL5). This seems to correlate with background invariance to be achieved already on the first (DM1), or only on the second or third (DL1, DL5) odor pulse. Moreover, we showed that background invariance of DM1 and DL1 ORNs requires synaptic transmission, whereas DL5 background invariance does not. Moreover, blocking GABA receptors has differential effects across glomeruli, which unlikely can be attributed solely to differences in drug penetration. Glomeruli such as DL5, which do not receive substantial GABAergic inputs under the condition tested, may instead rely on cell-intrinsic mechanisms - for example the regulation of internal calcium storages[75,76].

In other glomeruli, these intrinsic mechanisms may act in combination with feedback inhibition, which is recruited in a stimulus-dependent manner.

In all tested glomeruli, we find that a gain-of-function mutation of the Unc13-C1 domain, Unc13-C1^{HK}, occludes PNs background invariance. So far, we do not have direct evidence that plasticity involving Unc13 is mediated by the tonic and background-invariant presynaptic calcium nor that it is downstream of lateral inhibition. However, our current working model postulates a link between presynaptic calcium regulation and enhanced vesicle priming. As the Unc13-C1^{HK} mutant does not abolish background invariance for all stimulus conditions, other calcium-dependent mechanisms are likely involved in this plasticity, perhaps through modulation of other synaptic proteins (e.g. synaptotagmin-3 or -7[77]).

Overall, our data suggest a key role for presynaptic plasticity in PN background invariance, linking the same molecular pathways usually studied under artificially induced homeostasis[40,47,78] to sensory computations in natural conditions. At ORN-PN synapses, the homeostatic set point is the non-adapted response. Differently from other models of synaptic homeostasis, the feedback compensation is not calculated based on synaptic output (PN response) but based on the input drive to synaptic release (ORN firing rate). This synaptic strategy is, to our knowledge, unique in its design and perhaps specific to the computational demands of the olfactory system.

The undoing of a neural computation: evolutionary considerations

Undoing an upstream computation is rather an uncommon observation that becomes counterintuitive from an efficient coding perspective, where computations are expected to optimize information processing across neuronal layers. However, if we look at neural circuits as ongoing projects of evolution that continue to adapt to optimize behaviorally relevant trade-offs[79,80], more examples of undoing can be found. For example, some amacrine cells in the visual system undo the color opponency calculated in upstream neurons to preserve the balance between opponent and non-opponent units in the retina[81] such that both types of information are transferred in downstream neurons. The logic of this computation could result from the order in which these mechanisms evolved (discussed in[81]).

From an evolutionary perspective, the olfactory system is designed to ensure adaptability, which is implemented primarily by the evolution of chemosensory genes. Our considerations focused on the combinatorial aspect of odor coding, and therefore the fact that stimuli are encoded in populations of sensory neurons, with identity defined by the OR they express. However, this system evolved from an ancestor that expressed only one or few ORs[82]. In such a low dimensional system, firing rate adaptation might not only have been parsimonious, but also an efficient strategy for odor encoding, as it is the case for visual neurons. The olfactory system might have selected for mechanisms that support background invariance only after the emergence of a combinatorial coding strategy with multiple ORs.

Olfactory systems also evolved specialized channels that encode unique chemicals, such as pheromones[83] or harmful substrates[84], crucial in certain ecological contexts. These stimuli therefore do not rely on a population code and might implement different strategies for adaptation. A combination of mechanisms can be therefore expected within the same sensory system depending on the function of specific subcircuits. Further insight into these questions might benefit from the study of downstream areas like the LH that read out combinatorial or specialized representations for behavioral-relevant computations.

Material and methods

Experimental model / fly husbandry

All flies were kept on a standard molasses-based food at 25°C and on a 12h:12h light-dark cycle or at room temperature in the laboratory. For optogenetic experiments, flies were kept in the dark and on food that was supplement with 1mM all-trans retinal (Sigma-Aldrich, Table S1) for at least 4 days before experiments. For shibire^{ts} experiments, flies were incubated for at least 1h at 36-37°C before the start of recordings, which lasted a maximum of 45min. Female flies were used for all experiments. The complete genotypes are given in Table S2.

Fly mutagenesis Unc13-C1^{HK}

The mutation of the Unc13-C1 domain was based on the corresponding mutation of the mouse homologues Munc-13-1 where histidine 567 was changed to lysine[52]. Sequence alignment with *Drosophila* Unc13A identified histidine 1723 as the relevant target. Note that the two *Drosophila* splice isoforms Unc13A and Unc13B harbor a C1 domain[46] and that this modification therefore affects both. CRISPR-mediated mutagenesis was performed by WellGenetics Inc. using modified methods of Kondo and Ueda[85] to generate a break in unc-13/CG2999. A PBacDsRed cassette containing two PBac terminals and 3xP3-DsRed and two homology arms with point mutations (one to induce the amino acid change and one to introduce a TTAA sequence to recognize proper integration on the other homology arm) were used for repair. The DsRed marker was intermittently used to identify flies with successful integration events in the F1 generation. The marker was later excised and the presence of the point mutation and successful removal of the cassette in the final fly line validated by PCR and sequencing from genetic DNA.

In vivo calcium imaging

Flies 6-10 days post-eclosion were anesthetized on ice and mounted on a custom holder using the Bondic repair system (Bondic cartridge with Bondic liquid plastic and Bondic UV-LED). The proboscis was secured, and the maxillary palps were covered using low melting temperature wax. Saline solution

(5mM Hepes, 130 mM NaCl, 5mM KCl, 2 mM MgCl2, 2mM CaCl2, 36 mM Saccharose – pH 7.3) was added and the cuticle covering the fly's brain, as well as obstructing trachea and fat tissue, were removed.
Functional imaging was performed on an Investigator two-photon microscope (Bruker) coupled to a tunable laser (Spectraphysics Insight DS+) with a 25×/1.1 water-immersion objective (Nikon). Laser excitation was tuned to 920 nm, and less than 20 mW of excitation was delivered to the specimen. Emitted light passed through a SP680 short-pass filter, a 560 lpxr dichroic filter and a 525/70 filter. PMT gain was set to 850 V. The microscope was controlled with the PrairieView (5.4) software.

Stimulation

Test and control stimuli were 5 sec long, background stimuli were 15 sec. In Fig. 4,5,6, test and control stimuli were repeated 8 times with 10 sec between repetitions.
Optogenetics: light from a 625 nm LED was directed to the fly's antenna using an optic fiber. The LED was controlled by the imaging software and activated during the laser flight-back, allowing simultaneous acquisition and excitation. In electrophysiological experiments, the LED was controlled by an Arduino board.
Odor delivery: a flow of clean air was presented to the fly continuously (1L/min). To this main airflow, either an odor (odorant airflow; 100mL/min) or more clean air (balancer airflow; 100 mL/min) was added through a solenoid valve (LEE), so that the final airflow reaching the fly was always around 1.1L/min. To create the gas dilutions for the odorants, four mass flow controllers (MFCs) were used (Analyt-MTC) and controlled using a custom MATLAB (MathWorks) script and an Arduino board. Another 3 MFCs were required to keep the constant airflows for the main airflow and the balancer airflows. Odors were prepared in 20ml glass vials as a liquid volumetric dilution with a total volume of 5 mL in mineral oil. Airflow dilutions used are described in Table S3. Liquid dilutions were prepared in 20 ml glass vials always to a total volume of 5 mL in mineral oil.

Electrophysiology

Single-sensillum recordings were performed as previously described[14] using a silver-chloride electrode and glass pipettes filled with sensillum lymph ringer. Electrical signals were amplified using an extracellular amplifier (EXT-02F-1, npi) with head stage (EXTEH), bandpass filtered (300–5000 Hz), digitized at 20KHz using a NI board (NI-6212). Data were acquired with the MATLAB toolbox kontroller[27] (https://github.com/emonetlab/kontroller). Spikes were sorted using a custom MATLAB script. Odor delivery: flies were exposed to a constant airflow (1L/min) and an odor stimulus was delivered by switching a 3-way solenoid valve that directed a secondary airflow (100 mL/min) through a Pasteur pipette as in[14,36]. The pipette contained a filter paper with 50ml of the odor dilution. Volumetric odor dilutions were prepared in either mineral oil or MiliQ Water. Stimuli were controlled by custom-made software in MATLAB and Arduino.

Pharmacology

Acetylcholine receptor blockage was performed using 100 µM atropine + 20 µM tubocurarine + 200 nM imidacloprid (IMI). Stock solutions of 2 mM atropine and 20 mM tubocurarine were prepared in water and aliquoted and frozen at -20ºC. Stock solution of 1 mM IMI was prepared in DMSO and kept at room temperature. Final solution was dissolved in saline solution used for *in vivo* calcium imaging and kept at 4 ºC. For controls, instead of the drug solution, vehicle solution was applied, consisting of the saline solution previously mentioned with 5.1% water + 0.02% DMSO. It was also kept at 4 ºC.
GABA receptor blockage was done using 25 µM CGP54626 + 5 µM picrotoxin (PTX). Stock solutions of 25 mM CGP54626 and 100 mM PTX were prepared in DMSO, aliquoted and kept at -20ºC. Final solution was dissolved in saline solution used for *in vivo* calcium imaging and kept at 4 ºC.
For all pharmacology experiments, flies were prepared for *in vivo* calcium imaging as explained before, with the addition of a final step during dissection where the brain was de-sheathed. All flies were imaged before application of drug solutions with the same stimulation protocol used after drug was added in bath application.
For acetylcholine receptor blockage experiments, normal saline solution was replaced by 100 µM atropine + 20 µM tubocurarine + 200 nM IMI solution 2 consecutive times and then again 10 min after.

Recordings were started 20 min after the drug solution was initially applied. Vehicle solution was applied in the same manner to control flies.
For GABA receptor blockage, normal saline solution was replaced by 25 µM CGP54626 + 5 µM PTX. This was repeated 1 min, 2 min and 10 min after this initial drug application. Recordings were started 40 min after the drug solution was initially applied.

Adaptation model: population response

For a population of ORNs, we model the peak firing rate of each individual neuron i , $F_i(s)$, as a function of the odor stimulus, s , as

$$F_i(s) = \alpha_i \left[\frac{\tanh(s - \beta_i) + 1}{2} - \gamma_i \right] \quad (1)$$

where we have included an explicit dependence on the parameters α_i, β_i and γ_i that control the amplitude-compression, sensitivity-shift, and amplitude-shift adaptation respectively. Neurons within the population are set with an initial random stimulus tuning β_i and equal parameters $\alpha_i = \alpha$ and $\gamma_i = \gamma$. The adapted firing rate, $F'_i(s)$, is described by the same equation but different parameters, β'_i, α'_i and γ'_i, which are updated in a background response-dependent way. For the simulations in Fig. 1, we used the update rules,

$$\begin{aligned} &I. \quad \beta'_i = \beta_i + c_\beta F_i(s_B) \ \text{ fixed } \alpha_i, \gamma_i \\ &II. \quad \alpha'_i = \alpha_i - c_\alpha F_i(s_B) \ \text{ fixed } \beta_i, \gamma_i \\ &III. \quad \gamma'_i = \gamma_i + c_\gamma F_i(s_B) \ \text{ fixed } \alpha_i, \beta_i \end{aligned} \quad (2)$$

with $c_\alpha = c_\gamma = 0.8$ and $c_\beta = 1$. Our results in Fig 1 show that the adaptation mechanisms II and III (response domain) lead to a population code whose variance is mostly explained by two main principal components. Yet, for the mechanism I (sensitivity domain), only one component is needed. We tested the generality of these results for a larger set of weight parameters $c_\beta, c_\alpha, c_\gamma \in \{0.5, 0.6, \ldots, 1.5\}$ for which we quantified the ratio of explained variance between the two first principal components. For each adaptation mechanism we got the ratios $r_\beta = 15.46 \pm 0.76, r_\alpha = 1.62 \pm 0.53$ and $r_\gamma = 1.63 \pm 0.51$, where the error corresponds to the std across all the different weight parameters. Ratios near to unity indicate that both principal components contribute significantly to the population response, while large ratio values indicate a predominant representation of the first principal component. Altogether, we show that the results shown in Fig. 1 hold for different weights in the update rules of Eq. (1) and Eq. (2).

Adaptation model: firing rate and calcium response

We model the ORN calcium response R as a linear function of the difference between the ORN firing rate, $F_E(s,t)$,and an inhibitory rate, $F_I(s,t)$,coming from LNs:

$$R[F(s,t)] = a \cdot [F_E(s,t) - F_I(s,t)], \quad (3)$$

where a is the is the proportionality factor between calcium and firing rate in absence of background as shown in **Fig. 2e**. We model the dynamics of each ORN firing rate as the exponential process:

$$F_E(s,t) = F(s) \left[exp\left(-\frac{t}{\tau_E}\right) + I_E \right], \quad (4)$$

where τ_E is the excitatory time constant, $F(s)$ is the firing rate described by Eq. (1) and I_E is the excitatory baseline. We consider the inhibitory drive to have similar dynamics, inherited from the ORN responses, but a different baseline, that is $\tau_I = \tau_E$ and $I_E - I_I = \Delta_I = 0.05$ respectively. Note that here we do not model the LN firing dynamics, but a general inhibitory input to the pre-synapse. While some

LNs types have been shown to have more transient activity[86], this inhibitory drive could result from specific subtypes or from the signaling cascade downstream of the receptors[87].
Using Eq. (4) under these excitatory and inhibitory response conditions, the calcium response of Eq. (3) becomes proportional to the difference between the excitatory and inhibitory rates, that is,

$$R[F(s,t)] = a\Delta_I F(s). \quad (5)$$

The calcium sustained response to a given stimulus s in the presence of a background, s_B, is proportional to the sum of the sustained calcium response to the background and the stimulus calcium response after the firing rate is adapted, that is,

$$R[F(s,s_B,t)] = R[F(s_B,t)] + R[F'(s,t)]. \quad (6)$$

The background invariance of ORN calcium responses implies that $R[F(s,s_B,t)] = R[F(s,t)]$ for any background. By using Eq. (5) in Eq. (6) we obtain that the adapted firing rate response $F'(s)$ has to satisfy:

$$F'(s) = F(s) - F(s_B) .. \quad (7)$$

This implies that firing rate adaptation has to occur as a change in the response domain rather than in the stimulus domain. Using the firing rate model defined in Eq. (1), we calculate the adaptation rules that satisfy this calcium invariance for each type of adaptation strategy. Specifically, we calculate the adapted value of the parameters that control each of the three adaptation mechanisms considered:

$$\begin{aligned} \beta' &= s - tanh^{-1}\left[2\left(\tfrac{F(s)-F(s_B)}{\alpha}+\gamma\right)-1\right] && \text{for sensitivity-shift} \\ \alpha' &= \alpha\left[1-\tfrac{F(s_B)}{F(s)}\right] && \text{for amplitude-compression} \\ \gamma' &= \gamma + \tfrac{F(s_B)}{\alpha} && \text{for amplitude-shift} \end{aligned} \quad (8)$$

This demonstrate that the only adaptation mechanism that depends uniquely on the background adaptation response and satisfies the calcium invariant condition is the amplitude-shift adaptation. The other two mechanisms require information of both the adapted and non-adapted responses, which are not accessible simultaneously to the circuit.

Adaptation model: effects of inter-glomerular activity

To understand how inter-glomerular activity further shapes the adapted responses of ORNs, we modeled a second inhibitory mechanism that reads out odor information from the population of ORNs and acts at the single ORN level (see Fig. 8). Specifically, we introduce in our model an LN neuron that connects to several glomeruli[32,33] and provides an inhibitory input to the presynaptic terminals. This can be formalized by modifying Eq. (3) as,

$$R[F(s,t)] = a \cdot [F_E(s,t) - F_I(s,t) - F_G(s,t)], \quad (9)$$

where $F_G(s,t) = \sum_i \omega_i F_i(s,t)$ corresponds to the LN term that integrates the ORN population activity. Assuming that the dynamics of the global feedback is slower than the dynamics of the local feedback, our previous arguments hold up to Eq (6). Similarly, as we did before, we use Eq. (9) to write a new relation between the calcium responses of non-adapted and adapted ORNs:

$$F'(s) = F(s) - F(s_B) - F_G(s) + F_G(s_B) + F'_G(s) \quad (10)$$

We showed in **Fig. 1** that a population of ORNs encodes both stimulus intensity and contrast in a two-dimensional manifold, making it possible for two downstream neurons to extract such an information as a linear combination of single ORNs. Consequently, if we assume that the LN neuron that connects to multiple glomeruli extracts contrast information from the population, we can write $F_G(s) = s - s_B$, which at zero background equals the stimulus intensity. We can then write Eq. (10) as,

$$F'(s) = F(s) - F(s_B) - s + s_B + s - s_B, \qquad (11)$$

showing that the amplitude-shift mechanism continues to support ON-background invariance if contrast information is extracted from ORN populations by inter-glomerular LNs. In the absence of an odor background, the encoding of contrast information equals the encoding of the intensity value, which is in agreement with the literature on the role of inhibitory LNs[32,33,55].

PN model of asymmetric background invariance

We show that PNs inherit the ON background-invariant responses from ORN calcium responses. Consequently, we model the adapted responses of PNs in the same way as for the calcium responses of ORNs (Fig. 5). To account for the sharp but continuous transition from OFF to ON responses near small contrast stimuli (Fig 6c), we implement a noise model for the relative adapted responses of PN neurons with a probability $N(s - s_B, \sigma)$, where s_B is the background stimulus and σ is the noise standard deviation. We show that this noise model reproduces the transition from OFF to ON stimuli observed in the experiments (See S4). We then use this model to simulate the adapted responses of PNs (Fig. 8c).

Data Availability

All data are available in the main text or the supplementary materials. Raw data, scripts and software for data curation and analysis have been deposited in Zenodo and are accessible at 10.5281/zenodo.15937307.

Code Availability

Additional resources are available on GitHub https://gitlab.rlp.net/mrtlllab/brandao_ramirez_adaptation2024

Acknowledgment

We thank Filippo Calzolari for reading the first version of the manuscript, Giovanni D'Uva for developing methodology, Christopher Schnaitmann for help with *in vivo* imaging and comments on the manuscript, Christian Daniel for help with graphics, members of the Martelli and Silies lab for discussions, Sabine Schmitt, Simone Renner and Jonas Chojetzki for technical and administrative support. We further thank Douglas Storace for initial discussions on this project, Henrike Scholz for sharing fly lines and Mathias Böhme for help in the planning of the mutagenesis of the Unc13-C1 domain.

Funding

This work was supported by the DFG grant MA7804/2-1 to CM, the Research Unit FOR5289 (project P5 to MA and P4 to CM), the Emmy Noether Programme (project 261020751) and the Novo Nordisk Foundation (Young Investigator Award NNF19OC0056047) to AMW.

Author contribution

Conceptualization: SCB, CM
Methodology: SCB, LR, PZ, AMW, MS, CM
Investigation: SCB, LR, PZ, CM
Formal analysis: LR, CM
Visualization: SCB, LR, PZ, CM
Supervision: CM

680 Writing—original draft: LR, CM
681 Writing—review & editing: SCB, LR, AMW, MS, CM

682 # References
683
684 1. Wark, B., Lundstrom, B. & Fairhall, A. Sensory adaptation. *Curr Opin Neurobiol* **17**,
685 423–429 (2007).
686 2. Laughlin, S. B. The role of sensory adaptation in the retina. *Journal of Experimental*
687 *Biology* **146**, 39–62 (1989).
688 3. Simoncelli, E. P. Vision and the statistics of the visual environment. *Curr Opin*
689 *Neurobiol* **13**, 144–149 (2003).
690 4. Brenner, N., Bialek, W. & De Ruyter Van Steveninck, R. Adaptive Rescaling
691 Maximizes Information Transmission. *Neuron* **26**, 695–702 (2000).
692 5. Laughlin, S. B. & Hardie, R. C. Common strategies for light adaptation in the peripheral
693 visual systems of fly and dragonfly. *Journal of Comparative Physiology □ A* **128**, 319–
694 340 (1978).
695 6. Gür, B. *et al.* Neural pathways and computations that achieve stable contrast processing
696 tuned to natural scenes. *Nature Communications 2024 15:1* **15**, 1–18 (2024).
697 7. Malnic, B., Hirono, J., Sato, T. & Buck, L. B. Combinatorial receptor codes for odors.
698 *Cell* (1999) doi:10.1016/S0092-8674(00)80581-4.
699 8. Hallem, E. a & Carlson, J. R. Coding of odors by a receptor repertoire. *Cell* **125**, 143–
700 60 (2006).
701 9. Benda, J. Neural adaptation. *Current Biology* **31**, R110–R116 (2021).
702 10. Weber, A. I., Krishnamurthy, K. & Fairhall, A. L. Coding Principles in Adaptation. *Annu*
703 *Rev Vis Sci* **5**, 427–449 (2019).
704 11. Gutnisky, D. A. & Dragoi, V. Adaptive coding of visual information in neural
705 populations. *Nature 2008 452:7184* **452**, 220–224 (2008).
706 12. Reisert, J. & Matthews, H. R. Adaptation of the odour-induced response in frog olfactory
707 receptor cells. *Journal of Physiology* (1999) doi:10.1111/j.1469-7793.1999.0801n.x.
708 13. Nagel, K. I. & Wilson, R. I. Biophysical mechanisms underlying olfactory receptor
709 neuron dynamics. *Nat Neurosci* **14**, 208–216 (2011).
710 14. Martelli, C., Carlson, J. R. & Emonet, T. Intensity invariant dynamics and odor-specific
711 latencies in olfactory receptor neuron response. *Journal of Neuroscience* **33**, (2013).
712 15. Strausfeld, C. Z. & Kaissling, K.-E. Localized adaptation processes in olfactory sensilla
713 of Saturniid moths. *Chem Senses* **11**, 499–512 (1986).
714 16. Lemon, W. & Getz, W. Temporal resolution of general odor pulses by olfactory sensory
715 neurons in American cockroaches. *Journal of Experimental Biology* **200**, 1809–1819
716 (1997).
717 17. Raman, B., Joseph, J., Tang, J. & Stopfer, M. Temporally diverse firing patterns in
718 olfactory receptor neurons underlie spatiotemporal neural codes for odors. *Journal of*
719 *Neuroscience* **30**, 1994–2006 (2010).
720 18. Kurahashi, T. & Menini, A. Mechanism of odorant adaptation in the olfactory receptor
721 cell. *Nature* **385**, 725–729 (1997).
722 19. Dalton, P. Psychophysical and behavioral characteristics of olfactory adaptation. *Chem*
723 *Senses* **25**, 487–492 (2000).
724 20. Ramaswami, M. Network plasticity in adaptive filtering and behavioral habituation.
725 *Neuron* **82**, 1216–1229 (2014).
726 21. Sinding, C. *et al.* New determinants of olfactory habituation. *Sci Rep* **7**, 41047 (2017).
727 22. Wilson, D. A. Habituation of odor responses in the rat anterior piriform cortex. *J*
728 *Neurophysiol* **79**, 1425–1440 (1998).

23. Fishilevich, E. *et al.* Chemotaxis behavior mediated by single larval olfactory neurons in Drosophila. *Current Biology* (2005) doi:10.1016/j.cub.2005.11.016.
24. Baker, K. L. *et al.* Algorithms for Olfactory Search across Species. *J. Neurosci.* **38**, 9383–9389 (2018).
25. Sourjik, V. & Wingreen, N. S. Responding to chemical gradients: bacterial chemotaxis. *Curr Opin Cell Biol* **24**, 262–268 (2012).
26. Louis, M. Mini-brain computations converting dynamic olfactory inputs into orientation behavior. *Curr Opin Neurobiol* **64**, 1–9 (2020).
27. Gorur-Shandilya, S., Demir, M., Long, J., Clark, D. A. & Emonet, T. Olfactory receptor neurons use gain control and complementary kinetics to encode intermittent odorant stimuli. *Elife* **6**, e27670 (2017).
28. Martelli, C. & Storace, D. A. Stimulus Driven Functional Transformations in the Early Olfactory System. *Front Cell Neurosci* **15**, (2021).
29. Brandão, S. C., Silies, M. & Martelli, C. Adaptive temporal processing of odor stimuli. *Cell Tissue Res* **383**, 125–141 (2021).
30. Su, C.-Y., Menuz, K. & Carlson, J. R. Olfactory Perception: Receptors, Cells, and Circuits. *Cell* **139**, 45–59 (2009).
31. Kazama, H. & Wilson, R. I. Homeostatic matching and nonlinear amplification at identified central synapses. *Neuron* **58**, 401–413 (2008).
32. Olsen, S. R. & Wilson, R. I. Lateral presynaptic inhibition mediates gain control in an olfactory circuit. *Nature* **452**, 956–960 (2008).
33. Olsen, S. R., Bhandawat, V. & Wilson, R. I. Divisive normalization in olfactory population codes. *Neuron* **66**, 287–299 (2010).
34. Banerjee, A. *et al.* An Interglomerular Circuit Gates Glomerular Output and Implements Gain Control in the Mouse Olfactory Bulb. *Neuron* **87**, 193–207 (2015).
35. Laughlin, S. B. & Hardie, R. C. Common strategies for light adaptation in the peripheral visual systems of fly and dragonfly. *Journal of Comparative Physiology □ A* (1978) doi:10.1007/BF00657606.
36. Martelli, C. & Fiala, A. Slow presynaptic mechanisms that mediate adaptation in the olfactory pathway of Drosophila. *Elife* **8**, (2019).
37. Barth-Maron, A., D'Alessandro, I. & Wilson, R. I. Interactions between specialized gain control mechanisms in olfactory processing. *Curr Biol* **33**, 5109-5120.e7 (2023).
38. Cafaro, J. Multiple sites of adaptation lead to contrast encoding in the Drosophilaolfactory system. *Physiol Rep* **4**, e12762 (2016).
39. Chamberland, S. *et al.* Fast two-photon imaging of subcellular voltage dynamics in neuronal tissue with genetically encoded indicators. *Elife* **6**, (2017).
40. Jusyte, M. *et al.* Unc13A dynamically stabilizes vesicle priming at synaptic release sites for short-term facilitation and homeostatic potentiation. *Cell Rep* **42**, (2023).
41. Augustin, I., Rosenmund, C., Südhof, T. C. & Brose, N. Munc13-1 is essential for fusion competence of glutamatergic synaptic vesicles. *Nature* **400**, 457–461 (1999).
42. Walter, A. M., Böhme, M. A. & Sigrist, S. J. Vesicle release site organization at synaptic active zones. *Neurosci Res* **127**, 3–13 (2018).
43. Varoqueaux, F. *et al.* Total arrest of spontaneous and evoked synaptic transmission but normal synaptogenesis in the absence of Munc13-mediated vesicle priming. *Proc Natl Acad Sci U S A* **99**, 9037–9042 (2002).
44. Richmond, J. E., Davis, W. S. & Jorgensen, E. M. UNC-13 is required for synaptic vesicle fusion in C. elegans. *Nat Neurosci* **2**, 959–964 (1999).
45. Böhme, M. A. *et al.* Rapid active zone remodeling consolidates presynaptic potentiation. *Nat Commun* **10**, (2019).

46. Böhme, M. A. *et al.* Active zone scaffolds differentially accumulate Unc13 isoforms to tune Ca(2+) channel-vesicle coupling. *Nat Neurosci* **19**, 1311–1320 (2016).
47. Blaum, N. *et al.* Monoamine-induced diacylglycerol signaling rapidly accumulates Unc13 in nanoclusters for fast presynaptic potentiation. *bioRxiv* 2025.01.10.632340 (2025) doi:10.1101/2025.01.10.632340.
48. Fulterer, A. *et al.* Active Zone Scaffold Protein Ratios Tune Functional Diversity across Brain Synapses. *Cell Rep* **23**, 1259–1274 (2018).
49. Dittman, J. S. Unc13: a multifunctional synaptic marvel. *Curr Opin Neurobiol* **57**, 17–25 (2019).
50. Michelassi, F., Liu, H., Hu, Z. & Dittman, J. S. A C1-C2 Module in Munc13 Inhibits Calcium-Dependent Neurotransmitter Release. *Neuron* **95**, 577-590.e5 (2017).
51. Taschenberger, H., Woehler, A. & Neher, E. Superpriming of synaptic vesicles as a common basis for intersynapse variability and modulation of synaptic strength. *Proc Natl Acad Sci U S A* **113**, E4548–E4557 (2016).
52. Rhee, J. S. *et al.* β phorbol ester- and diacylglycerol-induced augmentation of transmitter release is mediated by Munc13s and not by PKCs. *Cell* **108**, 121–133 (2002).
53. Betz, A. *et al.* Munc13-1 is a presynaptic phorbol ester receptor that enhances neurotransmitter release. *Neuron* **21**, 123–136 (1998).
54. Basu, J., Betz, A., Brose, N. & Rosenmund, C. Munc13-1 C1 domain activation lowers the energy barrier for synaptic vesicle fusion. *J Neurosci* **27**, 1200–1210 (2007).
55. Root, C. M. *et al.* A presynaptic gain control mechanism fine-tunes olfactory behavior. *Neuron* **59**, 311–321 (2008).
56. Qiu, Y. *et al.* Natural environment statistics in the upper and lower visual field are reflected in mouse retinal specializations. *Current Biology* **31**, 3233-3247.e6 (2021).
57. Ramirez, L. & Dickman, R. Data-Driven Models of Efficient Chromatic Coding in the Outer Retina. *eNeuro* **9**, (2022).
58. Olshausen, B. A. & Field, D. J. Emergence of simple-cell receptive field properties by learning a sparse code for natural images. *Nature* **381**, 607–609 (1996).
59. Ganguli, D. & Simoncelli, E. P. Efficient sensory encoding and Bayesian inference with heterogeneous neural populations. *Neural Comput* **26**, 2103–2134 (2014).
60. Keller, A. & Vosshall, L. B. Influence of odorant receptor repertoire on odor perception in humans and fruit flies. *Proc Natl Acad Sci U S A* **104**, 5614–5619 (2007).
61. Zwicker, D., Murugan, A. & Brenner, M. P. Receptor arrays optimized for natural odor statistics. *Proc Natl Acad Sci U S A* **113**, 5570–5575 (2016).
62. Tesileanu, T., Cocco, S., Monasson, R. & Balasubramanian, V. Adaptation of olfactory receptor abundances for efficient coding. *Elife* **8**, (2019).
63. Cognigni, P., Felsenberg, J. & Waddell, S. Do the right thing: neural network mechanisms of memory formation, expression and update in Drosophila. *Curr Opin Neurobiol* **49**, 51–58 (2017).
64. Ling, D., Zhang, L., Saha, D., Chen, A. B. & Raman, B. Adaptation invariant concentration discrimination in an insect olfactory system. *Elife* **12**, (2023).
65. Gomez-Marin, A., Stephens, G. J. & Louis, M. Active sampling and decision making in Drosophila chemotaxis. *Nature Communications 2011 2:1* **2**, 1–10 (2011).
66. Gepner, R., Skanata, M. M., Bernat, N. M., Kaplow, M. & Gershow, M. Computations underlying Drosophila photo- taxis, odor-taxis, and multi-sensory integration. *Elife* **4**, (2015).
67. Vickers, N. J. Mechanisms of animal navigation in odor plumes. *https://doi.org/10.2307/1542524* **198**, 203–212 (2000).
68. Murlis, J., Elkinton, J. S. & Cardé, R. T. Odor plumes and how insects use them. *Annu Rev Entomol* **37**, 505–532 (1992).

69. Kadakia, N. *et al.* Odour motion sensing enhances navigation of complex plumes. *Nature 2022 611:7937* **611**, 754–761 (2022).
70. Dolan, M. J. *et al.* Neurogenetic dissection of the drosophila lateral horn reveals major outputs, diverse behavioural functions, and interactions with the mushroom body. *Elife* **8**, (2019).
71. Frechter, S. *et al.* Functional and anatomical specificity in a higher olfactory centre. *Elife* (2019) doi:10.7554/eLife.44590.
72. Taisz, I. *et al.* Generating parallel representations of position and identity in the olfactory system. *Cell* **186**, 2556-2573.e22 (2023).
73. Kim, H. S., Santana, G. M., Sancer, G., Emonet, T. & Jeanne, J. M. Divergent synaptic dynamics originate parallel pathways for computation and behavior in an olfactory circuit. *Current Biology* **35**, 3146-3162.e8 (2025).
74. Álvarez-Salvado, E. *et al.* Elementary sensory-motor transformations underlying olfactory navigation in walking fruit-flies. *Elife* **7**, e37815 (2018).
75. Murmu, M. S., Stinnakre, J. & Martin, J. R. Presynaptic Ca2+ stores contribute to odor-induced responses in Drosophila olfactory receptor neurons. *Journal of Experimental Biology* (2010) doi:10.1242/jeb.046474.
76. Murmu, M. S., Stinnakre, J., Réal, E. & Martin, J. R. Calcium-stores mediate adaptation in axon terminals of Olfactory Receptor Neurons in Drosophila. *BMC Neurosci* (2011) doi:10.1186/1471-2202-12-105.
77. Silva, M., Tran, V. & Marty, A. Calcium-dependent docking of synaptic vesicles. *Trends Neurosci* **44**, 579–592 (2021).
78. Rozenfeld, E., Ehmann, N., Manoim, J. E., Kittel, R. J. & Parnas, M. Homeostatic synaptic plasticity rescues neural coding reliability. *Nature Communications 2023 14:1* **14**, 1–14 (2023).
79. Ramirez, L. Trade-off between coding efficiency and color space in outer retinal circuits with colored oil droplets. *Vision Res* **208**, (2023).
80. Baden, T. The vertebrate retina: a window into the evolution of computation in the brain. *Curr Opin Behav Sci* **57**, (2024).
81. Wang, X., Roberts, P. A., Yoshimatsu, T., Lagnado, L. & Baden, T. Amacrine cells differentially balance zebrafish color circuits in the central and peripheral retina. *Cell Rep* **42**, 112055 (2023).
82. Brand, P. *et al.* The origin of the odorant receptor gene family in insects. *Elife* **7**, (2018).
83. Ruta, V. *et al.* A dimorphic pheromone circuit in Drosophila from sensory input to descending output. *Nature* **468**, 686–690 (2010).
84. Stensmyr, M. C. *et al.* A conserved dedicated olfactory circuit for detecting harmful microbes in drosophila. *Cell* **151**, 1345–1357 (2012).
85. Kondo, S. & Ueda, R. Highly improved gene targeting by germline-specific Cas9 expression in Drosophila. *Genetics* **195**, 715–721 (2013).
86. Nagel, K. I., Hong, E. J. & Wilson, R. I. Synaptic and circuit mechanisms promoting broadband transmission of olfactory stimulus dynamics. *Nature Publishing Group* **18**, 56–65 (2015).
87. Chou, Y. H. *et al.* Diversity and wiring variability of olfactory local interneurons in the Drosophila antennal lobe. *Nat Neurosci* (2010) doi:10.1038/nn.2489.

Supplementary Material

Table S1: Key resources

Reagent or Resource	Source	Identifier
Chemicals		
Methyl acetate	Sigma-Aldrich Co	Art. #45999, CAS 79-20-9
2-butanone	Carl Roth	Art. #T920.1, CAS 78-93-3
Mineral Oil	Sigma-Aldrich Co	Art. #330779, CAS 8042-47-5
CGP 54626 hydrochloride	Tocris Bioscience	Art. #1088, CAS 149184-21-4
Picrotoxin	Sigma-Aldrich Co	Art. #P1675, CAS 124-87-8
Atropine	Sigma-Aldrich Co	Art. #A0132, CAS 51-55-8
Tubocurarine	Sigma-Aldrich Co	Art. #T2379, CAS 6989-98-6
Imidacloprid	Sigma-Aldrich Co	Art. #37894, CAS 138261-41-3
All trans retinal	Sigma-Aldrich Co	Art. #R2500, CAS 116-31-4
Bondic cartridge with Bondic liquid plastic	Bondic	Art. #BONKART
Bondic UV-LED	Bondic	Art. #BONLED
Experimental Models: Organisms/Strains		
D. melanogaster: or42b-Gal4	Bloomington Drosophila Stock Center (BDSC)	RRID: BDSC_9972
D. melanogaster: or10a-Gal4	BDSC	RRID: BSDC_9944
D. melanogaster: GH146-Gal4	Gift from A. Fiala	Gift from A. Fiala
D. melanogaster: orco-Gal4	BDSC	RRID: BSDC_23292
D. melanogaster: UAS-GCaMP6f	BDSC	RRID: BSDC_42747
D. melanogaster: UAS-CsChrimson	BDSC	RRID: BSDC_82181
D. melanogaster: UAS- shibire^{ts}	Gift from M. Silies	
D. melanogaster: UAS-ASAP2s	Gift from T. Clandinin	
D. melanogaster: lexAop-GCaMP6f	BDSC	RRID: BSDC_44277
D. melanogaster: orco-LexA	Gift from H. Scholz	
Software and algorithms		
Fiji		RRID: SCR_002285
MATLAB	MathWorks	RRID: SCR_001622
Adobe Illustrator	Adobe	RRID: SCR_010279

Table S2: Genetic *D. melanogaster* strains

Name	Genotype	Figure
GH146 > GCaMP6f	*w-; GH146-Gal4/UAS-GCaMP6f ; +*	6a-c, 6e, S4a-c
GH146 > ASAP2s	*w+/w-; GH146-Gal4/UAS-ASAP2s ; +*	6d, S4d,e
or42b > GCaMP6f, csChrimson	*w+/w-; UAS-GCaMP6f/UAS-CsChrimson; or42b-Gal4/+*	3b-d
or42b > GCaMP6f, shibire^{ts}	*w+/w-; UAS-GCaMP6f/+; or42b-Gal4/UAS-shibire^{ts}*	4a-f
or42b > GCaMP6f (control)	*w+/w-; UAS-GCaMP6f/+; or42b-Gal4/+*	4a-f
or10a > GCaMP6f, shibire^{ts}	*w-; or10a-Gal4/UAS-GCaMP6f; UAS-shibire^{ts}/+*	S1a-d
or10a > GCaMP6f (control)	*w-; or10a-Gal4/UAS-GCaMP6f; +*	S1a-d
GH146 >shibire^{ts}; orco > GCaMP6f	*w-; GH146-Gal4/lexAop-GCaMP6f ; orco-LexA/UAS-shi[ts]*	S1e-f
GH146; orco > GCaMP6f (control)	*w-; GH146-Gal/lexAop-GCaMP6f ; orco-LexA/TM2*	S1e-f
orco > GCaMP6f	*w+/w-; UAS-GCaMP6f/+; orco-GAL4/+*	4g-n, 7b, S2
GH146 > GCaMP6f	*w-; GH146-Gal4/UAS-GCaMP6f ; +*	7c
GH146 > GCaMP6f; Unc13H1723K	*w-; GH146-Gal4/UAS-GCaMP6f ; +; Unc13H1723K*	7d

Table S3: Airflow dilutions for odor

C= test stimulus B = background	Odor airflow (sccm)	Equivalent dilution
C4/B4	0.03	$10^{-4.5}$
C5/B5	0.10	10^{-4}
C6/B6	0.30	$10^{-3.5}$
C7/B7	1	10^{-3}
C8/B8	3	$10^{-2.5}$
C9/B9	10	10^{-2}

Supplementary Figures

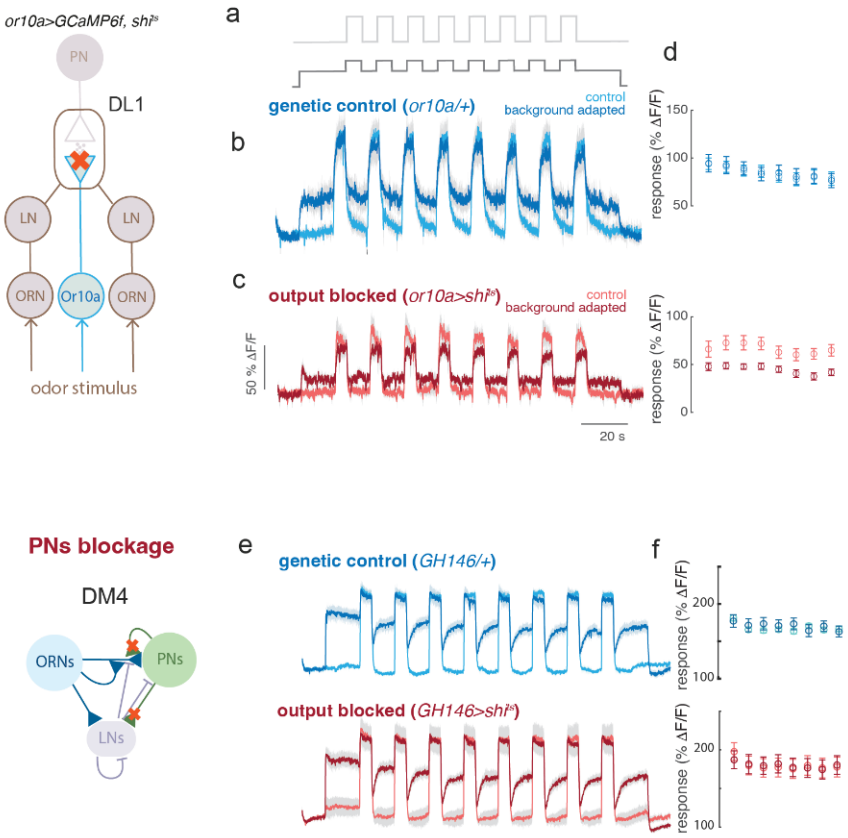

Figure S1: Role of synaptic release for ORN background invariance.
a) Genetic blockage of Or10a-ORNs neurotransmitter release. Stimulation protocol in control (light gray) and background adapted conditions (dark gray). **b)** Calcium response of the DL1 glomerulus in genetic control flies showing background-invariant responses. **c)** Calcium response in flies with blocked ORN synapses showing background dependent responses. **d)** Quantification of peak response for each of the 8 test pulses. Error bars indicate sem (N=4, 7).
e) Blocking of PN synaptic output does not affect ORN presynaptic calcium responses. Traces represent mean calcium responses of DM4 ORNs in control (light colors) and background adapted conditions (dark colors) for control (blue) and test flies (red). Test flies express shi^{ts} under control of GH146-GAL4 that labels PNs. **f)** Quantification of peak response for each of the 8 test pulses. Error bars indicate sem.

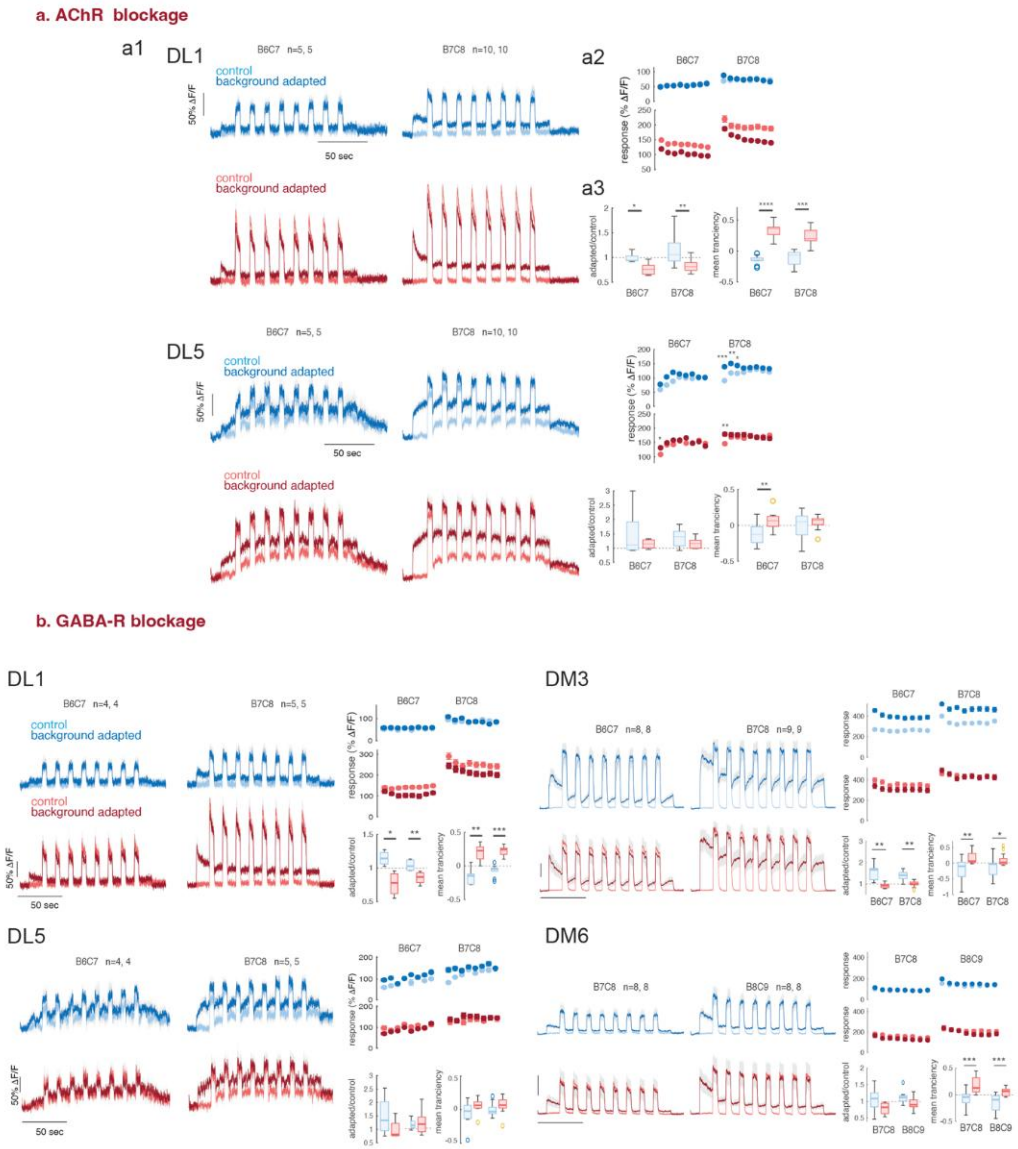

Figure S2: Glomerulus specific mechanisms for presynaptic calcium modulation.
a) Pharmacological blockage of AchRs (100 µM atropine + 20 µM tubocurarine + 200 nM imi, see Methods). **a1)** Traces represents mean calcium responses of DL1 ORNs in control (light colors) and background adapted conditions (dark colors) before (blue) and after (red) drug application. **a2)** Quantification of peak response for each of the 8 test pulses. Error bars indicate SEM but might not be visible. **a3)** Boxplot quantification of the degree of adaptation and response transiency, indicating median, quartiles max/min and outliers. Same organization for glomerulus DL5.
b) Pharmacological blockage of GABA receptors (25 µM CGP54626 + 5 µM picrotoxin, see Methods) in 4 glomeruli. Same organization of the plots as in **a)**. 2-butanone was used for DL1 and DL5 and butyl acetate for DM3 (10^{-2} liquid dilution in PO) and DM6 (10^{-3} liquid dilution in PO). *p<0.05, **p<0.01, ***p<0.001. Sample size is indicated for each dataset in the figure.

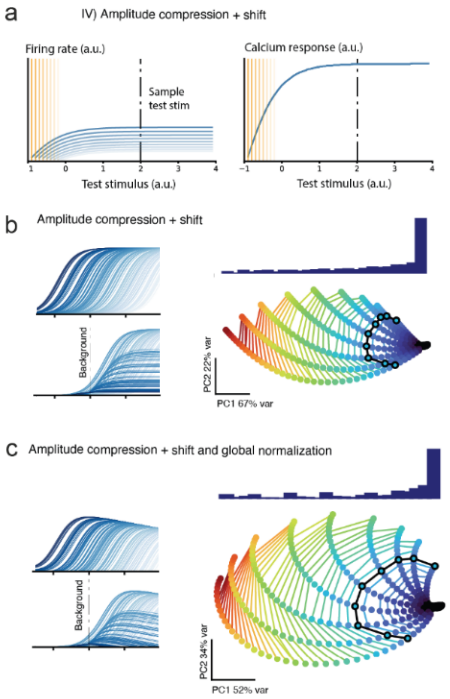

Figure S3: Population of ORNs with divisive normalization. a) Firing rate and calcium response for an adaptive function combining amplitude-compression and amplitude-shift as predicted by a model of background compensation and response normalization (Appendix 1). As in Fig. 5, Orange lines indicate the value of the adaptive background stimulus. Curves with different shades of red/blue correspond to different adapted conditions. Dotted lines indicate a representative test stimulus. **b)** 2D-manifold of the ORN population response to stimuli of different ON (color coded) and OFF (black) contrast in different background adapted conditions. The histogram represents the distribution of population states calculated on the first principal component. Same as plots b) and e) in Fig. 8 but now for the combined amplitude adaptation mechanism.

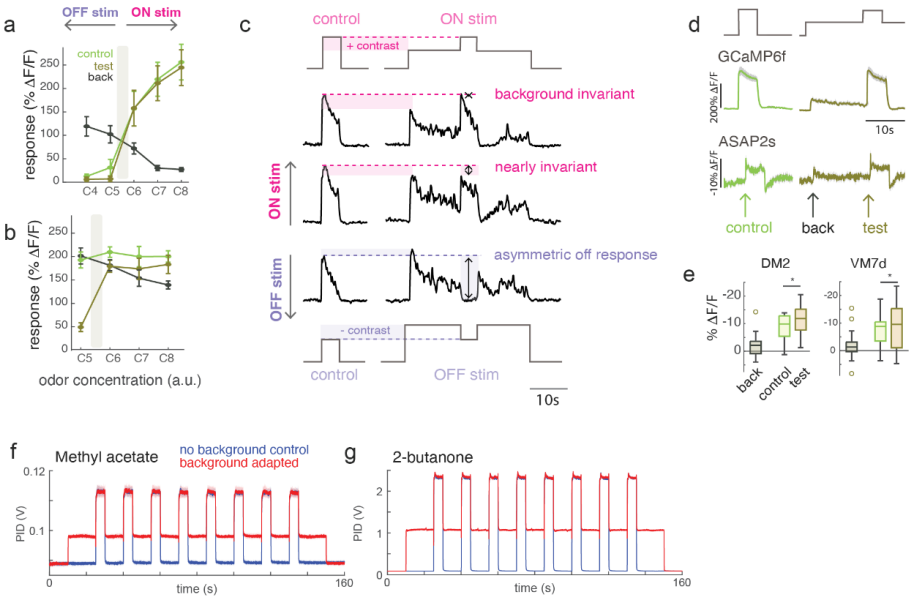

Figure S4: PNs response to ON and OFF stimuli. To cover a range of ON and OFF responses of PNs, we conducted two sets of experiments using different liquid solutions of the odors. To generate main **Fig. 6c** we analyzed the single trials of these two datasets. Here we show mean responses (**a, b**) and some examples of response to small contrast stimuli (**c**).

a-b) Peak calcium response to different combinations of ON, OFF and background stimuli using methyl acetate. *Green*: mean response to non-adapted control. *Black*: mean response to background stimulus. *Dark green*: mean response to the same stimulus as in green after 15 seconds of background adaptation. Error bars indicate SEM, the shaded area indicated the stimulus that equals the background concentration. Liquid dilution of methyl acetate for the background was 10^{-4} in **a)** and 10^{-3} in **b)**, therefore the higher background response in **b)**. The liquid dilution for the pulse was 10^{-2} in **a)** and 10^{-3} in **b)**. Labels on the x-axis corresponds to gas phase dilutions generated by the odor delivery system as indicated in **table S3**.

c) Three single trials from the dataset showing responses to ON and OFF stimuli with small contrast. The shaded area indicates the difference in response between test and background stimulus. The dotted line indicates the response to the control stimulus. These traces show how a small positive contrast leads to nearly perfectly invariant response (same as controls), while a small negative contrast leads to a strong decrease in calcium, much lower than the test stimulus amplitude. **d)** Control and background adapted response measure in DM2 using either a calcium or voltage sensor. Thick lines indicate the mean ΔF/F and the shaded areas sem. Liquid dilution of methyl acetate is 10^{-4} for the background and 10^{-2} for the pulse. **e)** Boxplot representing median, quartiles, min/max values and outliers of ASAP2s signals from two glomeruli. (DM2 N=19, VM7d N=23, *p<0.05, Kruskal-Wallis).

f) Average PID response to methyl acetate using a liquid dilution of 10^{-2} and background airflow dilution of C6 and pulse C7 (N=4) with stimulation protocol in control (blue) and background adapted conditions (red). **g)** Same as d) for pure 2-butanone with a background airflow dilution of C7 and pulse C8 (N=4).

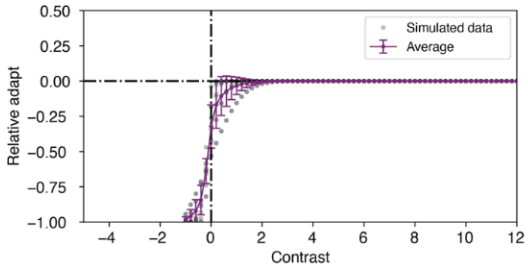

Figure S5: Modeling PNs relative adaptation for different contrast stimuli. We model the responses of PN neurons in a background adapted condition as a noisy process with probability $\mathrm{N}(s - s_B, \sigma)$, where s_B is the background stimulus and σ is the noise std. We simulate PN responses across different contrast stimuli and show that a standard deviation of $\sigma = 0.5$ fits the experimental observations shown in **Fig. 6c**. For each contrast value, we average the relative adaptation over a set of 10 different background conditions ranging from -4 to 4 in the stimulus log. scale.

Appendix 1

Adaptation model: firing rate and calcium response with divisive normalization

In the main text we have modeled the dynamics of calcium responses in ORNs as a linear function of their firing rate and the inhibitory inputs from LNs (**Fig. 5** and Methods). However, previous work by Olsen et al. [1] has shown that LN inhibition in the AL performs a divisive (rather than linear) transformation from ORNs to PNs firing rates. Therefore, we ask if a divisive model would also be able to support the background compensation. It should be noted that the divisive model was not originally proposed to fit the transformation between ORN firing rate and ORN axonal calcium. Moreover, the model is based on mean responses and does not capture response dynamics nor considers adaptive processes. Nonetheless, in the following we show that also when assuming a divisive effect of LN activity on ORN calcium, background invariance can only be achieved if the firing rate adapts in the amplitude domain, rather than by a shift in sensitivity.

We consider the calcium response of ORNs without odor background to be:

$$R[F(s)] = \frac{F(s)}{F(s) + \sigma} \qquad (s.1)$$

This relationship implies that the effect of inhibition is not linear (as in Eq. 3 of the main text) but dependents on the input stimulus: $\Delta_I = 1/(F(s) + \sigma)$ with σ a constant. Background invariance is achieved if $R[F(s, s_B)] = R[F(s)] = R[F(s_B)] + R[F'(s)]$ (Eq. 4 of main text). Using Eq. (s.1), we obtain:

$$\frac{F'(s)}{L(F'(s))} = \frac{F(s)}{F(s) + \sigma} - \frac{F(s_B)}{F(s_B) + \sigma} \qquad (s.2)$$

where we assume a general form of the normalization factor $L(F'(s))$ in adapted conditions. For equation s.2 to hold, it is required both that:

$$F'(s) = \sigma \cdot (F(s) - F(s_B))$$

and, using s.3 in s.2, that:

$$L\big(F'(s)\big) = A \cdot F'(s) + \sigma'$$

with $A = \frac{F(S_B)+\sigma}{\sigma}$ and $\sigma' = (F(s_B) + \sigma)^2$. Eq. (s.3) indicates that to achieve background invariance the adapted firing rate should be a combination of an amplitude compression (first term) and an amplitude shift (second term), as we obtained in the case of the dynamic linear model (Eq. 7, 8 in main text). In addition, Eq. (s.4) indicates that background invariance with divisive normalization requires adaptation of the LN feedback and therefore a background dependent normalization term. Specifically, in adapted conditions the normalization factor is still linear but a stronger effect ($A > 1$ *and* $\sigma' > \sigma$)

Including Eq. (1) into Eq. (s.4), we find the update rules,

$$\begin{aligned} \beta' &= \beta \\ \alpha' &= \alpha\big[1 + R_{Ca}[F(s_B)]\big] \\ \gamma' &= \gamma + \frac{\sigma R_{Ca}[F(s_B)]}{\alpha(1 + R_{Ca}[F(s_B)])} \end{aligned} \qquad (s.5)$$

This shows that the combined adaptation mechanism depends uniquely on the background adaptation response in both ORNs and LNs. Furthermore, it satisfies the calcium invariant condition. As done for the main dynamic model, we studied the consequences of this combined adaptation mechanism for single ORNs and for the population responses. We show that background invariance is indeed preserved for all test odors similarly to the ORNs implementing an amplitude-based adaptation (**Fig. S3a**). Regarding the encoding of ORNs at the population level, we performed the same analysis shown in Fig. 8, and show that the combination of both amplitude -shift and -compression mechanisms also preserve information about input contrast and lead to ON-background invariant responses in populations of PN neurons (**Fig. S3b**).

1. Olsen, S. R., Bhandawat, V. & Wilson, R. I. Divisive normalization in olfactory population codes. *Neuron* 66, 287–299 (2010).

4.3 Impact of developmental temperature on neural growth, connectivity, and function

This manuscript is published in Science Advances (January 2025) and is available under the DOI: https://doi.org/10.1126/sciadv.adp9587 (Züfle et al., 2025).

I performed the imaging experiments and data visualization for figure 4C,D. I also helped to review and edit the manuscript.

SCIENCE ADVANCES | RESEARCH ARTICLE

DEVELOPMENTAL NEUROSCIENCE

Impact of developmental temperature on neural growth, connectivity, and function

Pascal Züfle[1]†, Leticia L. Batista[1]†, Sofia C. Brandão[1], Giovanni D'Uva[1], Christian Daniel[1], Carlotta Martelli[1,2]*

Environmental temperature dictates the developmental pace of poikilothermic animals. In *Drosophila*, slower development at lower temperatures results in higher brain connectivity, but the generality of such scaling across temperatures and brain regions and its impact on function are unclear. Here, we show that brain connectivity scales continuously across temperatures, in agreement with a first-principle model that postulates different metabolic constraints for the growth of the brain and the organism. The model predicts brain wiring under temperature cycles and the nonuniform temporal scaling of neural development across temperatures. Developmental temperature has notable effects on odor-driven behavior. Dissecting the circuit architecture and function of neurons in the olfactory pathway, we demonstrate that developmental temperature does not alter odor encoding in first- and second-order neurons, but it shifts the specificity of connections onto third-order neurons that mediate innate behaviors. We conclude that while some circuit computations are robust to the effects of developmental temperature on wiring, others exhibit phenotypic plasticity with possible adaptive advantages.

INTRODUCTION

The wiring of the nervous system follows a complex genetic plan during development. However, because of stochastic processes and environmental factors, genetically identical individuals seldomly show the same phenotypic outcome (*1*). Temperature is the environmental factor with the broadest effects in biology, as it determines the rates of all biophysical reactions of an organism (*2*). In poikilothermic animals, such as insects, worms, fish, amphibians, and reptiles, temperature determines the speed of development. Mathematical theories of growth have shown that developmental times scale exponentially with temperature because of a constraint imposed by the rate-limiting metabolic reaction (*3*). The development of the nervous system is certainly not exempted by the effects of temperature.

It has been widely reported that development at different temperatures correlates with variation in behavioral phenotypes with examples in amphibians (*4*), reptiles (*5*–*7*), bees (*8*, *9*), ants (*10*), and fruit flies (*11*, *12*). Social insects invest a lot of resources to keep their broods at the correct temperature throughout daily and seasonal cycles. Even small variations in developmental temperature can affect learning in bees (*13*) and the synaptic organization of key brain areas for learning (*12*, *14*, *15*). Therefore, temperature does not just determine the speed, but also the outcome of development, although the mechanistic bases of this phenotypic variation are largely unknown.

A recent study in *Drosophila* reported that the number of synaptic connections between neurons of the visual system inversely correlate to temperature, i.e., when flies develop at lower temperature, these neurons make more synapses and have more postsynaptic partners (*16*). This leads to the questions of whether synaptic scaling occurs similarly throughout the brain and what consequences it has on neural computations and behavior. Answering these questions is key not only to predict the consequences of temperature changes on animal behavior in the wild, but also to fully understand the organization of development in poikilothermic animals.

Here, we investigate how developmental temperature affects the wiring and function of the fly olfactory circuit. We show that development at lower temperatures leads to higher connectivity at all stages of olfactory processing and changes the neural composition of local circuits. To explain these findings, we develop a first-principle theory that postulates the existence of different metabolic constraints for the growth of the whole animal and the brain. This theoretical framework explains changes in connectivity associated with different developmental conditions and predicts the nonuniform temporal scaling of neural growth across temperatures. Temperature manipulation during pupal development affects odor approach behavior, even when flies are adapted for 10 days at a common temperature. By measuring odor responses in first- and second-order olfactory neurons, we conclude that the behavioral differences cannot be attributed to a change in odor representations or sensitivity, which are robust to developmental temperature. Instead, we provide evidence that these odor representations are processed differently in downstream circuits that drive innate behaviors. Our results therefore indicate that the effect of developmental temperature on neural circuit function is not due to a general scaling in connectivity, but to a change in connection specificity across brain regions.

RESULTS

Impact of developmental temperature on the connectivity of an olfactory glomerulus

To investigate the effects of temperature on the development of similar, but functionally distinct neural circuits, we focus on the olfactory system of *Drosophila*. Olfaction mediates key behaviors in animals, including foraging and mating, plays a major role in the organization of animal societies, and supports adaptation to the environment. We set out to investigate the effect of developmental temperature on the wiring of olfactory receptor neurons (ORNs) within the antennal lobe (AL), the main olfactory area in the insect brain. We used trans-Tango (*17*), a genetic tool for trans-synaptic labeling, to analyze postsynaptic

[1]Johannes Gutenberg University, Mainz, Germany. [2]Institute for Quantitative and Computational Biosciences, Mainz, Germany.
*Corresponding author. Email: cmartell@uni-mainz.de
†These authors contributed equally to this work.

neurons of *Or42b*-ORNs, i.e., ORNs that express the odorant receptor *Or42b* and target the glomerulus DM1 (Fig. 1A). Flies were developed at either 18° or 25°C between the larval stage L3 and the end of pupal development (which we name P-100%, because the absolute developmental time depends on temperature). Flies were then kept at 25°C for 10 days before dissection, to minimize acute effects of temperature on brain wiring and transgene expression. Notably more postsynaptic neurons were labeled in flies that developed at 18°C, as suggested by denser innervations in both the AL and downstream areas (Fig. 1, B and C). We quantified these differences by counting the cell bodies of the postsynaptic cells in each fly, which were more than double at 18°C as compared to 25°C (Fig. 1D).

To demonstrate that the anatomically labeled postsynaptic neurons are functionally connected to the ORNs, we modified the *trans*-Tango experiment to express a calcium reporter (GCaMP6s) in the postsynaptic neurons, and CsChrimson in *Or42b*-ORNs (Fig. 1E).

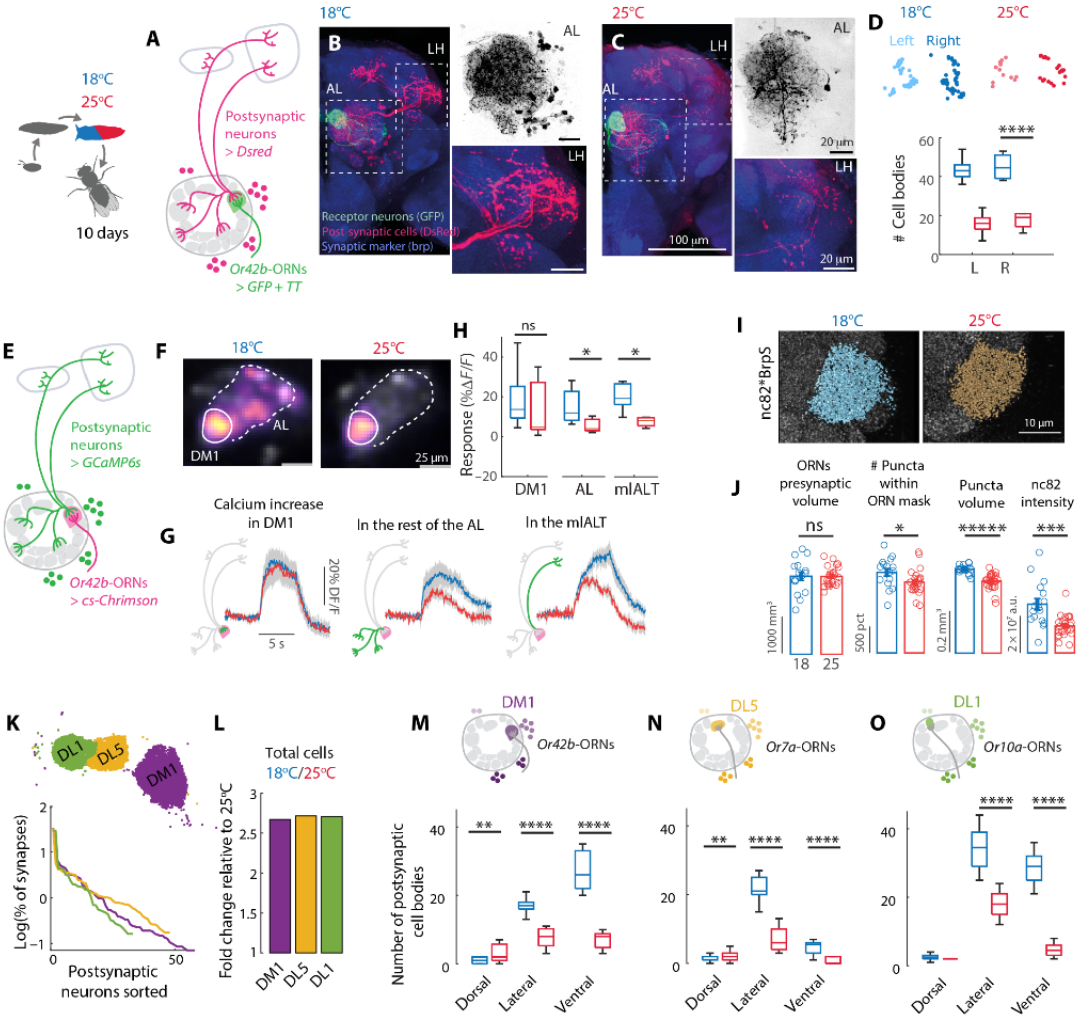

Fig. 1. Developmental temperature affects the connectivity of ORNs in the AL. (**A**) Schematics of the *trans*-Tango tool. (**B** and **C**) Example brains from flies developed at 18° and 25°C. Immunostaining labels ORNs that express green fluorescent protein (GFP, green), postsynaptic partners expressing dsRed (red), and all synapses (Brp, blue). (**D**) Cell body locations of postsynaptic partners in left (L) and right (R) hemispheres in two individual flies and corresponding boxplot, Kruskal-Wallis, $P < 10^{-7}$, $n = 10$ (18°C) and 10 (25°C). (**E**) Schematics of the experiment: The usual *trans*-Tango reporter dsRed was replaced by GCaMP6s, and activity of presynaptic neurons was induced by CsChrimson. (**F**) Example responses for flies developed at different temperatures. Color bar indicates $\Delta F/F$ calculated for each pixel. White lines indicate the region of interests used for quantification. (**G**) Optogenetic response to 0.05 mW/mm^2 quantified in the DM1 glomerulus, in the rest of the AL and in the mlALT. (**H**) Boxplot quantifies the response in 9 s following stimulus onset. Significant differences were observed in the AL [Kruskal-Wallis, $P = 0.02$, $n = 4$ (18°C), and 7 (25°C)] and in the mlALT [$P = 0.01$, $n = 4$ (18°C), and n = 7 (25°C)]. (**I**) Anti-Brp staining of synaptic puncta and 3D reconstruction within the ORN mask created from Brp^{Short}-GFP fluorescence. (**J**) Volume of the Brp^{Short}-mask, number of puncta, puncta volume, and intensity within the ORN mask (error bars indicate SEM, $n = 16$ hemibrains at 18°C and $n = 25$ at 25°C, Kruskal-Wallis test). (**K**) Allocation of ORN output synapses onto individual partners for the three glomeruli, as quantified from electron microscopy (EM) data (see Materials and Methods). Top: Spatial location of the synapses analyzed. (**L**) Fold change in number of synaptic partners relative to 25°C. (**M** to **O**) Number of synaptic partners labeled by trans-Tango in different cell clusters of the AL. Sample size at 18° and 25°C: DM1 $n = 20$ and 23, DL5 $n = 10$ and 10, DL1 $n = 10$ and 10, Kruskal-Wallis. $*P < 0.05$, $**P < 10^{-2}$, $***P < 10^{-3}$, $*****P < 10^{-5}$. Boxplots indicate median and quartiles, and whiskers indicate maximum and minimum values.

This allowed us to optogenetically activate *Or42b*-ORNs and measure the response of their postsynaptic partners. Optogenetic activation of ORNs is sufficient to induce postsynaptic responses in a dose-dependent manner (fig. S1A). We then measured calcium signals in the *trans*-Tango experiment upon optogenetic activation of the ORNs. Calcium transients measured within the DM1 glomerulus mostly report activity from the single uniglomerular projection neuron (uPN, which receives most of the ORN synapses) and do not differ between the two temperatures (Fig. 1G and fig. S1A). However, activation in the rest of the AL is higher in flies developed at 18°C (Fig. 1, F to H), which is consistent with a larger number of multiglomerular neurons being connected to DM1. Moreover, activity is stronger in the mediolateral AL track (mlALT; Fig. 1, G and H) through which a class of multiglomerular inhibitory PNs (vPNs) project their axons to the lateral horn (LH). Therefore, the *trans*-Tango labeled neurons are functionally connected to *Or42b*-ORNs; moreover, ORNs drive more activity in flies developed at 18°C, which is consistent with the recruitment of new synaptic partners compared to higher temperatures.

The observed phenotypes are unlikely caused by the effect of temperature on the expression strength of the UAS-GAL4 system, as higher temperature should increase (and not decrease) the activity of this yeast-derived expression system (*18*). This was also confirmed by a quantification of the expression of the *trans*-Tango components [figure S3 in (*17*)]. Although we cannot exclude that other aspects of this tool might be temperature dependent, these effects should be minimized by our protocol because we have kept adult flies at a reference temperature of 25°C for 10 days before dissection. Furthermore, we show that the differences between temperatures are consistent across ages (fig. S1B) and that *trans*-Tango can potentially even report a decrease in connectivity induced by antennal clipping (fig. S1C), together arguing that this is a suitable tool to track changes in connectivity related to developmental temperature.

Higher connection at lower temperatures could result from either a different distribution of synapses across postsynaptic partners, an increase in synapse number, or both. To quantify the number of synapses, we expressed a green fluorescent protein (GFP)–tagged Brp^{Short} in *Or42b*-ORNs to label presynapses specifically in these cells and stained the endogenous Brp to count synaptic puncta (*19*) (nc82; Fig. 1I). The *Or42b*-ORNs presynaptic volume defined by the Brp^{Short} signal was consistent across the two developmental temperatures, indicating no change in the glomerulus volume (Fig. 1J). However, flies developed at 18°C had higher Brp^{Short} intensity, an increased number of nc82-labeled Brp puncta within the presynaptic volume, larger puncta volumes, and stronger intensity (Fig. 1J). A similar increase was observed when considering the whole volume of the DM1 glomerulus, which includes connections between other neuron types (fig. S1D). Together, these results demonstrate that a lower developmental temperature leads both to more synapses, larger active zones, and more synaptic partners which are functionally connected to the ORNs.

Temperature-induced wiring differences across olfactory glomeruli

We asked whether developmental temperature scales connectivity similarly across glomeruli. *Trans*-Tango likely reports synaptic partners with synapse counts above a certain threshold. We used the hemibrain connectome data (*20*, *21*) from flies developed at 25°C to quantify the number of synapses per synaptic partner in *Or42b*-ORNs (fig. S1E). Comparing this with the number of postsynaptic neurons reported by *trans*-Tango at 25°C, we estimated that *trans*-Tango reports connected neurons with more than 10 synapses (total across ORNs of the same type; fig. S1E). Development at 18°C likely increases connectivity with available partners, which perhaps are already connected with few synapses at 25°C (fig. S1E). To test this hypothesis, we considered two additional ORN types (expressing *Or7a* and *Or10a*) that, based on connectome data, distribute similarly their synapses onto synaptic partners (Fig. 1K). We reasoned that the same fold change in synaptic partners should be expected for these ORN types if lower temperature shifted the overall connectivity up. Consistently, the fold change in postsynaptic partners between 18° and 25°C was remarkably similar for the three glomeruli (Fig. 1L).

We next looked at the identity of the postsynaptic partners of these ORNs. We hypothesized that, despite a similar scaling of connectivity, the identity of synaptic partners recruited by these different ORNs should depend on available neurons in the relevant glomerulus volume. AL neurons postsynaptic to ORNs have their cell bodies distributed in four clusters (*22*). We used cell body location as a proxy for cell type. On the basis of *trans*-Tango experiments, there were more neurons postsynaptic to *Or42b*-ORNs in the ventral and ventrolateral clusters (Fig. 1M) that host cell bodies of 66.6% of all multiglomerular PNs (mPNs) (*23*) including vPNs (*24*–*27*). This suggests that *Or42b*-ORNs might drive more activity in this population of neurons when flies develop at 18°C as compared to 25°C. This anatomical finding is consistent with increased calcium activity in the mlALT, which is used by these neurons to reach the LH (Fig. 1H). On the contrary, in glomeruli DL5 and DL1, ORNs increase connectivity more prominently with neurons of the lateral cluster (Fig. 1, N and O) that contains a large population of LNs, and mPNs mostly of unknown function (*28*). An analysis of the connectome data confirms that more mPNs innervate the DM1 glomerulus than the DL1 or DL5 glomeruli, where we instead find a larger percentage of LNs, which are mostly inhibitory (S1F). These findings suggest different functional consequences of developmental temperature in different glomeruli. In general, we predict a stronger recruitment of local inhibition in all glomeruli at lower temperatures. For the DM1 glomerulus, we predict it might drive activity in more mPNs that send axons to the LH with potential consequences for behavior.

Scaling of brain connectivity across temperatures

Next, we asked whether synaptic connectivity scales continuously across a wider range of temperatures. *Drosophila melanogaster* lives in different climates, with a thermal range between 11° and 31°C (*29*). The extreme conditions are highly stressful, and if persistent, female reproductive success would approach zero (*30*). However, flies were viable when temperature shifts were restricted to pupal development. We first looked at the anatomy of the ORNs axons targeting the DM1 glomerulus in flies developed at 12°C. Compared to 25°C, ORNs grow axonal extensions protruding radially from the glomerulus (Fig. 2, A and B) and innervate a more anterior glomerulus, VA2, that is normally not targeted by this receptor type (Fig. 2, B and C). We used *trans*-Tango to characterize connectivity patterns of *Or42b*-ORNs and its postsynaptic partners in flies that developed at extreme temperatures (12 to 31°C). In flies developed at 12°C, ORNs established a larger number of synaptic partners, including neurons that target regions outside the canonical olfactory pathway (Fig. 2, D and F), including neurons that arborize in the saddle (details and controls in fig. S2A). Development at lower

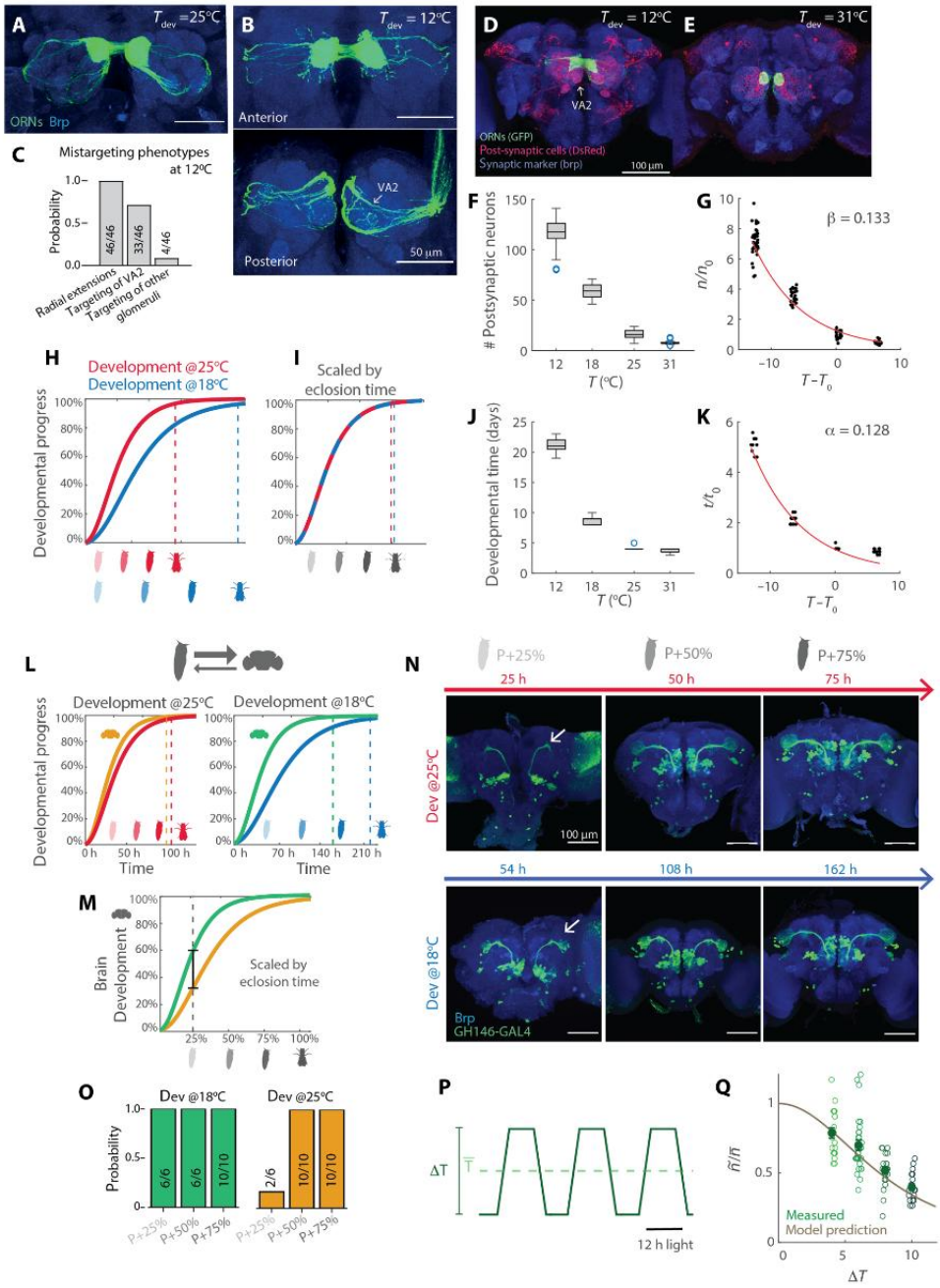

Fig. 2. A first-principle model for network connectivity at different temperatures. (**A** and **B**) *Or42b*-ORN axons labeled by GFP in flies developed at 25° and 12°C. (**C**) Probability of the mistargeting phenotypes at 12°C. Sample size is indicated on the bars. (**D** and **E**) Example brains of flies expressing *trans*-Tango under control of *Or42b-Gal4* developed at 12° or 31°C. (**F**) Boxplot of the number of postsynaptic partners as a function of developmental temperature. (**G**) Single data points as in (F), normalized by the mean number of neurons connected at a reference temperature (25°C) and plotted as a function of the difference from the reference temperature (n = 20 to 38 hemibrains). The line indicates the exponential fit. (**H**) Hypothetical growth curve showing the effects of developmental temperature. (**I**) Same as (H) but normalized by eclosion time. (**J**) Developmental times for the four temperature regimes. (**K**) Fold change in developmental time with respect to the temperature difference from 25°C and exponential fit (n = 8 to 20). (**L**) Schematics of the growth model showing percentage of development as a function of time for the brain and whole animal at two developmental temperatures. Parameters of the growth dynamics are hypothetical. (**M**) Brain growth curved scaled by body developmental time. (**N**) Staining of PNs labeled by *GH146* at three developmental times corresponding to 25, 50, and 75% of ontogenesis at the two temperatures. The arrow indicates the LH. (**O**) Probability that PNs axon terminals innervate the LH (n = 6 to 10 hemibrains). (**P**) Schematics of the temperature and light cycles. (**Q**) Fold change with respect to the mean temperature in the number of synaptic partners for development on temperature cycles of amplitude ΔT (n = 18 to 30 hemibrains). The solid line indicates model prediction (see Materials and Methods).

temperatures therefore leads to the recruitment of new synaptic partners. Flies developed at 31°C instead showed very few neurons connected to *Or42b*-ORNs (Fig. 2, E and F). Across all developmental temperatures tested, the number of ORNs was constant (fig. S2B), but the number of synaptic partners scaled exponentially with temperature (Fig. 2G).

A metabolic theory for brain wiring at different temperatures

To understand this scaling in connectivity, we took a theoretical approach. We started from the observation that temperature determines developmental time, which we define as the time of eclosion of the adult. We assumed that development follows a growth process whose rate depends on temperature, such that the adult ecloses later at lower temperatures (Fig. 2H). In general, one could expect that normalizing time by the adult eclosion should collapse the developmental process at the two temperatures on the same growth curve (Fig. 2I). This would be consistent with the model introduced by Gillooly *et al.* (*3*), which links growth rate to metabolism and temperature. The model postulates that the rate of development scales with temperature proportionally to the Boltzmann factor $e^{-\frac{E}{KT_k}}$ of a hypothetical rate-limiting metabolic reaction (*3*) (E being its activation energy). Assuming that flies eclose at a similar mass across temperatures, developmental time t should scale with the temperature T as $\frac{t}{t_0} = e^{-\frac{E}{KT_a^2}(T-T_0)}$ (see Materials and Methods), where t_0 is the developmental time at a reference temperature T_0 (here $T_0 = 25\,^\circ$C), E is the activation energy of the rate-limiting metabolic reaction, K is the Boltzmann constant, and T_a is the water freezing point (273 K; see Materials and Methods). This model fits our experimental data, with a scaling factor for the developmental time ($\alpha = \frac{E}{KT_a^2}$) equal to 0.128($\pm$0.009) (Fig. 2, J and K), which is in agreement with estimates in other animals (*3*). This simple exponential model fails to fit developmental times at the highest temperatures above 30°C (*31*); nonetheless, we took it as a starting point for our theoretical framework.

We reasoned that if the development of the neural circuit was limited by the same reaction rate as ontogenesis (development of the whole organism), then development should result in the same brain connectivity at all temperatures (Fig. 2I). If, otherwise, the development of the neural system was limited by a reaction with lower activation energy $E' < E$, then it should scale differently compared to body development when temperature changes (Fig. 2L). The neural circuit will therefore develop (extend axons and form synapses) at its own, faster pace, but for an amount of time that is determined by ontogenesis, therefore leading to a larger number of synapses. To calculate the fold change in connectivity, we assumed that axonal growth and synaptogenesis scale with a $^3/_4$ power law: $\frac{dn}{dt} \sim an^{\frac{3}{4}}$ (n indicating a measure of neuronal mass and synapses; see Materials and Methods), as for body mass (*3*). Many biological processes, including growth, scale allometrically with the $^3/_4$ law (*32*, *33*). This phenomenological observation has received a first-principle explanation based on the fractal nature of the distribution of nutrients and resources in a three-dimensional (3D) volume by a space-filling network of branching tubes (*34*, *35*). Given the tree-like structure of axons, along which mitochondria and proteins need to be transported, and of other energy suppliers in the brain (such as trachea and glia), the $^3/_4$ law is a reasonable assumption for the growth of the neural system. From this, we derived an analytical function for the scaling of synaptic connectivity with temperature: $\frac{n}{n_0} = e^{-4\frac{\Delta E}{KT_a^2}(T-T_0)}$ with $\Delta E = E - E'$ (see Materials and Methods). We define $\beta = \frac{4\Delta E}{KT_a^2}$ as the scaling factor for synaptic connectivity. When $\Delta E = 0$, the same number of connections is established across temperatures. This law fits well the exponential change in connectivity in the olfactory circuit (Fig. 2K) with $\beta = 0.133(\pm 0.011)$. From β and, we calculate the activation energy $E' = 0.61$ eV of the rate-limiting metabolic reaction for brain development, which falls in the range of feasible value for the metabolism (*36*). It should be noted that β can, in principle, be different across subcircuits if their development and growth are differently regulated. In the visual system, Kiral *et al.* (*16*) reported a fold change of ~1.5 that corresponds to a smaller value of β compared to what we find in the olfactory system. Whether these differences are technical or biological remains to be determined, but the proposed model could easily accommodate differences across circuits.

Nonuniform scaling of neural growth during development

Our model makes some predictions, which might be counterintuitive. First of all, by normalizing the time axis of the brain growth curves based on eclosion time (ontogenesis; Fig. 2L), the model predicts that the brain is in a more advanced developmental stage at lower as compared to higher temperatures (Fig. 2M). This implies that at proportional times of pupal metamorphosis (P-25%, P-50%, and P-75%), the branching anatomy of a given neuron type is expected to be more advanced in flies developed at 18°C, as compared to 25°C. We experimentally tested this prediction by looking at the advancement of PN development across times and temperatures. Consistent with the model prediction, we found that PN axons already targeted the LH at P-25% when flies developed at 18°C, while these axonal innervations were not yet visible at P-25% in flies developed at 25°C (Fig. 2, N and O), consistent with previous data (*37*). This prediction of the model is independent of the analysis of synaptic partners. Overall, the model and the experimental data agree that developmental temperature induces a nonuniform temporal scaling of neural circuit development as compared to ontogenesis.

Brain wiring under temperature cycles

A second prediction of the model concerns development on diurnal temperature cycles. In more ecologically relevant conditions, an animal does not experience constant temperatures during development. Does development under cycling temperatures result in the same wiring outcome as for flies developed at the mean temperature? We first answered this question using our metabolic model. Integrating the growth equation over temperature cycles (see Materials and Methods), we derived that circuit connectivity scales inversely with the amplitude ΔT of the temperature fluctuations as: $\frac{\tilde{n}}{\bar{n}} = \left[\frac{\cosh(\gamma\Delta T)}{\cosh(\alpha\Delta T)}\right]^4$, where $\tilde{n}$ and $\bar{n}$ are the number of connections for development on temperature cycles and at the mean temperature, and $\gamma = \alpha - \frac{\beta}{4}$ with α and β estimated from the fixed temperature experiments (Fig. 2, G and K). Because $\gamma < \alpha$, fluctuating temperatures should always lead to less connections than at the mean temperature $\overline{T}$. An intuitive explanation of this result is to be found in the fact that the time spent at low and at high temperature does not lead to equal amount of development. Rather, the brain grows more

in the high-temperature phase of the cycle compared to the low temperature phase. Therefore, the outcome is skewed toward the high-temperature phenotype, leading to less connections during cycles compared to the mean temperature. To test this experimentally, we developed flies on ecologically realistic temperature cycles with the same mean temperature but different amplitudes (20° to 28°, 18° to 30°, 16° to 32°, and 14 to 34°C; Fig. 2P). *Trans*-Tango experiments showed that these conditions lead to different connectivity of *Or42b*-ORNs in the AL, which make more synaptic partners when temperature cycles had smaller amplitudes, following the prediction of the theory (Fig. 2Q). Moreover, the temperature experienced after eclosion does not strongly affect connectivity (fig. S2C). We noticed that developmental times, however, seem to deviate from the theory prediction (fig. S2D), probably because the temperature fluctuations reach extreme values up to 34°C (Fig. 2K). Overall, we conclude that temperature-dependent wiring is consistent with a growth model with different rate-limiting metabolic reactions for the development of the whole organisms and for the development of neural circuits, although deviations to this rule might occur at extreme high temperatures.

Impact of developmental temperature on odor-driven behavior

We next asked whether wiring consequences of developmental temperature affect odor-driven behavior. We tested the odor response of individual, 10-day-old flies, tethered to walk on a spherical treadmill (Fig. 3A). On average, a puff of 2-butanone elicited a stronger increase in walking speed in flies developed at 18°C compared to 25°C (Fig. 3B). These odor responses were highly reproducible across repetitions of the stimulus (Fig. 3D, left), although variable across individuals (Fig. 3D, right). Similar results were obtained with vinegar (fig. S3, A to C). Basal walking speed was, on average, lower for flies developed at 25°C (Fig. 3C). In general, we found no correlation between basal speed and response, as slow and fast walking flies could respond equally well to odors (fig. S3B).

To test whether these findings were specific to this assay and to better understand the effect of temperature on walking behavior, we used a "free-walking" arena. We tracked the flies' positions while they explored a large circular arena (40 cm in diameter) hiding an odor source in a random position. At all times, more flies raised at 18°C visited the odor source and spent more time at the odor than flies raised at 25°C (Fig. 3E). The difference in behavior between developmental conditions was maximal in the first 7 min of the assay, when the odor landscape was novel. Similar results were obtained with vinegar (fig. S3, D to F) and for a higher testing temperature of 32°C (fig. S3, G and H).

To separate the effect of developmental temperature on baseline walking speed and odor approach, we analyzed data collected in control experiments with no odor. Because flies move in bouts of activity (Fig. 3F, top trace), we asked whether developmental and test temperatures affect how often the fly is walking (activity level) and/or how fast it walks when it is active (mean speed). To assess this, we plotted the probability of walking speed for all conditions tested (Fig. 3F). The peak at zero represents flies that are not walking. The second peak contains all walking flies and can be fitted by a Gaussian. The mean of the Gaussian indicates how fast flies walk when they are moving (mean speed; Fig. 3H). The amplitude of the Gaussian indicates how often the flies are walking instead of standing still (activity level; Fig. 3G). An increase in testing temperature shifts the Gaussian curve right, to higher walking speed, while an increase in developmental temperature slightly lowers the amplitude of the Gaussian, to lower activity. This means that developmental temperature does not affect walking speed but activity level, two parameters that were confounded in the analysis of the ball assay data (Fig. 3C). We conclude that developing flies at 18°C rather than 25°C does not induce major motor deficits but has a slight influence on the propensity of the flies to walk. Because the activity levels of

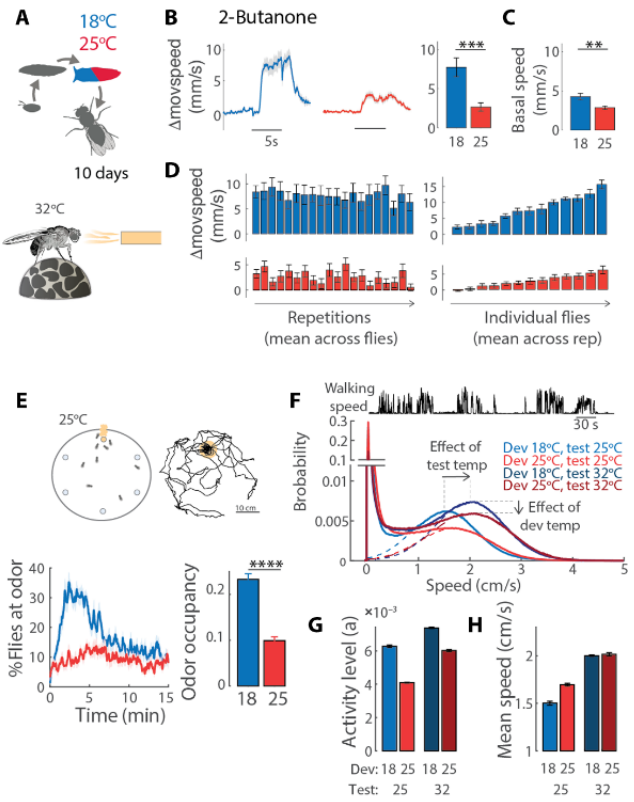

Fig. 3. Developmental temperature affects odor-driven behavior. (**A**) Flies were kept at 25°C for 10 days before behavioral experiments. Odor response was tested at 32°C on a spherical treadmill (see Materials and Methods). (**B**) Odor response was calculated as change in moving speed as a function of time in response to 5-s stimulation (Δmovspeed = speed − basal speed); bar plot, mean change in moving speed within the first 2 s of stimulation [$P < 10^{-3}$, $n = 13$ (18°C) and 13 (25°C)]. (**C**) Basal walking speed is estimated within 3 s before stimulus onset ($P = 0.02$). (**D**) Mean response to each consecutive stimuli repetitions averaged across all flies (right), and mean response of each individual fly across repetitions (left). (**E**) Top: Same protocol as in (A), but odor preference was tested at 25°C in a free walking assay consisting in a circular arena of 40-cm radius with an odor source randomly placed in one of six possible locations. Flies were tracked for 15 min (see Materials and Methods). Bottom: Average percentage of flies at the odor source and odor occupancy (bar plot). Shaded area and error bars indicate SEM [$P < 10^{-6}$, $n = 19$ (18°C) and 20 (25°C)]. (**F**) Top: Example of walking speed for one fly, showing bouts of activity. Bottom: Probability of walking speed calculated from all data (flies and times) at each of four conditions, showing a bimodal distribution with a large peak in zero that represents inactive flies; dotted lines indicate Gaussian fit $ae^{-\left(\frac{x-b}{c}\right)^2}$ to the walking speed of active flies. (**G** and **H**) Parameter estimates from the Gaussian fit: amplitude (a) as an estimate of the activity levels (probability to be active) and mean (b) as an estimate of the mean walking speed during active times. Error bars indicate confidence intervals on the fitted parameters.

flies developed at 18°C are higher and the walking speed is the same compared to 25°C, the higher odor occupancy of these flies cannot be attributed to inactivity nor to poor locomotion. Together, this argues that approach behavior toward 2-butanone and vinegar is increased when flies develop at lower temperatures.

The effect of developmental temperature on odor coding

Next, we asked whether the enhanced response to appetitive odors is due to altered odor representations in the AL and related to temperature-dependent wiring. Extracellular recordings from single sensilla showed that *Or42b*-ORNs transduction currents (fig. S4A) and firing rates (Fig. 4A) elicited by odor stimuli do not differ in flies developed at different temperatures. Similar results were obtained for *Or59b*-ORNs, innervating glomerulus DM4 (fig. S4, B and C). Moreover, within the antenna, the number of cell bodies labeled by the Or-specific GAL4 line did not differ between the two temperatures (Fig. 4B). We then expressed the calcium sensor GCaMP6f in ORNs (labeled by *Orco-GAL4*) and imaged activity in their axon terminals in the AL in response to odor stimuli. The glomeruli DM1 and DM4 showed higher presynaptic calcium responses in flies developed at 18°C (Fig. 4C). Because the number of action potentials and the number of ORNs did not differ with temperature, we conclude that larger calcium transients in these glomeruli reflect the larger number (and size) of synapses (Fig. 1, I and J). This raises the possibility that uPNs postsynaptic to the *Or42b*- or *Or59b*-ORNs might be activated more strongly by an odor stimulus. Unexpectedly, the odor responses of uPNs in all glomeruli tested were not different in flies developed at 18° and 25°C (Fig. 4D). Similarly, we found that the odor responses of a subset of mPNs—measured from their axonal projections in the LH—were the same in flies developed at the two temperatures, with a significant difference only for benzaldehyde (fig. S4D).

We conclude that odor representations in the output of the AL are robust to changes in developmental temperature, also for the appetitive odors that we tested behaviorally. Innate odor preference is certainly affected by metabolic and feeding state (*38*) and usually so through modulation of olfactory sensory pathways (*39*, *40*). The fact that the odor responses in PNs are the same at the two developmental temperatures indicate that feeding-dependent pathways previously reported to modulate odor preference are not activated, probably because flies are adapted to the same temperature for 10 days before the experiments and are not in an acute feeding deficit.

Impact of developmental temperature on wiring and function of the LH

Because the measured output activity of the AL is invariant to developmental temperature (Fig. 4), the different behavioral phenotypes observed could result from differences downstream of the AL. Innate odor preference is determined by the wiring of uPNs onto LH neurons (*41*) and modulated by mPNs (*24*–*27*). We therefore asked whether the connections of these cell types onto LHNs were also altered by developmental temperature.

First, we used a pan-neuronal retrograde tracer, *retro*-Tango (*42*), to label all the presynaptic partners of the LHN PD2a1/b1 (Fig. 5A). We chose PD2a1/b1 because it was shown to be functionally connected to DM1 (*43*), although its role in driving innate behavior remains unclear and could be context dependent (*44*–*46*). *Retro*-Tango labels a larger number of presynaptic neurons at the lower developmental temperature, consistent with a general scaling of connectivity throughout the brain. The change in connectivity

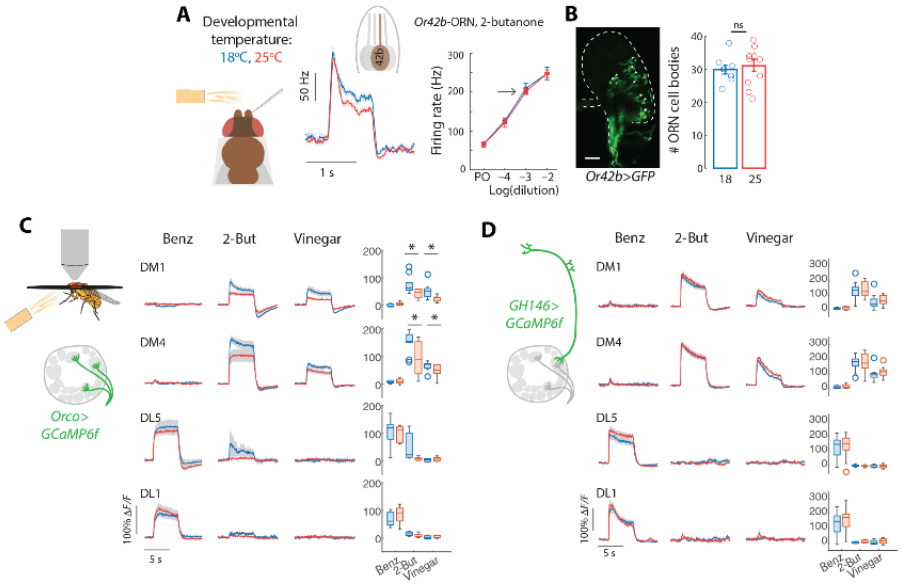

Fig. 4. Scaling and normalization of odor responses in input and output neurons of the AL. (**A**) Single-sensillum recordings from the ab1 sensillum containing a single *Or42b*-ORN. Left: Firing rate response to a 1-s pulse of 2-butanone at 10^{-3} dilution calculated in 100-ms sliding window. Right: Mean peak response for each concentration tested [$n = 10$ (18°C) and 11 (25°C)]. (**B**) Confocal image of the antenna showing GFP expression in *Or42b*-ORNs. Bar plot indicates mean and SEM [$n = 9$ (18°C) and 11(25°C)]. (**C**) Calcium imaging from ORN axon terminals in the AL, quantified within four glomeruli for flies developed at the different temperatures [$*P < 0.05$, *P* value calculated for the average activity during the first second of the stimulus, $n = 6$ (18°C) and 10(25°C)]. (**D**) Same as (C), but the calcium reporter was expressed in uPNs and responses were quantified in the dendritic arborizations within corresponding AL glomeruli, $n = 16$ (18°C) and 18 (25°C). Shaded areas indicate SEM.

was larger in the ventral cluster, which contains mPNs (Fig. 5A). An analysis of the AL innervations revealed denser and more symmetric AL innervations of PD2a1/b1 presynaptic partners at 18°C compared to 25°C (Fig. 5, B to D). This is consistent with a more reliable recruitment of mPNs that innervate the whole AL at 18°C. At 25°C mPNs seem to be more stochastically connected to PD2a1/b1 leading to notable asymmetries and patchy innervations of the AL (Fig. 5B and fig. S5A).

In a second approach, we aimed at identifying the glomeruli connected to PD2a1/b1 by uPNs, by using the genetically encoded retrograde tracing tool BAcTrace (*47*) (Fig. 5E). Differently from *retro*-Tango, this tool only labels presynaptic partners from a pool of genetically targeted neurons, in this case 27 uPNs and three mPNs (*VT033006-LexA*). Although the innervation of uPNs' axons into the LH have been shown to be stereotypic across individuals (*48*), we found a large degree of interindividual variation and asymmetry in connectivity across AL hemispheres (Fig. 5F) [also reported in (*47*)]. An analysis of connection probability shows that developmental temperature influences the connectivity pattern of PD2a1/b1 to AL glomeruli, with a stronger effect in the DM4 glomerulus (Fig. 5, G to I). Temperature, however, does not affect the total number of connected glomeruli (fig. S5, B and C) nor the number of PD2a1/b1 neurons labeled (fig. S5D). Similarly small, but significant shifts in connectivity were observed for two other LHNs, AV4a1 and AD1c1 (Fig. 5J, and fig. S5, E to H).

To link these changes in wiring to function, we performed calcium imaging from PD2a1/b1 neurons. We separated the a1 and b1 subtypes by imaging from two focal planes (Fig. 5K). The b1 subtype showed differences in odor response in flies developed at the two temperatures (Fig. 5K). This demonstrates that PD2b1 function is not robust to developmental temperature, leading to a different LH output in response to odor stimuli. Therefore, while a general scaling of connectivity occurs across the brain, functional consequences are circuit specific and depend on the type of synaptic partners recruited.

DISCUSSION

The development of a whole organism requires the parallel and coordinated growth of body mass and, in the brain, the establishment of functional synaptic connections. Developmental programs are highly temporally structured, raising the question of how they are affected by a temperature-dependent change in developmental speed. Here, we propose that if developmental speed is constrained by varying metabolic reactions across cell types, then temperature manipulation could potentially disrupt the temporal coordination of their developmental programs. We demonstrate that this temporal mismatch can provide an explanation for the change in neural growth and connectivity induced by developmental temperature (Fig. 6, left). Developmental temperature has consequences on odor-driven behavior, but we show that this is not due to different odor responses or sensitivity across the olfactory glomeruli. Therefore, despite a scaling in connectivity, odor encoding is robust to developmental temperature. Odor information, however, converges differently onto LH neurons, with possible consequences for behavior (Fig. 6, right).

Metabolic constraints on the development of the neural system

Through an analysis of filopodia dynamics, Kiral *et al.* (*16*) had proposed that an increased number of synapses at lower developmental temperature is the result of a difference between the scaling of neural and animal growth rates. Here, we have formalized this hypothesis in a mathematical model of growth. We show that fly developmental times scale exponentially with temperature in agreement with proposed theories that assume a metabolic constraint to growth rate. We then extended this theoretical framework to model the rate of neural growth and synapse formation, with two main assumptions. The first is that neural/synaptic growth scales with the fractional power $z = {}^{3}/_{4}$. This value was previously justified starting from geometrical considerations on the fractal nature of the distributions of resources throughout capillaries in a 3D volume (*34*). Our data at fixed temperatures are consistent with any $z < 1$, but the developmental outcome measured in presence of cycling temperatures is well predicted by a ${}^{3}/_{4}$ exponent (*49*). Nonetheless, this scaling law requires further experimental confirmation in the neural system.

The second assumption we made is that the pace of ontogenesis (whole animal development) and neural development are limited by different metabolic reactions. We currently have no direct evidence to support this hypothesis. However, recent works have linked developmental pace to metabolic rates. For example, species-specific developmental rates have been associated to differences in mitochondrial metabolism (*50*, *51*) and manipulations of metabolism directly scale developmental rates (*51*). An intriguing possibility is that these metabolic processes may vary across cell types, particularly in neurons, though this remains to be clarified (*52*). Recent analysis of single-cell transcriptomes in zebrafish demonstrated that developmental temperature has cell type–specific effects on proteostasis (*53*) with possible consequences on developmental pace. Future studies will have to clarify whether differences in cell metabolism determine the effect of temperature on brain wiring. In the meantime, the role of metabolism in this context remains an assumption.

Mechanisms for robust function in a synaptically enriched circuit

The analysis of neural connectivity of distinct glomeruli reveals that lower developmental temperature leads to an overall increase in synaptic partners, as well as a larger number and size of synapses (fig. S6A). This synaptic scaling is consistent with the larger calcium transients measured in some of the glomeruli, in the corresponding ORN axons (fig. S6A). Because ORNs are cholinergic, this increased presynaptic activity could lead to higher excitatory responses in postsynaptic PNs that send odor information to higher brain areas. Unexpectedly, this was not the case, and the responses of PNs was mostly invariant for the two temperatures considered (fig. S6, B and C). This compensation might rely on inhibitory LNs that are recruited in larger numbers at lower temperatures. The balance between excitation and inhibition is key for the function of healthy brains, and there is evidence that this balance is achieved developmentally during synapse formation (*54*). In the fly olfactory system, γ-aminobutyric acid (GABA) mediated inhibition is distributed at both pre- and postsynapses in ORN-uPN connections (*55*, *56*). Presynaptic inhibition could therefore explain why in some glomeruli (DL1 and DL5) calcium transients are already compensated at the ORN axon terminals (fig. S6A), although this remains to be confirmed experimentally. Last, inhibition might not be the sole mechanism that keeps responses temperature invariant. It is possible that the presynaptic scaling is also a homeostatic response to weaker postsynapses (*57*, *58*) or lower release probability (*59*). Overall, we conclude that within a range of temperatures, the peripheral olfactory system is designed to compensate for the developmental effects

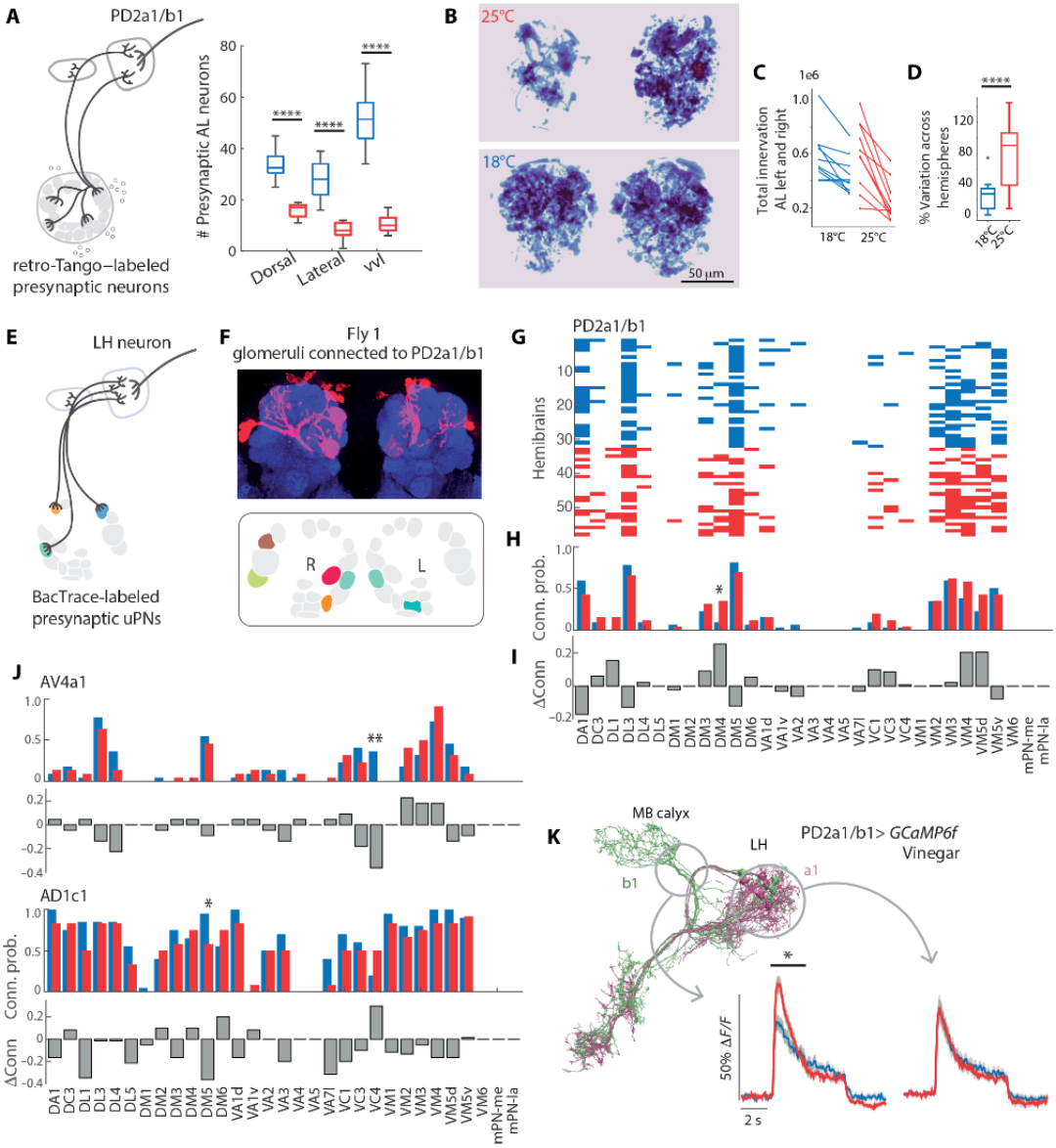

Fig. 5. Developmental temperature affects LH neurons' connectivity to PNs and their odor response. (**A**) Schematics of the *retro*-Tango experiment starting from PD2a1/b1. Boxplot shows median, quartiles, and minimum/maximum values for the number of PD2a1/b1 presynaptic partners from three AL cell clusters; vvl includes cell bodies in the ventral and ventrolateral cluster [$P < 10^{-4}$, $n = 12$ (18°C), and 11 (25°C) hemibrains]. (**B**) Example of *retro*-Tango labeling of the AL (Z-projection of the binary mask of fluorescence intensity). (**C**) Quantification of volumes of segmented neurons labeled by *retro*-Tango in L and R hemispheres. Areas are in pixels squared. (**D**) Symmetry in volume innervation calculated as 100 × (volume left − volume right)/(2 × tot volume). $P < 0.0001$, *t* test. (**E**) Schematics of the BAcTrace experiment, showing a LH neuron and candidate presynaptic uPNs from the AL. (**F**) Confocal image of a sample brain showing labeled uPNs arborizations in the AL and binary connectivity patterns of the uPNs (identified by their glomerular innervation) to PD2a1/b1 in a sample brain. (**G**) Connectivity matrix between glomeruli (*x* axis) and PD2a1/b1 in individual hemibrains (*y* axis) in flies developed at 25°C (red) or 18°C (blue). (**H**) Probability to find a certain glomerulus connected to PD2a1/b1 for each temperature. (**I**) Difference in wiring probability (25° to 18°C). $^*P < 0.05$, $^{**}P < 0.01$, chi-square test, $n = 32$ (18°C) and 26 (25°C). (**J**) Difference in wiring probability for two other LH neuron types, AV4a1: $n = 12$ (18°C) and 20 (25°C); AD1c1: $n = 10$ (18°C) and 20 (25°C). (**K**) Calcium responses of PD2a1/b1 to vinegar in flies developed at 25°C (red) or 18°C (blue). Imaging was performed on two focal planes to capture potential differences between the a1 and b1 subtypes, indicated by circles in the EM skeleton. Shaded areas indicate SEM.

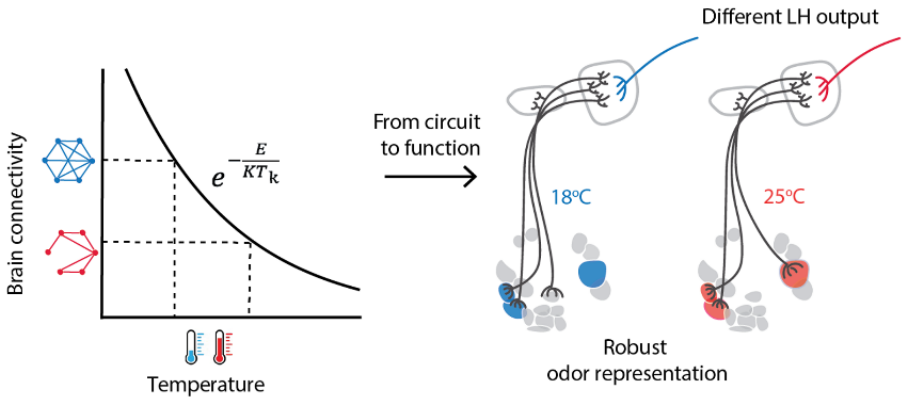

Fig. 6. Linking developmental temperature to neural circuit function. Brain connectivity scales inversely to developmental temperature. This general scaling is consistent with a theory that postulates different metabolic constraints on neural and body development. In the AL, odor representations are invariant to the effect of temperature on circuit organization. In the LH, a downstream area that controls innate behavior, developmental temperature affects the olfactory inputs into some LHNs.

on circuit wiring and to keep odor information invariant to this environmental factor.

Circuits for the modulation of odor preference downstream of the AL

Despite the robust odor representations within the AL, behavioral responses to appetitive odor cues are strongly affected by developmental temperature in two different assays (Fig. 3). This indicates that the scaling in brain connectivity is not fully functionally compensated, and the odor induced activity in circuits downstream of the AL is dependent on developmental temperature. Innate odor preference arises in the LH, where PNs target LHNs within a complex wiring logic. Here, LHNs pull information from subsets of glomeruli with ecologically related odor response profiles (*43*, *44*). Our analysis demonstrates that the odor information received by the LH is temperature dependent because of small but significant differential wiring of PNs (fig. S6D). PD2b1 neurons have different odor responses in flies developed at different temperatures, and therefore, LH output is not invariant to developmental temperature.

These changes in connectivity and function are likely only a lower bound on the effect of developmental temperature. First, only half of the uPN types was included in our analysis, and we might have neglected more relevant connections. Second, the connectivity and odor responses of other LHNs might be affected. PD2a1/b1 neurons are required for memory retrieval (*45*), but their role in innate behavior is likely context dependent (*46*). They might be involved in approach toward appetitive cues, although their activation is not sufficient to drive behavior (*44*). Most likely, PD2a1/b1 neurons act synergistically or redundantly with other LHNs with temperature-dependent wiring, although the logic of these circuits remains to be understood.

Last, odor information is transmitted to higher brain areas not only by uPNs but also by mPNs that target the LH and the protocerebrum. The connectivity of mPNs to ORNs and LHNs is also affected by temperature (fig. S6, C and D). The function of this large population of neurons (>50% of the total number of PNs), however, is still unclear. Half of mPNs are predicted to be GABAergic (*23*): These modulate odor preference and discrimination (*24*, *26*, *27*), and silencing inhibitory mPNs reduces approach toward appetitive odors (*24*). The other half of mPNs is predicted to be cholinergic (*23*), with a still unknown contribution to both downstream odor processing and behavior. Therefore, further understanding of mPN function and LH circuit organization is required to link the temperature-dependent plasticity to the behavior we observe.

Linking temperature-dependent wiring to behavior: Current limitations

The observation that developmental temperature scales connectivity throughout the brain presents a substantial challenge in establishing a causal link between circuit architecture and behavior. We were able to exclude the early olfactory circuit as the origin of the observed behavioral differences. However, we cannot conclusively demonstrate that these differences arise from changes in the output of the LH, as other downstream pathways could also be affected by developmental temperature. Therefore, the relationship between LH output and behavior in flies developed at different temperatures must be regarded as correlative. Overall, our analysis shows that predicting circuit function—whether in terms of neural activity or behavioral outcomes—based on circuit connectivity remains a challenge in the context of these developmental manipulations.

Phenotypic variation and constrained pathways

Overall, our study suggests that the effect of developmental temperature on neural circuit wiring and function is heterogeneous across circuits and likely depends on the spatiotemporal availability of synaptic partners (*1*). Clearly, some connections in the brain are critical for survival, and these have probably evolved to correctly wire and function no matter the temperature. Developing flies on extremely high temperatures revealed what is considered to be the backbone of the olfactory pathway, i.e., the wiring of ORNs onto a single uPN and a few mPNs and LNs (glomerulus DM1, Fig. 2B). Studying these extreme conditions might provide insights on evolutionary constraints on circuit design.

The brain has evolved many strategies to keep circuits' function robust to environmental factors (*60*, *61*). While such robustness holds true within some subcircuits (individual glomeruli in this study), it cannot be assumed to occur throughout the brain (LH output in this study). In this way, environmental factors can lead to observable variation in behavioral phenotypes. Our study raises the question of whether such variation in brain wiring is an

evolutionary selected feature for adaptation to the environment, posing new challenges for understanding brain development in poikilothermic animals.

MATERIALS AND METHODS

Experimental model and fly husbandry

Flies were raised on standard molasses-based food, at 65% humidity and on controlled 12-hour:12-hour light-dark cycles. All flies were kept at 25°C as embryos and after eclosion. Flies were placed at different temperatures (12°, 18°, 25°, and 31°C depending on the experiment) between the third-instar larva stage (L3) and the end of metamorphosis. As the time of development depends on temperature, we call the end point of metamorphosis P-100%. For optogenetics experiments, flies were kept in standard molasses-based food with 1 mM all-trans retinal (Sigma-Aldrich) in the dark for ≥72 hours before experiments. In all experiments, only females were used. Exact genotypes are given in tables S1 and S2.

Temperature cycle experiment

For temperature cycle experiments, flies were kept on 12-hour:12-hour light-dark cycles. Temperature varied in parallel to light with the high temperature corresponding to the light cycle. The temperature ranges (minimum to maximum) used were 20° to 28°C, 18° to 30°C, 16° to 32°C, and 14° to 34°C. The maximum temperatures were held for 8 hours and shifted to the minimum temperature gradually in 4 hours.

Immunohistochemistry and confocal

Female flies (9 to 11 days after eclosion) were anesthetized with ice and then briefly submerged in ethanol 70%. Flies were dissected on cold phosphate-buffered saline (PBS) for no longer than 20 min and fixated for 50 min in 2% paraformaldehyde (Polysciences, diluted in PBS) rotating at room temperature. All subsequent incubation and washes were done while rotating, in the dark. Brains were washed three times in PBT (PBS with 0.5% Triton X-100, Roth) for 15 min and then blocked for 1 hour in 5% normal goat serum (Thermo Fisher Scientific, in 0.3% PBT). Samples were incubated in primary antibody mixture (chicken anti-GFP 1:1000; rabbit anti-DsRed 1:500; mouse anti-nc82 1:25) for 48 hours at 4°C, then washed in PBT (3× of 15 min) and incubated in secondary antibody mix (goat anti-chicken Alexa Fluor 488; donkey anti-rabbit Alexa Fluor 568; donkey anti-mouse Alexa Fluor 647, all at 1:200) for 48 hours at 4°C. Last, brains were washed three times in PBT and mounted in VectaShield (Biozol). Brains were imaged on a Leica SP8 microscope with a 20×, 40×, or 63× objective depending on the experiment. After image acquisition, the number cell bodies of postsynaptic partners were manually counted using Fiji's cell counter plugin. Cell body numbers were classified according to the position around the AL: dorsal, lateral, or ventrolateral (including both ventrolateral and ventral clusters). For reagents, see table S1.

Brp^{Short} analysis

Confocal images of individual DM1 glomeruli were processed using a custom code in Python, with the package pyclesperanto (*62*). Images contained a Brp^{Short} (GFP) and Brp (nc82) channel. Both channels were preprocessed with Gaussian blur (1.0, 1.0, 1.0) and top hat box (20.0, 20.0, 1.0). The DM1-ORN mask was made using the Brp^{Short} channel, by applying Voronoi Otsu Labeling and then merging the touching labels. For the whole DM1 glomerulus mask, the DM1-ORN volume was closed using the function closing labels. Single nc82-labelled puncta were segmented by Voronoi Otsu Labeling and restricted to the DM1 glomerulus mask. The volume and fluorescence intensity of labeled regions were acquired using the statistics of labeled pixels in pyclesperanto.

Retro-Tango quantification

As for Brp^{Short} analysis, *retro*-Tango confocal stacks were processed using a custom Python script. For each AL, a manual mask was done to delimit the region of interest and crop the original images. Presynaptic neurons were preprocessed by applying Gaussian blur (1.0, 1.0, 1.0) followed by top hat box (10.0, 10.0, 1.0). Presynaptic neurons were then binarized with Gauss Otsu Labeling. Volumes of labeled regions were acquired using the statistics of labeled pixels (pyclesperanto).

In vivo calcium imaging

Flies were developed at either 18° or 25°C. At 9 to 11 days after eclosion, flies were anesthetized on ice and mounted on a custom holder using ultraviolet (UV)–cured glue (Bondic). Saline solution [5 mM Hepes, 130 mM NaCl, 5 mM KCl, 2 mM $MgCl_2$, 2 mM $CaCl_2$, and 36 mM saccharose (pH 7.3)] was added. The cuticle covering the fly's head, as well as obstructing trachea, were removed. Functional imaging was done on an Investigator two-photon microscope (Bruker) coupled to a tunable laser (Spectraphysics Insight DS+) with a 25×/1.1 water-immersion objective (Nikon). Laser excitation was tuned to 920 nm, and less than 20 mW of excitation was delivered to the specimen. Emitted light passed through a SP680 short-pass filter, a 560 lpxr dichroic filter, and a 525/70 filter. PMT gain was set to 850 V. The microscope was controlled with the PrairieView (5.4) software.

Optogenetics

For optogenetic activation light from a 625-nm light-emitting diode (LED) was directed using an optic fiber to the fly's antenna. The LED was controlled in flight-back mode from the imaging software using an Arduino board, allowing simultaneous acquisition and excitation. The light stimulus protocol consisted of 5-s series of light pulses, presented five times with intervals of 30 s. Stimulus intensity in fig. S1A was measured at the fly position with this protocol.

Odor delivery

Flies were exposed to a continuous clean air airflow (1 liter/min), in which either an odor stream (100 ml/min) or a clean balancer airflow (100 ml/min) was redirected through a solenoid valve (LEE), so that the final airflow reaching the fly was around 1.1 liters/min. For creating the gas dilutions, four mass flow controllers were used (Analyt-MTC) and controlled using a custom MATLAB (MathWorks) script and an Arduino board. Odors were prepared as a liquid 5-ml 10^{-2} volumetric dilution in 20-ml glass vials (2-butanone and benzaldehyde in mineral oil and apple cider vinegar in MiliQ Water). The final volumetric gas dilution used was 10^{-5}. Odor stimulation consisted of three repetitions of a 5 s, with 30-s intervals in between. For chemicals, see table S1.

Electrophysiology

Single-sensillum recordings were performed as previously described (*63*) using a silver chloride electrode and glass pipettes filled with sensillum lymph ringer. Electrical signals were amplified using an extracellular amplifier (EXT-02F-1, npi) with head stage (EXT-EH), band-pass filtered (300 to 5000 Hz), and digitized at 20 KHz using a NI board (NI-6212). Data were acquired with the matlab toolbox kontroller (*64*) (https://github.com/emonetlab/kontroller). Spikes were sorted using a custom MATLAB routine available at https://gitlab.rlp.net/mrtlllab/zuefle_batista_etal_2024.

Odor delivery

Flies were exposed to a constant airflow (1 liter/min), and an odor stimulus was delivered by switching a three-way solenoid valve that directed a secondary airflow (100 ml/min) through a Pasteur pipette as in (*63*, *65*). The pipette contained a filter paper with 50-ml odor dilution. Volumetric odor dilutions were prepared in either mineral oil or MiliQ Water. Stimuli were controlled by custom made software in MATLAB and Arduino.

Behavioral experiments

Spherical treadmill

Experiments were conducted at 32°C in a closed custom arena. The spherical treadmill consisted of a 15-mm-diameter polyurethane foam sphere (FR-7120 foam, General Plastics) floating on an air column. The sphere was coated with two layers of classic wood glue (Ponal, 25% in water), and then a random nonuniform pattern was drawn using two layers of acrylic black paint (Black 3.0, Culture Hustle). All coats of paint were allowed to dry overnight. The odor delivery system was similar to the one described above for in vivo calcium imaging experiments but with a differing airflow rate controlled by Alicat Scientific MFCs. Continuous clean airflow was 90 ml/min, and both the odor and balancer airflows were 10 ml/min. Videos were acquired with a XIMEA xiQ video camera, placed 10 cm from the treadmill. The treadmill ball was illuminated by a panel of 940-nm LEDs (Solarox) and an extra LED on the air column was visible in the video and turned on simultaneously to the odor stimulus to trigger the data.

Experimental protocol. For experiments, 9- to 10-day-old female flies were cold anesthetized and secured to a needle at their thorax on the dorsal side using a UV-hardening glue (Bondic) and positioned on the sphere with the help of a 3D micromanipulator. Before recording, flies were acclimatized to walking on the sphere for 10 to 15 min with no stimulus being presented. Subsequently, video recording and the odor stimulation were started. Videos were acquired using the XIMEA CamTool software: The exposure was set to 10,725 ms, the gain to 2.6 Db, and the frame rate to 80 fps. The odor stimulation was controlled through MATLAB by an Arduino UNO Rev3 and consisted of at least 19 repetitions of 5-s-long odor stimuli and 20-s-long interval without odor.

Video processing and analysis. Fly moving speed was calculated a posteriori from the video recordings using the open-source software library FicTrac (*66*), which provided direction and walking speed of the animal for each frame in the video. The video recordings were also analyzed in MATLAB to extract the stimulus trigger from the LED placed in the field of view. Last, the output data from Fictrac and the time points obtained from the video were analyzed in MATLAB so that the moving speed during and outside odor presentation could be quantified. Flies that had a basal walking speed lower than 2 mm/s were discarded.

Free-walking assay

A free walking area was contained in a thermally controlled black box (100 cm by 45 cm by 45cm) shielded from room light, fully closed with a frontal door, and equipped with a heating system and thermostat (H-TRONIC GmbH, Product ID: 1114430). The box was heated up by an air stream created by a fan and homogeneously distributed by a diffuser. A blue LED stripe (470 nm, Paulmann Licht GmbH, product ID: 78979) was positioned around the walking arena to ensure stable illumination during experiments. Videos were recorded with a Basler Camera (Basler acA2040-90um) placed on the ceiling of the box and equipped with f12mm lens (Basler C10-1214-2 M-S), using Pylon viewer (64-Bit, 6.3.0.10295). The walking arena had 40.2-cm diameter and 2-cm height and was composed of four stacked layers and three overlapping plates (glass or plexiglass). The bottom layer contained six holes, arranged at the corners of a hexagon, where 1.5-ml glass vials (Fisherbrand 11565874) containing the test odor could be screwed in. On top of this, a Teflon-coated porous sheet (FIBERFLON GmbH & Co. KG, product ID: 408.07 P) provides a walking surface for the flies hiding the odor location. The mid-arena layer consists in a sloped (at 11°, 5-cm length) ring that defines the accessible walking area. To seal the walking arena, we used a glass plate coated with Sigmacote (Sigma-Aldrich Co.) to prevent fly walking upside down. This behavioral setup was built by the workshop of the Biology Department at Johannes Gutenberg Universität Mainz.

Experimental protocol. We tested female flies developed at 18° or 25°C, 5 to 7 days after eclosion. One hour before the experiment, flies were transferred into a vial with only a small piece of filter paper soaked in water and kept at room temperature. For experiments carried at 32°C, the fly vials were incubated for 15 min in a 32°C water bath. To create an odor gradient inside the arena, 5 min before the start of each experiment, a 1.5-ml glass vial containing 1 ml of test odor was placed in one of the six possible odor positions in the behavioral setup. For each trial, a fresh odor vial was used, and the position was pseudo-randomized. Each trial consisted of 10 to 15 female flies exposed to either apple cider vinegar (10^{-2} in MilliQ water) or 2-butanone (10^{-2} in mineral oil) or tested with empty vials. Flies were gently pushed inside the arena using a custom fly transfer tube and the recording was immediately started. All experimental videos were recorded at 20 fps for 15 min and saved in mp4 format. At the end of each trial, the flies were removed and discarded. The initial condition was restored by removing the odor vial and the cover glass plate, replacing the Teflon sheet with a clean one, and letting the whole system ventilate for 5 min.

Video processing and analysis. All required steps to preprocess the raw videos were done using the Python 3.9.12 distribution ANACONDA (version 4.13.0). Scripts were written using Virtual Studio Code (version 1.81.1). Recorded mp4 videos were processed and video tracked with the software TRex (version 1.1.8_3) (*67*). The output files were analyzed using custom Python and MATLAB scripts available at https://gitlab.rlp.net/mrtlllab/zuefle_batista_etal_2024. A threshold of 5 cm was chosen to determine whether the fly had located the odor source; variations of this threshold do not alter the results. Odor occupancy was calculated as the integral under the curve in the first 7 min, being 1 if all flies spend 100% of the time at the odor.

Connectome analysis

We used the Hemibrain dataset (hemibrain:v.1.2.1) (*20*). For Fig. 1 (K and L) and fig. S1 (E and F), we considered all synapses from the *Or42b*-ORNs of the left and right antennae within the DM1 glomerulus of the right hemisphere, which were selected by clustering the synapses on the basis of their 3D coordinates. The analysis was restricted to synapses of the right hemisphere, as postsynaptic partners are fully reconstructed only on this side. We calculated the number of synapses between each ORN and each postsynaptic neuron. Connections with less than three synapses from a single ORN were discarded. Moreover, postsynaptic neurons that received less than 10 total synapses were discarded. The number of synapses was

normalized to the total number for this ORN type. Postsynaptic neurons were sorted on the basis of the number of synaptic inputs they received. The same procedure was used for DL1 and DL5. The percentages of LNs and mPNs in fig. S1F are lower bounds, as calculated from the available annotations.

Theory

To model ontogenetic growth, we follow the same approach of (*3*). We assume that growth scales as the three-fourth power of the mass m [see Discussion and (*34*)] following the equation

$$\frac{dm}{dt} = am^{\frac{3}{4}}\left[1-\left(\frac{m}{M}\right)^{\frac{1}{4}}\right] \tag{1}$$

where M is the asymptotic mass and a is proportional to metabolic rate

$$a = \frac{B_0 m_c}{E_c} \tag{2}$$

with m_c the cell mass, E_c the energy per cell, and B_0 is the normalization factor of the metabolic rate $B = B_0 m^{\frac{3}{4}}$ that scales proportionally to the Boltzmann factor: $B_0 \propto e^{-\frac{E}{KT_k}}$ (T_k is the temperature in Kelvin, K the Boltzmann constant, and E the activation energy). Therefore, $a \propto e^{-\frac{E}{KT_k}}$. Following (*3*), we calculate a with respect to a reference temperature (the water freezing point $T_a = 273$ K), and replacing $= T_k - T_a$, we obtain

$$a = a(T,E) = a(T_a,E)e^{\frac{E}{KT_a^2}\left(\frac{T}{1+T/T_a}\right)} \approx a(T_a,E)e^{\frac{E}{KT_a^2}T} \tag{3}$$

where now the temperature T is in degrees Celsius. The last approximation takes in account the fact that the relevant temperatures do not exceed 32°C; therefore, T/T_a is at most 0.1. This approximation leads to an error of about 10% on the exponential fits, but the quality of the model prediction remains unchanged. We keep the approximation for simplicity in the following calculations.

To find the relationship between developmental time and temperature, we integrate the growth Eq. 1 for $m \ll M$ (but see below)

$$\int_0^{m(t)} m^{-\frac{3}{4}}\,dm = \int_0^t a(T,E)dt \Longrightarrow 4m^{\frac{1}{4}} = a(T,E)\cdot t \tag{4}$$

Equations 3 and 4 lead to the exponential relationship between developmental time t and temperature T proposed in (*3*)

$$t = \frac{4m^{\frac{1}{4}}}{a(T_a,E)}e^{-\frac{E}{KT_a^2}T} \tag{5}$$

We calculate the fold change with respect to a reference temperature $T_0 = 25$°C by assuming that development results in the same final mass

$$\frac{t}{t_0} = e^{-\frac{E}{KT_a^2}(T-T_0)} = e^{-\alpha(T-T_0)} \tag{6}$$

with $= \frac{E}{KT_a^2}$. We use Eq. 6 to fit developmental times in Fig. 2K. This result remains the same if we use the general solution of Eq. 1 from (*3*) (relaxing the assumption $\ll M$) or if we integrate it from $m(0) = m_i$ instead of $m(0) = 0$.

We now assume that developmental time follows the exponential relationship in Eq. 6, while the wiring of the neural circuit is constrained by a different reaction rate with $E' < E$. In modeling the growth of the neural system, we use n instead of the mass m, which can be intended as number of synapses, synaptic partners, or axonal branching. n follows a similar equation as Eq. 5 leading to

$$\frac{t}{t_0} = \left(\frac{n}{n_0}\right)^{\frac{1}{4}} e^{-\frac{E'}{KT_a^2}(T-T_0)} \tag{7}$$

This results from an initial condition $n(0) = 0$, which is reasonable given the major pruning and regrowth of axons that happens during metamorphosis. Using Eqs. 6 and 7

$$\frac{n}{n_0} = e^{-4\frac{E-E'}{KT_a^2}(T-T_0)} \tag{8}$$

where we define $\beta = 4\frac{E-E'}{KT_a^2} = 4\frac{\Delta E}{KT_a^2}$. If $\Delta E = 0$, then there should be no change in the number of synaptic partners. Also note that β can be larger than α ($\Longrightarrow E > \frac{4}{3}E'$) or smaller than α ($\Longrightarrow E' < E < \frac{4}{3}E'$). We use Eq. 8 to fit fold changes in the number of synaptic partners in Fig. 2G.

Next, we calculate the developmental time of flies on temperature cycles with maximum and minimum temperatures T_1 and T_2. Here, we simplify the cycling temperature protocol to step changes such that the final mass on temperature cycles results from development that occurs half of the time at T_1 and half at T_{12}

$$\int_0^{m(\widetilde{t})} m^{-\frac{3}{4}}\,dm = \int_0^{\frac{\widetilde{t}}{2}} a(T_1,E)dt + \int_0^{\frac{\widetilde{t}}{2}} a(T_2,E)dt \tag{9}$$

$$\Longrightarrow m^{\frac{1}{4}} = \frac{\widetilde{t}}{8}\left[a(T_1,E)+a(T_2,E)\right] \tag{10}$$

Here, $\widetilde{t}$ indicates the developmental time on temperature cycles. Assuming an equal final mass, the fold change with respect to a fix temperature $\overline{T}$ is

$$\frac{\widetilde{t}}{t} = 2\frac{a(\overline{T},E)}{a(T_1,E)+a(T_2,E)} = 2\frac{1}{e^{-\alpha(\overline{T}-T_1)}+e^{-\alpha(\overline{T}-T_2)}} \tag{11}$$

To calculate the fold change in synaptic connectivity, we use the same logic as before to derive

$$\left(\frac{\widetilde{n}}{n}\right)^{\frac{1}{4}} = \frac{1}{2}\frac{\widetilde{t}}{t}\frac{a(T_1,E')+a(T_2,E')}{a(\overline{T},E')} \tag{12}$$

Moreover, using Eq. 11

$$\frac{\widetilde{n}}{n} = e^{\beta\overline{T}}\left(\frac{e^{\gamma T_1}+e^{\gamma T_2}}{e^{\alpha T_1}+e^{\alpha T_2}}\right)^4 \tag{13}$$

with $= \frac{E'}{KT_a^2} = \alpha - \frac{\beta}{4}$. We use Eq. 13 to predict the number of synaptic partners in flies developed on periodic temperature cycles in Fig. 2Q. The solutions in Eqs. 11 and 13 further simplify, if we take the mean temperature as the reference temperature $\overline{T} = \frac{T_1+T_2}{2}$ and $\Delta T = \frac{T_2-T_1}{2}$ that is

$$\frac{\tilde{t}}{t} = \frac{1}{\cosh(\alpha \Delta T)} \tag{14}$$

and

$$\frac{\tilde{n}}{n} = \left[\frac{\cosh(\gamma \Delta T)}{\cosh(\alpha \Delta T)}\right]^4 \tag{15}$$

which shows that the fold change in developmental time and connectivity scale inversely with the amplitude of the temperature cycles (as $\gamma < \alpha$).

Supplementary Materials

This PDF file includes:

Figs. S1 to S6
Tables S1 and S2

REFERENCES AND NOTES

1. P. R. Hiesinger, B. A. Hassan, The evolution of variability and robustness in neural development. *Trends Neurosci.* **41**, 577–586 (2018).
2. J. F. Gillooly, J. H. Brown, G. B. West, V. M. Savage, E. L. Charnov, Effects of size and temperature on metabolic rate. *Science* **293**, 2248–2251 (2001).
3. J. F. Gillooly, E. L. Charnov, G. B. West, V. M. Savage, J. H. Brown, Effects of size and temperature on developmental time. *Nature* **417**, 70–73 (2002).
4. M. E. B. Ohmer, T. T. Hammond, S. Switzer, T. Wantman, J. G. Bednark, E. Paciotta, J. Coscia, C. L. Richards-Zawacki, Developmental environment has lasting effects on amphibian post-metamorphic behavior and thermal physiology. *J. Exp. Biol.* **226**, jeb244883 (2023).
5. D. W. A. Noble, V. Stenhouse, L. E. Schwanz, Developmental temperatures and phenotypic plasticity in reptiles: A systematic review and meta-analysis. *Biol. Rev.* **93**, 72–97 (2018).
6. T. Abayarathna, J. K. Webb, Effects of incubation temperatures on learning abilities of hatchling velvet geckos. *Anim. Cogn.* **23**, 613–620 (2020).
7. M. de Jong, B. L. Phillips, J. Llewelyn, D. G. Chapple, B. B. M. Wong, Effects of developmental environment on animal personality in a tropical skink. *Behav. Ecol. Sociobiol.* **76**, 137 (2022).
8. J. Tautz, S. Maier, C. Groh, W. Rössler, A. Brockmann, Behavioral performance in adult honey bees is influenced by the temperature experienced during their pupal development. *Proc. Natl. Acad. Sci. U.S.A.* **100**, 7343–7347 (2003).
9. M. A. Becher, H. Scharpenberg, R. F. A. Moritz, Pupal developmental temperature and behavioral specialization of honeybee workers (Apis mellifera L.). *J. Comp. Physiol. A Neuroethol. Sens. Neural Behav. Physiol.* **195**, 673–679 (2009).
10. A. Weidenmüller, C. Mayr, C. J. Kleineidam, F. Roces, Preimaginal and adult experience modulates the thermal response behavior of ants. *Curr. Biol.* **19**, 1897–1902 (2009).
11. S. B. S. Baleba, V. P. Mahadevan, M. Knaden, B. S. Hansson, Temperature-dependent modulation of odor-dependent behavior in three drosophilid fly species of differing thermal preference. *Commun. Biol.* **6**, **905**, (2023).
12. X. Wang, D. S. Green, S. P. Roberts, J. S. de Belle, Thermal disruption of mushroom body development and odor learning in *Drosophila*. *PLOS ONE* **2**, e1125 (2007).
13. C. Zhu, H. Li, X. Xu, S. Zhou, B. Zhou, X. Li, H. Xu, Y. Tian, Y. Wang, Y. Chu, X. Zhang, X. Zhu, The mushroom body development and learning ability of adult honeybees are influenced by cold exposure during their early pupal stage. *Front. Physiol.* **14**, 1173808 (2023).
14. C. Groh, J. Tautz, W. Rössler, Synaptic organization in the adult honey bee brain is influenced by brood-temperature control during pupal development. *Proc. Natl. Acad. Sci. U.S.A.* **101**, 4268–4273 (2004).
15. A. Falibene, F. Roces, W. Rössler, C. Groh, Daily thermal fluctuations experienced by Pupae via rhythmic nursing behavior increase numbers of mushroom body microglomeruli in the adult ant brain. *Front. Behav. Neurosci.* **10**, 73 (2016).
16. F. R. Kiral, S. B. Dutta, G. A. Linneweber, S. Hilgert, C. Poppa, C. Duch, M. von Kleist, B. A. Hassan, P. R. Hiesinger, Brain connectivity inversely scales with developmental temperature in *Drosophila*. *Cell Rep.* **37**, 110145 (2021).
17. M. Talay, E. B. Richman, N. J. Snell, G. G. Hartmann, J. D. Fisher, A. Sorkaç, J. F. Santoyo, C. Chou-Freed, N. Nair, M. Johnson, J. R. Szymanski, G. Barnea, Transsynaptic mapping of second-order taste neurons in flies by *trans*-Tango. *Neuron* **96**, 783–795.e4 (2017).
18. E. L. Wilder, N. Perrimon, Dual functions of *wingless* in the *Drosophila* leg imaginal disc. *Development* **121**, 477–488 (1995).
19. D. A. Wagh, T. M. Rasse, E. Asan, A. Hofbauer, I. Schwenkert, H. Dürrbeck, S. Buchner, M.-C. Dabauvalle, M. Schmidt, G. Qin, C. Wichmann, R. Kittel, S. J. Sigrist, E. Buchner, Bruchpilot, a protein with homology to ELKS/CAST, is required for structural integrity and function of synaptic active zones in *Drosophila*. *Neuron* **49**, 833–844 (2006).
20. L. K. Scheffer, C. S. Xu, M. Januszewski, Z. Lu, S.-Y. Takemura, K. J. Hayworth, G. B. Huang, K. Shinomiya, J. Maitin-Shepard, S. Berg, J. Clements, P. M. Hubbard, W. T. Katz, L. Umayam, T. Zhao, D. Ackerman, T. Blakely, J. Bogovic, T. Dolafi, D. Kainmueller, T. Kawase, K. A. Khairy, L. Leavitt, P. H. Li, L. Lindsey, N. Neubarth, D. J. Olbris, H. Otsuna, E. T. Trautman, M. Ito, A. S. Bates, J. Goldammer, T. Wolff, R. Svirskas, P. Schlegel, E. R. Neace, C. J. Knecht, C. X. Alvarado, D. A. Bailey, S. Ballinger, J. A. Borycz, B. S. Canino, N. Cheatham, M. Cook, M. Dreher, O. Duclos, B. Eubanks, K. Fairbanks, S. Finley, N. Forknall, A. Francis, G. P. Hopkins, E. M. Joyce, S. Kim, N. A. Kirk, J. Kovalyak, S. A. Lauchie, A. Lohff, C. Maldonado, E. A. Manley, S. McLin, C. Mooney, M. Ndama, O. Ogundeyi, N. Okeoma, C. Ordish, N. Padilla, C. Patrick, T. Paterson, E. E. Phillips, E. M. Phillips, N. Rampally, C. Ribeiro, M. K. Robertson, J. T. Rymer, S. M. Ryan, M. Sammons, A. K. Scott, A. L. Scott, A. Shinomiya, C. Smith, K. Smith, N. L. Smith, M. A. Sobeski, A. Suleiman, J. Swift, S. Takemura, I. Talebi, D. Tarnogorska, E. Tenshaw, T. Tokhi, J. J. Walsh, T. Yang, J. A. Horne, F. Li, R. Parekh, P. K. Rivlin, V. Jayaraman, M. Costa, G. S. X. E. Jefferis, K. Ito, S. Saalfeld, R. George, I. A. Meinertzhagen, G. M. Rubin, H. F. Hess, V. Jain, S. M. Plaza, A connectome and analysis of the adult *Drosophila* central brain. *eLife* **9**, e57443 (2020).
21. A. S. Bates, J. D. Manton, S. R. Jagannathan, M. Costa, P. Schlegel, T. Rohlfing, G. S. X. E. Jefferis, The natverse, a versatile toolbox for combining and analysing neuroanatomical data. *eLife* **9**, e53350 (2020).
22. C. Sakuma, M. Anzo, M. Miura, T. Chihara, Development of olfactory projection neuron dendrites that contribute to wiring specificity of the *Drosophila* olfactory circuit. *Genes Genet. Syst.* **89**, 17–26 (2014).
23. A. S. Bates, P. Schlegel, R. J. V. Roberts, N. Drummond, I. F. M. Tamimi, R. Turnbull, X. Zhao, E. C. Marin, P. D. Popovici, S. Dhawan, A. Jamasb, A. Javier, L. Serratosa Capdevila, F. Li, G. M. Rubin, S. Waddell, D. D. Bock, M. Costa, G. S. X. E. Jefferis, Complete connectomic reconstruction of olfactory projection neurons in the fly brain. *Curr. Biol.* **30**, 3183–3199. e6 (2020).
24. A. Strutz, J. Soelter, A. Baschwitz, A. Farhan, V. Grabe, J. Rybak, M. Knaden, M. Schmuker, B. S. Hansson, S. Sachse, Decoding odor quality and intensity in the *Drosophila* brain. *eLife* **3**, e04147 (2014).
25. K. Shimizu, M. Stopfer, A population of projection neurons that inhibits the lateral horn but excites the antennal lobe through chemical synapses in *Drosophila*. *Front. Neural Circuits* **11**, 30 (2017).
26. L. Liang, Y. Li, C. J. Potter, O. Yizhar, K. Deisseroth, R. W. Tsien, L. Luo, GABAergic projection neurons route selective olfactory inputs to specific higher-order neurons. *Neuron* **79**, 917–931 (2013).
27. M. Parnas, A. C. Lin, W. Huetteroth, G. Miesenböck, Odor discrimination in *Drosophila*: From neural population codes to behavior. *Neuron* **79**, 932–944 (2013).
28. S. Lin, C.-F. Kao, H.-H. Yu, Y. Huang, T. Lee, Lineage analysis of *Drosophila* lateral antennal lobe neurons reveals notch-dependent binary temporal fate decisions. *PLoS Biol.* **10**, e1001425 (2012).
29. G. Pétavy, J. P. Morin, B. Moreteau, J. R. David, Growth temperature and phenotypic plasticity in two *Drosophila* sibling species: Probable adaptive changes in flight capacities. *J. Evol. Biol.* **10**, 875–887 (1997).
30. V. Trotta, F. C. F. Calboli, M. Ziosi, D. Guerra, M. C. Pezzoli, J. R. David, S. Cavicchi, Thermal plasticity in *Drosophila melanogaster*. A comparison of geographic populations. *BMC Evol. Biol.* **6**, 67 (2006).
31. D. Ludwig, R. M. Cable, The effect of alternating temperatures on the pupal development of Drosophila melanogaster Meigen. *Physiol. Zool.* **6**, 493–508 (1933).
32. H. A. Feldman, T. A. McMahon, The 3/4 mass exponent for energy metabolism is not a statistical artifact. *Respir. Physiol.* **52**, 149–163 (1983).
33. R. H. Peters, *The Ecological Implications of Body Size* (Cambridge Univ. Press, 1983).
34. G. B. West, J. H. Brown, B. J. Enquist, The fourth dimension of life: Fractal geometry and allometric scaling of organisms. *Science* **284**, 1677–1679 (1999).
35. G. B. West, J. H. Brown, B. J. Enquist, A general model for the origin of allometric scaling laws in biology. *Science* **276**, 122–126 (1997).
36. A. I. Dell, S. Pawar, V. M. Savage, Systematic variation in the temperature dependence of physiological and ecological traits. *Proc. Natl. Acad. Sci. U.S.A.* **108**, 10591–10596 (2011).
37. G. S. X. E. Jefferis, R. M. Vyas, D. Berdnik, A. Ramaekers, R. F. Stocker, N. K. Tanaka, K. Ito, L. Luo, Developmental origin of wiring specificity in the olfactory system of *Drosophila*. *Development* **131**, 117–130 (2004).
38. I. C. Grunwald Kadow, State-dependent plasticity of innate behavior in fruit flies. *Curr. Opin. Neurobiol.* **54**, 60–65 (2019).
39. C. Martelli, U. Pech, S. Kobbenbring, D. Pauls, B. Bahl, M. V. Sommer, A. Pooryasin, J. Barth, C. W. P. Arias, C. Vassiliou, A. J. F. Luna, H. Poppinga, F. G. Richter, C. Wegener, A. Fiala, T. Riemensperger, SIFamide translates hunger signals into appetitive and feeding behavior in *Drosophila*. *Cell Rep.* **20**, 464–478 (2017).

40. C. M. Root, K. I. Ko, A. Jafari, J. W. Wang, Presynaptic facilitation by neuropeptide signaling mediates {odor-driven} food search. *Cell* **145**, 133–144 (2011).
41. J. N. Schultzhaus, S. Saleem, H. Iftikhar, G. E. Carney, The role of the Drosophila lateral horn in olfactory information processing and behavioral response. *J. Insect Physiol.* **98**, 29–37 (2017).
42. A. Sorkaç, R. A. Moşneanu, A. M. Crown, D. Savaş, A. M. Okoro, E. Memiş, M. Talay, G. Barnea, retro-Tango enables versatile retrograde circuit tracing in *Drosophila*. *eLife* **12**, e85041 (2023).
43. J. M. Jeanne, M. Fişek, R. I. Wilson, The organization of projections from olfactory glomeruli onto higher-order neurons. *Neuron* **98**, 1198–1213.e6 (2018).
44. M.-J. Dolan, S. Frechter, A. S. Bates, C. Dan, P. Huoviala, R. J. V. Roberts, P. Schlegel, S. Dhawan, R. Tabano, H. Dionne, C. Christoforou, K. Close, B. Sutcliffe, B. Giuliani, F. Li, M. Costa, G. Ihrke, G. W. Meissner, D. D. Bock, Y. Aso, G. M. Rubin, G. S. X. E. Jefferis, Neurogenetic dissection of the *Drosophila* lateral horn reveals major outputs, diverse behavioural functions, and interactions with the mushroom body. *eLife* **8**, e43079 (2019).
45. M.-J. J. Dolan, B.-G. Ghislain, A. S. Bates, S. Frechter, A. Lampit-Saint-Amax, Y. Aso, R. J. V. Roberts, P. Schlegel, A. Wong, A. Hammad, D. Bock, G. M. Rubin, T. Preat, P.-Y. Plaçais, G. S. X. E. Jefferis, Communication from learned to innate olfactory processing centers is required for memory retrieval in *Drosophila*. *Neuron* **100**, 651–668.e8 (2018).
46. H. Lerner, E. Rozenfeld, B. Rozenman, W. Huetteroth, M. Parnas, Differential role for a defined lateral horn neuron subset in naïve odor valence in *Drosophila*. *Sci. Rep.* **10**, 6147 (2020).
47. S. Cachero, M. Gkantia, A. S. Bates, S. Frechter, L. Blackie, A. McCarthy, B. Sutcliffe, A. Strano, Y. Aso, G. S. X. E. Jefferis, BAcTrace, a tool for retrograde tracing of neuronal circuits in *Drosophila*. *Nat. Methods* **17**, 1254–1261 (2020).
48. G. S. X. E. Jefferis, C. J. Potter, A. M. Chan, E. C. Marin, T. Rohlfing, C. R. Maurer Jr., L. Luo, Comprehensive maps of *Drosophila* higher olfactory centers: Spatially segregated fruit and pheromone representation. *Cell* **128**, 1187–1203 (2007).
49. G. B. West, J. H. Brown, B. J. Enquist, A general model for ontogenetic growth. *Nature* **413**, 628–631 (2001).
50. R. Iwata, P. Vanderhaeghen, Metabolic mechanisms of species-specific developmental tempo. *Dev. Cell* **59**, 1628–1639 (2024).
51. M. Diaz-Cuadros, T. P. Miettinen, O. S. Skinner, D. Sheedy, C. M. Díaz-García, S. Gapon, A. Hubaud, G. Yellen, S. R. Manalis, W. M. Oldham, O. Pourquié, Metabolic regulation of species-specific developmental rates. *Nature* **613**, 550–557 (2023).
52. J. J. Bourn, M. W. Dorrity, Degrees of freedom: Temperature's influence on developmental rate. *Curr. Opin. Genet. Dev.* **85**, 102155 (2024).
53. M. W. Dorrity, L. M. Saunders, M. Duran, S. R. Srivatsan, E. Barkan, D. L. Jackson, S. M. Sattler, B. Ewing, C. Queitsch, J. Shendure, D. W. Raible, D. Kimelman, C. Trapnell, Proteostasis governs differential temperature sensitivity across embryonic cell types. *Cell* **186**, 5015–5027.e12 (2023).
54. H. Cline, Synaptogenesis: A balancing act between excitation and inhibition. *Curr. Biol.* **15**, R203–R205 (2005).
55. S. R. Olsen, R. I. Wilson, Lateral presynaptic inhibition mediates gain control in an olfactory circuit. *Nature* **452**, 956–960 (2008).
56. C. M. Root, K. Masuyama, D. S. Green, L. E. Enell, D. R. Nässel, C.-H. Lee, J. W. Wang, A presynaptic gain control mechanism fine-tunes olfactory behavior. *Neuron* **59**, 311–321 (2008).
57. M. A. Böhme, A. W. McCarthy, A. T. Grasskamp, C. B. Beuschel, P. Goel, M. Jusyte, D. Laber, S. Huang, U. Rey, A. G. Petzoldt, M. Lehmann, F. Göttfert, P. Haghighi, S. W. Hell, D. Owald, D. Dickman, S. J. Sigrist, A. M. Walter, Rapid active zone remodeling consolidates presynaptic potentiation. *Nat. Commun.* **10**, 1085 (2019).
58. C. A. Frank, T. D. James, M. Müller, Homeostatic control of *Drosophila* neuromuscular junction function. *Synapse* **74**, e22133 (2020).
59. E. Rozenfeld, N. Ehmann, J. E. Manoim, R. J. Kittel, M. Parnas, Homeostatic synaptic plasticity rescues neural coding reliability. *Nat. Commun.* **14**, 2993 (2023).
60. S. A. Haddad, E. Marder, Circuit robustness to temperature perturbation is altered by neuromodulators. *Neuron* **100**, 609–623.e3 (2018).
61. E. Marder, T. O'Leary, S. Shruti, Neuromodulation of circuits with variable parameters: Single neurons and small circuits reveal principles of state-dependent and robust neuromodulation. *Annu. Rev. Neurosci.* **37**, 329–346 (2014).
62. R. Haase, Image processing filters for grids of cells analogous to filters processing grids of pixels. *Front. Comput. Sci.* **3**, 774396 (2021).
63. C. Martelli, J. R. Carlson, T. Emonet, Intensity invariant dynamics and odor-specific latencies in olfactory receptor neuron response. *J. Neurosci.* **33**, 6285–6297 (2013).
64. S. Gorur-Shandilya, M. Demir, J. Long, D. A. Clark, T. Emonet, Olfactory receptor neurons use gain control and complementary kinetics to encode intermittent odorant stimuli. *eLife* **6**, e27670 (2017).
65. C. Martelli, A. Fiala, Slow presynaptic mechanisms that mediate adaptation in the olfactory pathway of *Drosophila*. *eLife* **8**, e43735 (2019).
66. R. J. D. Moore, G. J. Taylor, A. C. Paulk, T. Pearson, B. van Swinderen, M. V. Srinivasan, FicTrac: A visual method for tracking spherical motion and generating fictive animal paths. *J. Neurosci. Methods* **225**, 106–119 (2014).
67. T. Walter, I. D. Couzin, Trex, a fast multi-animal tracking system with markerless identi cation, and 2d estimation of posture and visual elds. *eLife* **10**, e64000 (2021).

Acknowledgments: We thank M. Silies for access to resources; M. Silies, F. Calzolari, and S. Cachero for critical reading of the manuscript; C. Schnaitmann for help with in vivo imaging; L. F. Ramirez Ochoa for discussions of the model; C. Müller, N. Benjamin, and P. Krasnova for help with behavioral experiments; the biology workshop at JGU for developing the behavioral assay; C. Rickert for help with confocal imaging; M. Ioannidou, T. Walter, F. Francisco, and A. Albi for help with video tracking; S. Cachero and G. Jefferis for sharing a new BAcTrace construct; R. Hiesinger, A. Fiala, and M. Silies for sharing fly strains; D. Deutsch for materials for the spherical treadmill; and R. Hiesinger, C. Duch, B. Hassan, members of the FOR5289, and members of the Silies laboratory for discussions. We further thank S. Schmitt, S. Renner, and J. Chojetzki for technical and administrative support and the anonymous reviewers for valuable feedback. **Funding:** This work was supported by the DFG grants MA7804/2-1, MA7804/3-1, and the FOR5289 to C.M. and by the Institute for Quantitative and Computational Biosciences. **Author contributions:** Conceptualization: P.Z., L.L.B., S.C.B., G.D.U., C.D., and C.M. Methodology: P.Z., L.L.B., S.C.B., G.D.U., C.D., and C.M. Software: G.D.U. and C.D. Formal analysis: C.M. Investigation: P.Z., L.L.B., S.C.B., G.D.U., C.D., and C.M. Data Curation: P.Z., L.L.B., S.C.B., G.D.U., C.D., and C.M. Writing—original draft: L.L.B. and C.M. Writing—review and editing: P.Z., L.L.B., S.C.B., G.D.U., C.D., and C.M. Visualization: P.Z., L.L.B., S.C.B., G.D.U., C.D., and C.M. Supervision: C.M. Funding acquisition: C.M. **Competing interests:** The authors declare that they have no competing interests. **Data and materials availability:** All data needed to evaluate the conclusions in the paper are present in the paper and/or the Supplementary Materials. Raw data, scripts, and software for data curation and analysis have been deposited in Zenodo and are accessible at https://doi.org/10.5281/zenodo.14203758. Additional resources are available on GitLab https://gitlab.rlp.net/mrtlllab/zuefle_batista_etal_2024.

Submitted 19 April 2024
Accepted 6 December 2024
Published 15 January 2025
10.1126/sciadv.adp9587

Science Advances
AAAS

Supplementary Materials for

Impact of developmental temperature on neural growth, connectivity, and function

Pascal Züfle *et al.*

Corresponding author: Carlotta Martelli, cmartell@uni-mainz.de

Sci. Adv. **11**, eadp9587 (2025)
DOI: 10.1126/sciadv.adp9587

This PDF file includes:

Figs. S1 to S6
Tables S1 and S2

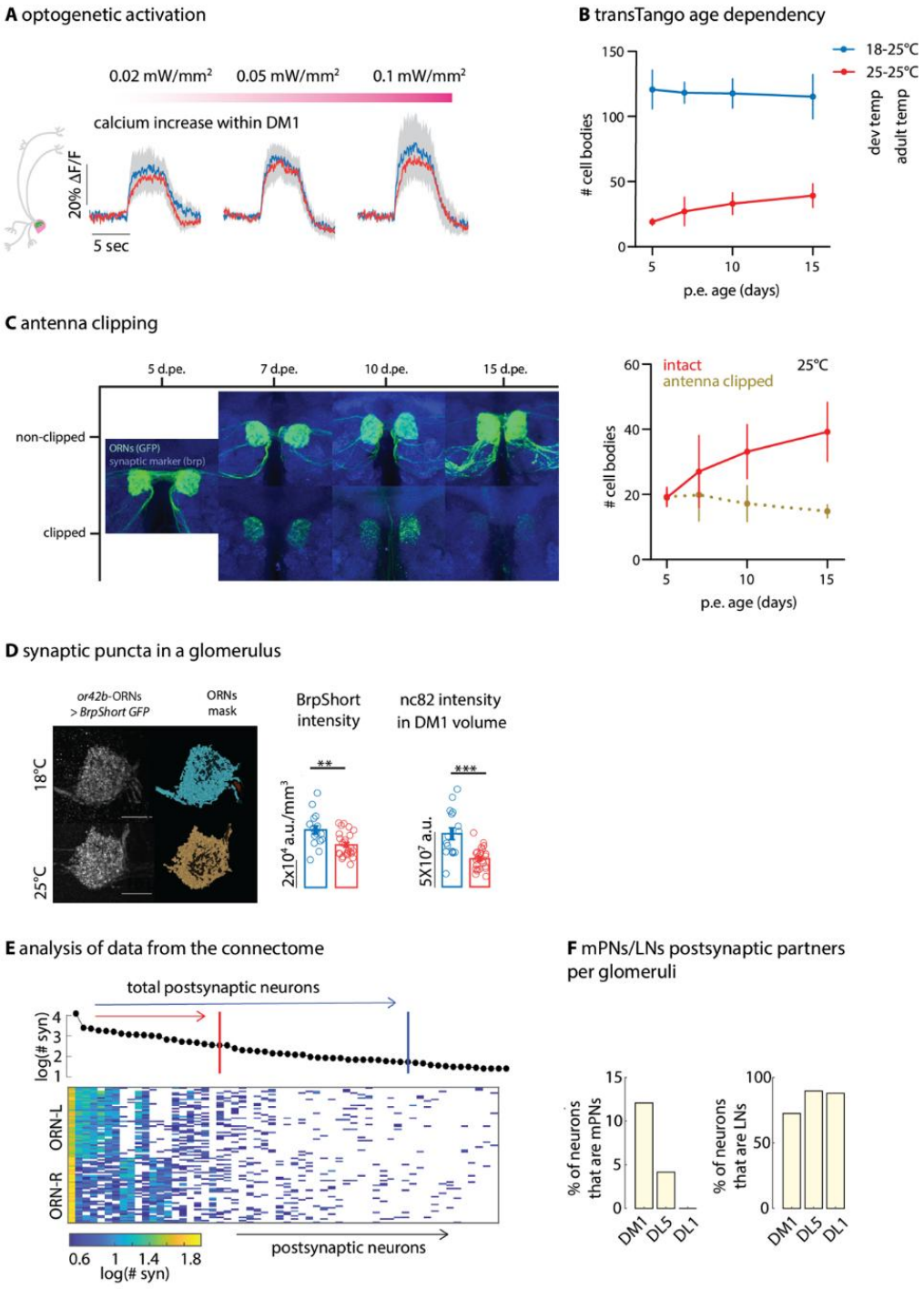

Fig. S1. Tool validation and anatomical quantifications. (A) Optogenetic activation of *Or42b*-ORNs in flies developed at different temperatures. The usual trans-Tango reporter dsRed was replaced by GCaMP6s, and activity of presynaptic neurons induced by CsChrimson. Mean optogenetic response of DM1-postsynaptic partners was quantified in the glomerulus for three stimuli intensities. **(B)** Mean number of cell bodies in the AL labeled by trans-Tango as post-

synaptic partners of *Or42b*-ORNs measured at different ages after eclosion. Error bars indicate standard deviation (N = 5-10). **(C)** Sample confocal images showing the axons of *Or42b*-ORNs across days post eclosion in control flies (top) and in flies whose antenna were clipped on day 5 (bottom). The decrease in GFP indicates axon degeneration. Right: mean number of cell bodies in the AL labeled by transTango as post-synaptic partners of *Or42b*-ORNs measured at different ages after eclosion in control and antenna-clipped flies (N = 8-12). Overall, these experiments indicate that the transTango reporter accumulates over time, nonetheless it is able to detect changes in synaptic connectivity that occur in the adult. The response time could be somewhat slow. **(D)** Left to right: $Brp^{[Short]}$-GFP fluorescence expressed in *Or42b*-ORNs and glomerulus 3D mask reconstructed from it for the two temperatures. Quantification of $Brp^{[Short]}$-GFP and nc82 puncta intensity within the whole glomerulus volume (error bars indicate SEM, n = 16 hemibrains at 18°C and n = 25 at 25°C, Kruskal-Wallis test, $**p<10^{-2}$, $***p<10^{-3}$). **(E)** Bottom: heatmap of the connectivity matrix from hemibrain EM data illustrating the number of synapses made by DM1-ORNs from both antennae on postsynaptic partners in the right hemisphere. Post-synaptic partners on the x-axis are ranked by the total number of input synapses from these ORNs, as quantified in the top plot. Color scale indicates the number of synapses in log scale. The red and blue bar indicate the mean number of postsynaptic partners counted within one hemisphere in the trans-Tango experiment. **(F)** Percentage of postsynaptic neurons that have been annotated in the Hemibrain dataset as multiglomerular projection neurons (mPNs, left) and local neurons (LNs, right).

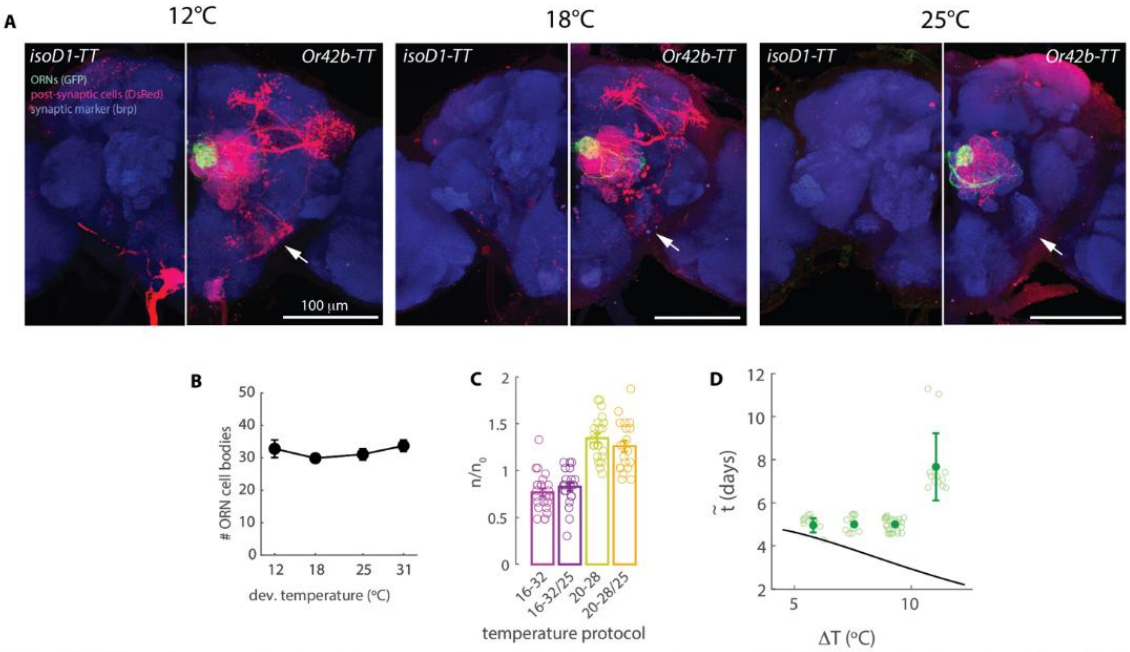

Fig. S2. Development at extreme and cycling temperatures. (A) Sample brains developed at three different temperatures show trans-Tango labeling of new cell types (arrows) connected to *Or42b*-ORNs at low temperatures. Images for 18 and 25°C are reproduced from Figure 1B. In flies developed at 12°C, trans-Tango labels neurons that innervate the saddle (SAD), one of the four SEZ subregions, which is not labeled at other temperatures. The left images are from genetic controls for the trans-Tango tool crossed to a control line (isoD1). **(B)** Mean number of ORNs cell bodies as a function of temperature (error bars indicate SEM, N=9-11). Note that this figures also includes data shown in main Fig. 4B. **(C)** Fold change in synaptic partners from 25°C for development on cycling temperatures. Temperature manipulations were applied only between L3 and P-100% then flies were moved to 25°C, except for the light-purple (16-32) and light-yellow (20-28) bars for which flies were kept through adulthood at the cycling temperatures (N=10-12). **(D)** Developmental times (adult eclosion) for pupae developed on temperature cycles of different amplitude (ΔT, mean temperature was 24°C) (N=12-25). The black line indicates the model prediction. Developmental times deviates from the model prediction, despite the nice agreement of the model with the measured connectivity (Fig. 2Q of main text), indicating a disruptive effect of temperatures above 30°C.

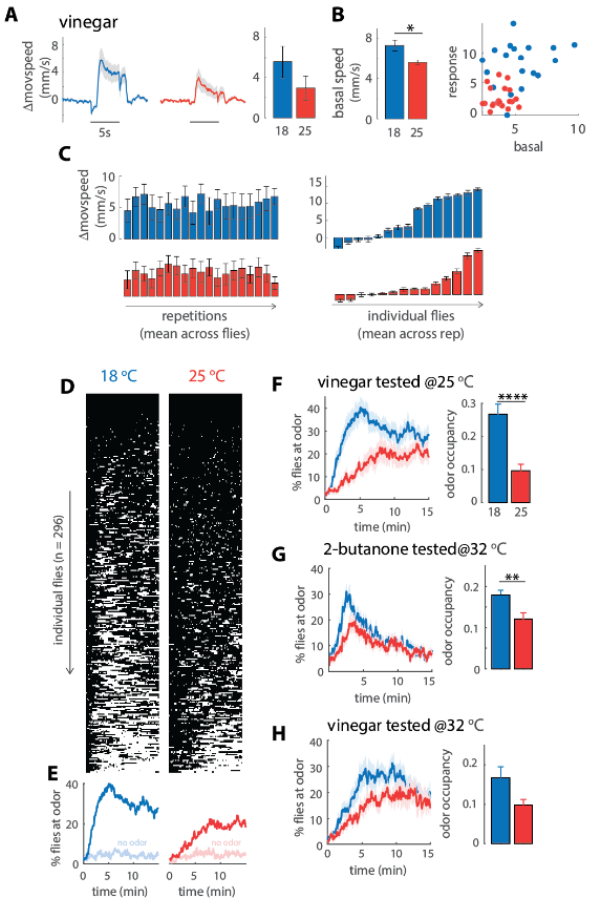

Fig. S3. Effects of developmental temperature on odor driven behavior. A-C) Response to vinegar on the spherical treadmill setup for flies developed at 18°C (blue) and 25°C (red). **(A)** Odor response calculated as change in moving speed as a function of time in response to 5s stimulation; bar plot: mean change in moving speed within the first 2s of stimulation ($p = 0.1$, N=14,13). **(B)** Left: mean basal walking speed is estimated from the 3s preceding stimulus onset ($p = 0.02$). Right: scatter plot of basal walking speed vs odor response for individual flies, showing that in both conditions basal and response behaviors are not correlated: both flies with high and low basal speed can respond strongly to the odor. **(C)** Mean response to each consecutive stimuli repetitions averaged across all flies (right), and mean response of each individual fly across repetitions, showing large variation across individuals (left). **(D-H)** Behavioral response in the free walking assay. **(D)** Binary maps showing individual flies located at the odor source (<5 cm, white) as a function of time and **(E)** percentage of flies at the odor (vinegar). An empty odor vial was used as control in an independent set of experiments (shaded curves). **(F)** Average percentage of flies at the odor source and odor occupancy (bar plot), for vinegar tested at 25°C ($p<10^{-4}$, N=21,20). **(G)** same as in (f) for a testing temperature of 32°C for 2-butanone ($p=0.006$, N=20,20) and **(H)** vinegar ($p=0.09$, N=19,18). Shaded area and error bars indicate SEM.

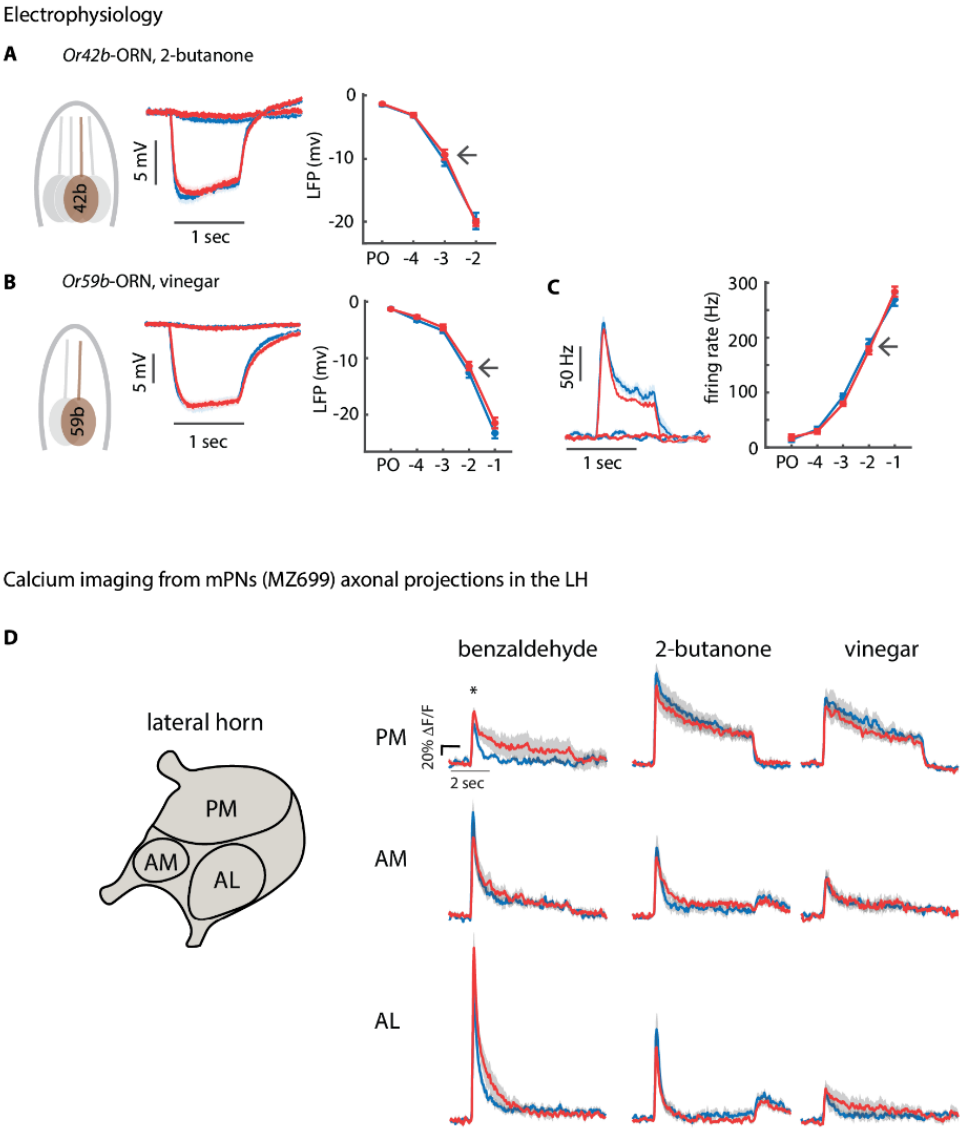

Fig. S4. Effects of developmental temperature on odor encoding. (A) Left to right: Single sensillum recordings from the ab1 sensillum containing a single *Or42b*-ORN. Mean response of the LFP to a 1s pulse of 2-butanone at 10^{-3} dilution and Paraffin Oil (PO) control. Amplitude of the LFP calculated as the maximum drop for each odor concentration. **(B)** Same as for the ab2 sensillum containing one *Or59b*-ORN. **(C)** Firing rate response of ab2 to a 1s pulse of 2-butanone at 10^{-3} dilution and PO control calculated in 100ms sliding window. Right: mean peak response for each concentration tested. **(D)** Calcium imaging from the axon terminals of mPNs labeled by *MZ699-Gal4*. For functional quantification, the LH was divided in regions based on Strutz et al. (24): posterior-medial (PM), anterior-medial (AM) and anterior-lateral (AL). As previously reported the posterior-medial LH is more sensitive to appetitive odors (N=6-10). All response curves are mean responses and shaded areas are SEM (*p<0.05).

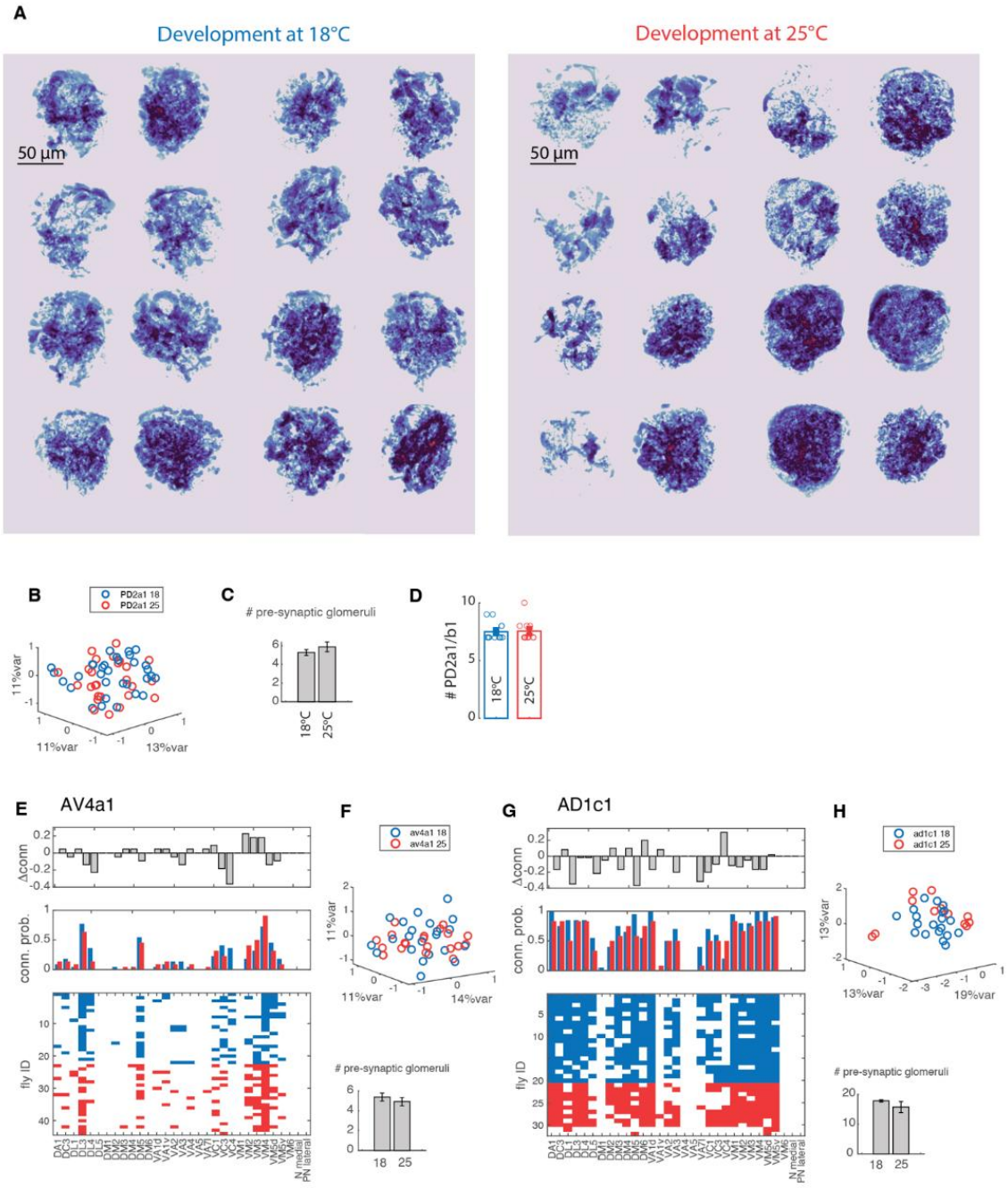

Fig. S5. Connectivity analysis of LH neurons. (A) Dendritic arborizations of neurons pre-synaptic to PD2a1/ as labeled by retro-Tango in individual brains. All brains developed at 18°C show stronger and more uniform innervation of the AL as compared to brain that developed at 25°C, which have more asymmetric innervations of the two hemibrains. **(B)** PCA of connectivity matrix of PD2a1/b1 to the AL glomeruli as quantified from BAcTrace in main Fig. 5G: each dot indicates a single hemibrain. (**C**) Mean number of pre-synaptic glomeruli for PD2a1/b1 in each hemibrain. (**D**) Bar plot showing mean number of PD2a1/b1 neurons labeled by the split-Gal4 line at the two developmental temperatures (error bars are SEM, N=12/11 hemibrains). (**E and G)** As main Fig.

5C-D-E for AV4a1 and AD1c1. Bottom: binary connectivity matrix. Middle: Connection probability to each glomerulus. Top: difference in connectivity between 25°C and 18°C. Middle and top panel are the same as in Fig. 5J. (**F and H**) As (C) and (D) for AV4a1 and AD1c1.

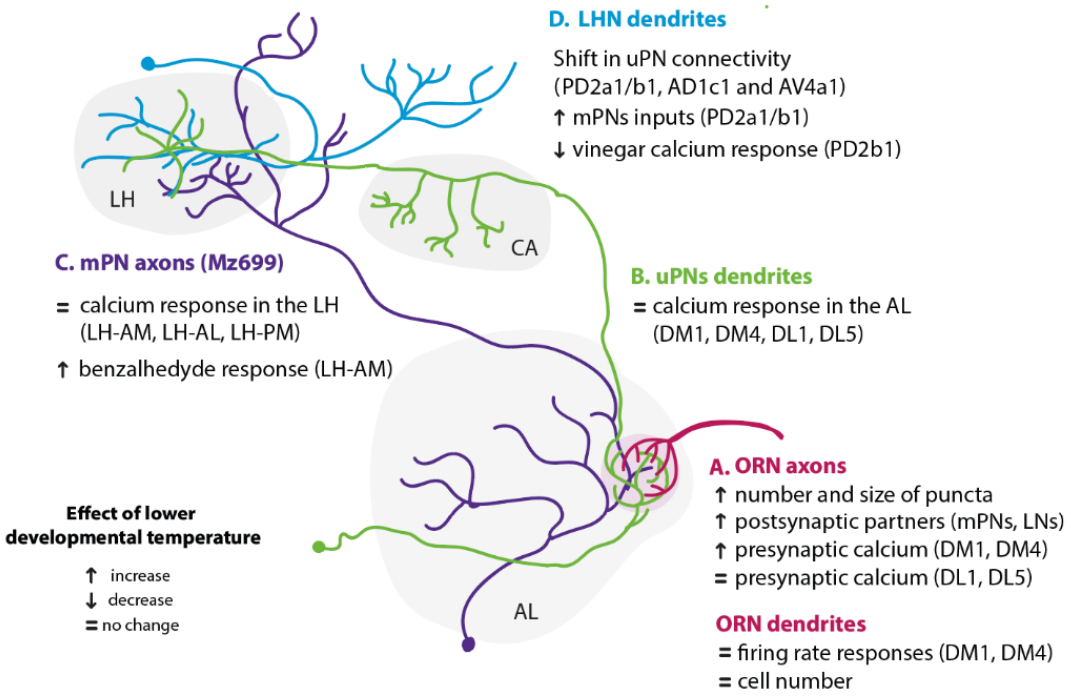

Fig. S6. Overview of study findings throughout the olfactory system. Changes are indicated as found in flies developed at 18°C relative to 25°C. Subpanels indicate different system levels analyzed. **(A)** ORN axons and dendrites, **(B)** uPNs dendrites, **(C)** mPNs axons, and **(D)** LHNs dendrites.

Reagent or Resource	Source	Identifier
Antibodies		
chicken anti-GFP	Abcam	Abcam Cat# ab13970, RRID:AB_300798
rabbit anti-DsRed	Takara Bio	Takara Bio Cat# 632496, RRID:AB_10013483
Mouse anti-nc82	deposited to the DSHB by Buchner, E.	DSHB Cat# nc82, RRID:AB_2314866
Goat anti-chicken Alexa Fluor 488	Jackson Immunoresearch	Jackson ImmunoResearch Labs Cat# 103-545-155, RRID:AB_2337390
Donkey anti-rabbit Alexa Fluor 568	Thermo Fisher Scientific	Thermo Fisher Scientific Cat# A10042, RRID:AB_2534017
Donkey anti-mouse Alexa Fluor 647	Thermo Fisher Scientific	Thermo Fisher Scientific Cat# A-31571, RRID:AB_162542
Chemicals		
PBS	GIBCO	Art. #70011044
Paraformaldehyde	Polysciences	Art. #00380-1
Triton X-100	Roth	Art. #3051.2
Normal goat serum	Thermo Scientific	Art. #31872
VectaShield	Biozol	Art. #VEC-H-1000
Apple Cider Vinegar	Ja! REWE, Apfel Essig	N/A
2-butanone	Sigma-Aldrich Co.	Art. #34861-M, CAS 78-93-3
Benzaldehyde	Sigma-Aldrich Co.	Art. #B1334, CAS 100-52-7
Mineral Oil	Sigma-Aldrich Co.	Art. #330779-1L, CAS 8042-47-5
All trans retinal	Sigma-Aldrich Co.	Art. #R2500
Sigmacote®	Sigma-Aldrich Co.	Art. #SL2
Experimental Models: Organisms/Strains		
D. melanogaster: *UAS-brpD3::GFP*	Gift from R. Heisinger	N/A
D. melanogaster: *Or42b-Gal4*	Bloomington Drosophila Stock Center (BDSC)	RRID: BDSC_9972
D. melanogaster: *Or7a-Gal4*	BDSC	RRID: BSDC_23907
D. melanogaster: Or10a-Gal4	BDSC	RRID: BSDC_9944
D. melanogaster: trans-Tango	BDSC	RRID: BSDC_77124

D. melanogaster: QUAS-GCamp6s; trans-Tango	BDSC	RRID: BSDC_95316
D. melanogaster: PD2a1/b1 split-Gal4 (R48F03-p65AD; R37G11-Gal4DBD)	BDSC	RRID: BSDC_86654
D. melanogaster: BAcTrace (w^+,QUAS-mtdTomato_UAS-CD2(attp8); pJFRC19-Syb::GFP-P10(VK37) VT033006-LexAp65(JK22C) LexAop-minQf-noV5-minSNAP25-HIVNES-Syntaxin(VK18);P{20XUASI-B3R.PEST}attp2 pJFRC161-B3RT-B2B3RT-HBMBoNTa2xGFPnb(VK5) QUAS-mtdTomato::HA)	Gift from S. Cachero	N/A
D. melanogaster: GH146-Gal4	Gift from A. Fiala	N/A
D. melanogaster: Orco-Gal4	BDSC	RRID: BSDC_23292
D. melanogaster: isoD1	Gift from M. Silies	N/A
D. melanogaster: UAS- GCaMP6f	BDSC	RRID: BSDC_42747
D. melanogaster: UAS-CsChrimson	BDSC	RRID: BSDC_82181
D. melanogaster: retro-Tango	BDSC	RRID: BSDC_99661
Software and algorithms		
ImageJ		RRID:SCR_003070
Leica Application Suite X	Leica	RRID:SCR_013673
MATLAB	MathWorks	RRID:SCR_001622
Adobe Illustrator	Adobe	RRID:SCR_010279
Hemibrainr (v. 0.1.0)	*(21)*	https://github.com/natverse/hemibrainr
Pylon viewer (64-Bit, 6.3.0.10295)		
FicTrac	*(64)*	
Trex 1.1.8_3	*(65)*	RRID:SCR_022361
Python 3.9.12		RRID:SCR_008394
RStudio		RRID:SCR_000432
Napari-pyclesperanto	*(60)*	https://github.com/clEsperanto/pyclesperanto_prototype

Supplementary Table 1. Resources table for all used antibodies, chemicals and experimental organisms used in this study, with their respective source and identifier.

Name	Genotype	Figure
Or42b > trans-Tango	*w+, UAS-myrGFP.QUAS-mtdTomato-3xHA; trans-Tango / CyO ; Or42b-Gal4 / +*	Fig. 1B-D, Fig. 1M, Fig. 2A-E, Fig. S1B,C, Fig S2
Or42b > trans-Tango QUAS-GCaMP6s	*w+ 10x QUAS-GCaMP6s; trans-Tango / UAS-CsChrimson; or42b-Gal4 / +*	Fig. 1F-G, Fig S.1A
Or42b > Brp^{Short} GFP	*;+;UAS-BRP D3::GFP/or42b-Gal4*	Fig. 1I-J, Fig S.1D
Or7a > trans-Tango	*w+, UAS-myrGFP.QUAS-mtdTomato-3xHA; trans-Tango / Or7a-Gal4*	Fig. 1N
Or10a > trans-Tango	*w+, UAS-myrGFP.QUAS-mtdTomato-3xHA; trans-Tango / Or10a-Gal4*	Fig. 1O
GH146 > GCaMP6f	*w+; UAS-GCaMP6f/ GH146-Gal4*	Fig. 2N,O Fig. 4D
Or42b > GFP	*w+, UAS-myrGFP.QUAS-mtdTomato-3xHA; trans-Tango / CyO ; or42b-Gal4 / +*	Fig. 4B
Orco > GCaMP6f	*w+; UAS-GCamp6f / +; orco-Gal4 / +*	Fig. 4A,C, Fig. S4A-B
PD2a1/b1 > *BacTrace*	*w+, QUAS-mtdTomato,UAS-CD2/+; Syb::GFP, VT033006-LexAp65, LexAop-minQf-noV5-minSNAP25-HIVNES-Syntaxin/R48F03-p65AD; UASI-B3R.PEST,B3RT-B2B3RT-HBMBoNTa2xGFPnb, QUAS-mtdTomato::HA / R37G11-Gal4DBD*	Fig. 5E-I, Fig. S5B-D
PD2a1/b1 > *GCaMP6f*	*w+; UAS-GCaMP6f/ R48F03-p65AD ; R37G11-Gal4DBD / +*	Fig. 5K
AD1c1 > *BacTrace*	*w+, QUAS-mtdTomato,UAS-CD2/+; Syb::GFP, VT033006-LexAp65, LexAop-minQf-noV5-minSNAP25-HIVNES-Syntaxin/R55C09-GAL4; UASI-B3R.PEST,B3RT-B2B3RT-HBMBoNTa2xGFPnb, QUAS-mtdTomato::HA / +*	Fig. 5J, Fig. S5G,H
AV4a1 > *BacTrace*	*w+, QUAS-mtdTomato,UAS-CD2/+; Syb::GFP, VT033006-LexAp65, LexAop-minQf-noV5-minSNAP25-HIVNES-Syntaxin/ R34C08-p65.AD; UASI-B3R.PEST,B3RT-B2B3RT-HBMBoNTa2xGFPnb, QUAS-mtdTomato::HA / R22C12-GAL4DBD}*	Fig. 5J, Fig. S5E,F
PD2a1 > *retro-Tango*	*y w+ QUAS-mtdTomato-3xHA; retro-Tango / + ; 10xUAS-retro-Tango/ R48F03-p65AD; R37G11-Gal4DBD / +*	Fig. 5A-D, Fig. S5A
isoD1 > *trans-Tango*	*w+, UAS-myrGFP.QUAS-mtdTomato-3xHA/isoD1; trans-Tango / isoD1*	Fig. S2A
MZ699 > GCaMP8f	*w+; UAS-GCaMP8f/+; MZ699-Gal4/+*	Fig. S4D

Supplementary Table 2. Fly strains used in the paper, separated by used name, full genotype and figure in which it appears.

5 Discussion

In this dissertation I have explored how plasticity impacts robustness of neuronal function and behavior in the olfactory system of *Drosophila melanogaster*. I have focused on the effects of two types of plasticity - long-term developmental plasticity and short-term stimulus-driven plasticity (adaptation) – on the first neuropil of the olfactory system, the antennal lobe (AL), a key structure that relays information directly to higher brain regions.

We employed developmental temperature as a tool to probe developmental plasticity, since it was known that lower developmental temperatures (compared to the laboratory standard of 25°C) yield more synaptic connections and more postsynaptic partners in the fly visual system (Kiral et al., 2021). We observed similar results in the olfactory system, in the AL: the number of postsynaptic partners of olfactory receptor neurons (ORNs) was increased in flies developed at 18°C when compared to flies developed at 25°C (Züfle et al., 2025 - manuscript in section 4.3 - figure 1L). However, different ORN types (which innervate different glomeruli) recruited different postsynaptic cells (defined by their cell body location), with possible differential effects on odor coding across glomeruli (Züfle et al., 2025 - manuscript in section 4.3 - figure 1M-O). Consistently with this, I found that ORN responses (measured from their axon terminals) are larger in flies developed at lower temperatures for some of the glomeruli but not for all (Züfle et al., 2025 - manuscript in section 4.3 - figure 4C). Surprisingly, the responses of projection neurons postsynaptic to each of these glomeruli were independent of developmental temperature (Züfle et al., 2025 - manuscript in section 4.3 - figure 4D). **This result is exciting because it shows that the antennal lobe can wire differently and process stimuli differently while still producing a robust outcome**, i.e. the same odor representations. In the future, it will be interesting to study how. Our hypothesis is that inhibitory LNs are differentially recruited across temperatures and drive different amounts of inhibition. This hypothesis can be tested experimentally, for example, by silencing LNs (blocking their synaptic output) and testing if odor representations are disrupted at lower temperatures.

Background adaptation is observed in the peripheral firing rate responses of ORNs (Brandão et al., 2025 - manuscript in section 4.2 - figure 2b). My main project investigated if and how adaptation in single ORNs leads to robust combinatorial odor representations in downstream circuits in the olfactory system. We find that ORN adaptation is undone in the antennal lobe: odor representations in both presynaptic ORNs and postsynaptic PNs are robust to the background for ON stimuli (Brandão et al., 2025 - manuscript in section 4.2 - figures 3 and 6). On the other hand, responses for OFF stimuli collapse in a low activity state (Brandão et al., 2025 - manuscript in section 4.2 - figures 3 and 6). This undoing of adaptation is possible thanks to a homeostatic inhibitory feedback loop and synaptic plasticity (Brandão et al., 2025 - manuscript in section 4.2 - figures 4 and 7). Interestingly, we found that only an adaptation strategy of firing rate where modulation occurs in the activity domain (as opposed to the stimulus domain, as is the case for photoreceptors) can achieve this background invariance (Brandão et al., 2025 - manuscript in section 4.2 - figure 5). We propose that **the antennal lobe uses contrast information encoded in the ORN populations to enhance the separation between ON and OFF stimuli, while keeping odor identity information robust for ON stimuli**.

5.1 The neurons behind the homeostatic inhibitory feedback loop

We have identified LNs as the likely neurons implementing the homeostatic inhibitory feedback loop but have not determined which LN subtype is specifically relevant for background normalization

(Brandão et al., 2025 - manuscript in section 4.2 - figure 4k). The AL is innervated by a very heterogeneous population of LNs with different anatomical and physiological properties (Chou et al., 2010; Barth-Maron et al., 2023; Schenk and Gaudry, 2023). Schlegel et al. (2021) have described 4 anatomical types of LNs based on EM connectome data. Two of these, patchy and full LNs, have been functionally characterized (Barth-Maron et al., 2023). Full LNs have widespread responses throughout the AL, making them good candidates to implement inter-glomerular background compensation (Barth-Maron et al., 2023). On the other hand, patchy LNs have been found to respond in graded potentials that are restricted to the activated glomerulus and could be involved in local background compensation (Barth-Maron et al., 2023; Schenk and Gaudry, 2023). However, future work is required to determine which LNs are responsible for undoing ORN adaptation. This can be done by silencing specific LNs. Besides physiological characteristics discussed above, an in-depth analysis of the connectome should inform which LNs to investigate, since we know we are looking, for example, for LNs that not only receive substantial inputs from ORNs but also have outputs on the same ORNs. **Overall, we reveal background compensation as a novel function of antenna lobe LNs, providing a new functional framework to understand the role of this very diverse family of neurons**.

5.2 Glomerular variability

While lateral inhibition clearly plays a role for background compensation in most glomeruli, it might not be the sole mechanism. At least in one glomerulus (DL5), blocking of acetylcholine (ACh) receptors and of gamma-aminobutyric acid (GABA) receptors did not affect responses, and the outcome of these experiments had some variability between some glomeruli where a phenotype was observed (Brandão et al., 2025 - manuscript in section 4.2 - figure S2b). In these experiments, the glial sheath around the AL is removed manually and only where it is exposed. However, glial cells also establish a network of processes inside the AL (Oland et al., 2008). This network is quite sparse when compared to other organisms, not forming a continuous border around the glomeruli (Oland et al., 2008). Moreover, it is not homogeneous, with different amounts of glial processes not only around but also infiltrating each glomerulus (Oland et al., 2008). If the glial processes formed a complete glial envelope around each glomerulus, one would expect that only surface glomeruli that are exposed and where the glial sheath is removed would be affected by drug application. This means all the other glomeruli would be equally protected and not affected, which would not explain our findings. It is the variability of glial infiltration combined with its sparseness that makes it possible that the differences in pharmacology we observe are a result of the different degrees of insulation by the glial sheath, leading to differences in drug penetration that would not be explained only by the anatomical location of the glomeruli. But variability in pharmacology can be overcome by using genetic tools. One approach is to downregulate GABA receptors in ORNs; another possibility is to silence LNs by blocking their synaptic output. If glomerular variability is still observed, other mechanisms must be considered, such as a potential role for PNs, which was only excluded so far for glomerulus DM4 (Brandão et al., 2025 - manuscript in section 4.2 - figure S1e).

5.3 Background invariance – from ORNs to PNs

We have discovered an inhibitory feedback compensation responsible for undoing peripheral adaptation in ORNs, resulting in calcium responses in ORN axon terminals that are not only background invariant but also tonic. Moreover, we found that synaptic plasticity is required for background invariance to be relayed to PNs. Our working model posits that the tonic calcium response in ORNs during the background modulates synaptic transmission resulting in background-invariant PN responses, thereby linking presynaptic to postsynaptic background invariance.

Unc13 proteins have been previously shown to mediate different types of presynaptic plasticity through calcium-dependent pathways at the neuromuscular junction in *Drosophila melanogaster* (Böhme et al., 2016, 2019; Walter et al., 2018; Jusyte et al., 2023; Blaum et al., 2025). We have shown that synaptic plasticity through Unc13 proteins is required for PNs to maintain background-invariant responses (Brandão et al., 2025 - manuscript in section 4.2 - figure 7). It remains unclear, however, whether this requirement comes directly from the ORN-PN synapses or from ORN synapses to/from LNs. This question will be answered in the future by comparing presynaptic ORN calcium responses in Unc13 mutant flies to control flies.

More work is also required to clarify which GABA receptors are involved in background compensation in ORNs, since both ionotropic GABA-A and metabotropic GABA-B are expressed in the AL (Wilson and Laurent, 2005; Root et al., 2008; McLaughlin et al., 2021). This can be assessed by downregulating each receptor type in ORNs and measuring presynaptic ORN calcium responses. By repeating this experiment but measuring postsynaptic PN responses instead, we can confirm if tonic calcium responses in ORNs are indeed required for PN responses to be background invariant.

Finally, we must elucidate how GABAergic inhibition modulates presynaptic ORN calcium and synaptic plasticity, which will depend on the GABA receptors found to be involved. In a preliminary experiment, I depleted calcium from internal stores with caffeine (data not shown) and found that ORN calcium responses in glomerulus DL1 became transient and background dependent, recapitulating the phenotype of blocking GABA receptors in this glomerulus (Brandão et al., 2025 - manuscript in section 4.2 - figure 4k). This indicates that calcium release from internal stores is required for background compensation in ORNs, suggesting the involvement of metabotropic GABA-B receptors. Subsequent experiments will focus on disrupting the different mechanisms that can lead to calcium release from internal stores to identify the responsible pathway.

Altogether, future research is imperative to understand how GABAergic inputs to ORNs undo peripheral adaptation and how synaptic output is modulated to elicit background-invariant PN responses. **Nevertheless, this study marks the beginning of the generalization of synaptic plasticity mechanisms that, in *Drosophila melanogaster*, were once confined to the neuromuscular junction to central brain computations that are fundamental to sensory processing**.

5.4 Odor representations downstream of the antennal lobe

Why would a neuronal circuit implement a computation – single neuron adaptation – just so that it can be later undone? We have found that ORN firing rate adaptation makes it possible to reach asymmetry between ON and OFF stimuli, with ORN calcium responses to OFF stimuli collapsing in a low-response state while responses to ON stimuli become background invariant. Another potential benefit regards decreased energy consumption, but one would have to quantify how much energy is saved by ORN firing rate adaptation and compare it to the energy cost of undoing it at the AL to verify this possibility.

The asymmetric background-invariant odor representation that we found in PNs is then sent to the lateral horn and the mushroom body. We have discussed before that finding an odor source in an environment without wind would simply require the encoding of the odor gradient through contrast (see Introduction, section 3.3). While we found that contrast is not encoded explicitly at the level of the AL, background-invariant PN responses allow for contrast computations for ON stimuli in downstream circuits while also having access to other stimulus information such as odor identity. The lateral horn could be the substrate for such computations (Kim et al., 2025). Interestingly, we found that representations of OFF stimuli collapse in a low response state. This suggests that precise information about the OFF stimulus, such as identity and contrast, cannot be accessed, and perhaps is

not needed during navigation. Asymmetry between ON and OFF coding is consistent with the very different behaviors elicited by ON (upwind walk) and OFF (local search) stimuli (Álvarez-Salvado et al., 2018).

Background invariance of ON responses might also be useful in associative learning. In the mushroom body, associative learning occurs when an odor and a reinforcement are experienced concurrently and it leads to a change in the animal's response to the odor (Cognigni et al., 2018). This memory can only be functional if retrieval can happen independently of any possible odor backgrounds, which is only feasible if the odor representation is background invariant. However, whether odor representations in the mushroom body are also background invariant remains to be tested and could be the subject of a follow-up study.

While we have gained a new insight into how first- and second-order neurons at the periphery of the olfactory system manage background stimuli to ensure that robust odor representations reach higher brain regions, further work is needed to confirm the functional advantages of asymmetric background invariance. This will help to elucidate how such coding strategies shape odor representations in downstream regions and how they ultimately influence behavior.

5.5 Conclusions and outlook

In this dissertation I have looked at plasticity in the olfactory system in response to changes in temperature during development and in response to odor background stimuli. In both studies, my focus was on the first relay in the olfactory system – the antennal lobe. I have found evidence that odor representations in this neuropil are robust in both contexts, with functional output being unchanged by developmental temperature and by background odors. Our data point to a critical role for inhibitory local neurons in both these conditions. These results suggest a possible strategy where the antennal lobe consolidates the combinatorial odor representation (through background compensation, *divisive normalization* and intraglomerular inhibition) while prioritizing robustness. This should ensure that all important information about the stimulus can be sent to and recovered in all these conditions by higher brain regions such as the lateral horn and the mushroom body.

In both conditions, the local network of inhibitory neurons in the antennal lobe seems to play central roles. Throughout development, LNs are flexibly recruited to keep AL function invariant across temperatures; acutely, different amounts of LN activity are recruited across background conditions to ensure odor coding invariance. In the future, these two frameworks will be useful to assign functions to the different LN types and to explain their functional and anatomical diversity.

Altogether, this work advances our understanding of the computations performed in the complex network of the antennal lobe while establishing new paths for future research. Moreover, it highlights the remarkable ability of neuronal circuits to maintain robustness despite variation-induced plasticity across a wide range of timescales.

6 Bibliography

Álvarez-Salvado E, Licata AM, Connor EG, McHugh MK, King BMN, Stavropoulos N, Victor JD, Crimaldi JP, Nagel KI (2018) Elementary sensory-motor transformations underlying olfactory navigation in walking fruit-flies. Elife 7: e37815.

Anton S, Rössler W (2020) Plasticity and modulation of olfactory circuits in insects. Cell Tissue Res.

Barlow HB (1961) Possible Principles Underlying the Transformations of Sensory Messages. In: Sensory Communication (Walter A. Rosenblith, Ed.). The MIT Press, p. 217–234.

Barth-Maron A, D'Alessandro I, Wilson RI (2023) Interactions between specialized gain control mechanisms in olfactory processing. Current Biology 33(23): 5109–5120.

Benda J (2021) Neural adaptation. Current Biology 31(3): R110–R116.

Bhandawat V, Olsen SR, Gouwens NW, Schlief ML, Wilson RI (2007) Sensory processing in the Drosophila antennal lobe increases reliability and separability of ensemble odor representations. Nat Neurosci 10(11): 1474–1482.

Blaum N, Ghelani T, Götz TWB, Chronister KS, Bengochea M, Ceresnova L, Christensen CF, Moulin TC, Kern H, Thomas U, Heine M, Sigrist SJ, et al. (2025) Monoamine-induced diacylglycerol signaling rapidly accumulates Unc13 in nanoclusters for fast presynaptic potentiation. PNAS 122(34): e2514151122.

Boccaccio A, Menini A (2007) Temporal Development of Cyclic Nucleotide-Gated and Ca^{2+}- Activated Cl^- Currents in Isolated Mouse Olfactory Sensory Neurons. J Neurophysiol 98(1): 153–160.

Boekhoff I, Tareilus E, Strotmann J, Breer H (1990) Rapid activation of alternative second messenger pathways in olfactory cilia from rats by different odorants. EMBO J 9(8): 2453–2458.

Böhme MA, Beis C, Reddy-Alla S, Reynolds E, Mampell MM, Grasskamp AT, Lützkendorf J, Bergeron DD, Driller JH, Babikir H, Göttfert F, Robinson IM, et al. (2016) Active zone scaffolds differentially accumulate Unc13 isoforms to tune Ca^{2+} channel–vesicle coupling. Nat Neurosci 19(10): 1311–1320.

Böhme MA, McCarthy AW, Grasskamp AT, Beuschel CB, Goel P, Jusyte M, Laber D, Huang S, Rey U, Petzoldt AG, Lehmann M, Göttfert F, et al. (2019) Rapid active zone remodeling consolidates presynaptic potentiation. Nat Commun 10(1): 1085.

Brandão SC, Ramirez L, Züfle P, Walter AM, Silies M, Martelli C (2025) Undoing of firing rate adaptation enables invariant population codes. bioRxiv.

Brandão SC, Silies M, Martelli C (2021) Adaptive temporal processing of odor stimuli. Cell Tissue Res 383: 125–141.

Breer H, Boekhoff I, Tareilus E (1990) Rapid kinetics of second messenger formation in olfactory transduction. Nature 345: 65–68.

Brunet LJ, Gold GH, Ngai J (1996) General Anosmia Caused by a Targeted Disruption of the Mouse Olfactory Cyclic Nucleotide–Gated Cation Channel. Neuron 17(4): 681–693.

Buck L, Axel R (1991) A Novel Multigene Family May Encode Odorant Receptors: A Molecular Basis for Odor Recognition. Cell 65(1): 175–187.

Burkhardt DA (1994) Light Adaptation and Photopigment Bleaching in Cone Photoreceptors in situ in the Retina of the Turtle. The Journal of Neuroscience 14(3): 1091–1105.

Cain WS (1970) Odor intensity after self-adaptation and cross-adaptation. Percept Psychophys 7(5): 271–275.

Cardé RT (2021) Navigation Along Windborne Plumes of Pheromone and Resource-Linked Odors. Annu Rev Entomol 66: 317–336.

Chen T-Y, Yau K-W (1994) Direct modulation by Ca^{2+}- calmodulin of cyclic nucleotide- activated channel of rat olfactory receptor neurons. Nature 368(6471): 545–548.

Chou YH, Spletter ML, Yaksi E, Leong JCS, Wilson RI, Luo L (2010) Diversity and wiring variability of olfactory local interneurons in the Drosophila antennal lobe. Nat Neurosci 13(4): 439–449.

Clyne P, Grant A, O'connell R, Carlson JR (1997) Odorant response of individual sensilla on the Drosophila antenna. Invertebrate Neuroscience 3: 127–135.

Cognigni P, Felsenberg J, Waddell S (2018) Do the right thing: neural network mechanisms of memory formation, expression and update in Drosophila. Curr Opin Neurobiol 49: 51–58.

Colbert HA, Bargmann CI (1995) Odorant-Specific Adaptation Pathways Generate Olfactory Plasticity in C. elegans. Neuron 14(4): 803–812.

Couto A, Alenius M, Dickson BJ (2005) Molecular, Anatomical, and Functional Organization of the Drosophila Olfactory System. Current Biology 15(17): 1535–1547.

Dean I, Harper NS, McAlpine D (2005) Neural population coding of sound level adapts to stimulus statistics. Nat Neurosci 8(12): 1684–1689.

Deshpande M, Venkatesh K, Rodrigues V, Hasan G (2000) The Inositol 1,4,5-Trisphosphate Receptor is Required for Maintenance of Olfactory Adaptation in Drosophila Antennae. J Neurobiol 43(3): 282–288.

Falibene A, Roces F, Rössler W, Groh C (2016) Daily Thermal Fluctuations Experienced by Pupae via Rhythmic Nursing Behavior Increase Numbers of Mushroom Body Microglomeruli in the Adult Ant Brain. Front Behav Neurosci 10: 73.

Fechner G (1966) Elements of Psychophysics. Holt, Rinehart and Winston, Inc., New York.

Firestein S (2001) How the olfactory system makes sense of scents. Nature 413: 211–218.

Fishilevich E, Vosshall LB (2005) Genetic and Functional Subdivision of the Drosophila Antennal Lobe. Current Biology 15(17): 1548–1553.

Guo H, Kunwar K, Smith D (2017) Odorant Receptor Sensitivity Modulation in Drosophila. The Journal of Neuroscience 37(39): 9465–9473.

Gür B, Ramirez L, Cornean J, Thurn F, Molina-Obando S, Ramos-Traslosheros G, Silies M (2024) Neural pathways and computations that achieve stable contrast processing tuned to natural scenes. Nature Communications 15: 8580.

Hallem EA, Carlson JR (2006) Coding of Odors by a Receptor Repertoire. Cell 125(1): 143–160.

Hallem EA, Ho MG, Carlson JR (2004) The Molecular Basis of Odor Coding in the Drosophila Antenna. Cell 117(7): 965–979.

Heimbeck G, Bugnon V, Gendre N, Keller A, Stocker RF (2001) A central neural circuit for experience-independent olfactory and courtship behavior in Drosophila melanogaster. PNAS 98(26): 15336–16341.

Heisenberg M (2003) Mushroom body memoir: from maps to models. Nat Rev Neurosci 4: 266–275.

Hudson R, Distel H (1998) Induced Peripheral Sensitivity in the Developing Vertebrate Olfactory System. Ann N Y Acad Sci 855: 109–115.

Jefferis GSXE, Potter CJ, Chan AM, Marin EC, Rohlfing T, Maurer CR, Luo L (2007) Comprehensive Maps of Drosophila Higher Olfactory Centers: Spatially Segregated Fruit and Pheromone Representation. Cell 128(6): 1187–1203.

Jones DT, Reed RR (1989) Golf: An Olfactory Neuron Specific-G Protein Involved in Odorant Signal Transduction. Science 244(4906): 790–795.

Joseph RM, Carlson JR (2015) Drosophila chemoreceptors: A molecular interface between the chemical world and the brain. Trends Genet 31(12): 683–695.

Jusyte M, Blaum N, Böhme MA, Berns MMM, Bonard AE, Vámosi ÁB, Pushpalatha K V., Kobbersmed JRL, Walter AM (2023) Unc13A dynamically stabilizes vesicle priming at synaptic release sites for short-term facilitation and homeostatic potentiation. Cell Rep 42(6): 112541.

Kazama H, Wilson RI (2008) Homeostatic Matching and Nonlinear Amplification at Identified Central Synapses. Neuron 58(3): 401–413.

Ketkar MD, Shao S, Gjorgjieva J, Silies M (2023) Multifaceted luminance gain control beyond photoreceptors in Drosophila. Current Biology 33(13): 2632–2645.

Kim HS, Santana GM, Sancer G, Emonet T, Jeanne JM (2025) Divergent synaptic dynamics originate parallel pathways for computation and behavior in an olfactory circuit. Current Biology 35(13): 3146–3162.

Kiral FR, Dutta SB, Linneweber GA, Hilgert S, Poppa C, Duch C, Kleist M von, Hassan BA, Hiesinger PR (2021) Brain connectivity inversely scales with developmental temperature in Drosophila. Cell Rep 37(12): 110145.

Kleene SJ, Gesteland RC (1991) Calcium-activated Chloride Conductance in Frog Olfactory Cilia. The Journal of Neuroscience 11(11): 3624–3629.

Kolb B, Harker A, Gibb R (2017) Principles of plasticity in the developing brain. Dev Med Child Neurol 59(12): 1218–1223.

Kramer RH, Siegelbaum SA (1992) Intracellular Ca^{2+} Regulates the Sensitivity of Cyclic Nucleotide-Gated Channels in Olfactory Receptor Neurons. Neuron 9(5): 897–906.

Kucharski R, Maleszka J, Foret S, Maleszka R (2008) Nutritional Control of Reproductive Status in Honeybees via DNA Methylation. Science 319(5871): 1827–1830.

Kurahashi T, Menini A (1997) Mechanism of odorant adaptation in the olfactory receptor cell. Nature 385: 725–729.

Laughlin SB (1989) The role of sensory adaptation in the retina. Journal of Experimental Biology 146: 39–62.

Laughlin SB, Hardie RC (1978) Common Strategies for Light Adaptation in the Peripheral Visual Systems of Fly and Dragonfly. J comp Physiol 128: 319–340.

Leinders-Zufall T, Ma M, Zufall F (1999) Impaired Odor Adaptation in Olfactory Receptor Neurons after Inhibition of Ca^{2+}/Calmodulin Kinase II. The Journal of Neuroscience 19(14): RC19.

Lin HH, Lai JSY, Chin AL, Chen YC, Chiang AS (2007) A Map of Olfactory Representation in the Drosophila Mushroom Body. Cell 128(6): 1205–1217.

Liu M, Chen TY, Ahamed B, Li J, Yau KW (1994) Calcium-calmodulin modulation of the olfactory cyclic nucleotide-gated cation channel. Science 266(5189): 1348–1354.

Luo L (2015) Principles of Neurobiology. Garland Science, New York.

Marin EC, Jefferis GSXE, Komiyama T, Zhu H, Luo L (2002) Representation of the Glomerular Olfactory Map in the Drosophila Brain. Cell 109(2): 243–255.

Martelli C, Carlson JR, Emonet T (2013) Intensity Invariant Dynamics and Odor-Specific Latencies in Olfactory Receptor Neuron Response. The Journal of Neuroscience 33(15): 6285–6297.

Martelli C, Fiala A (2019) Slow presynaptic mechanisms that mediate adaptation in the olfactory pathway of Drosophila. Elife 8: e43735.

Martelli C, Storace DA (2021) Stimulus Driven Functional Transformations in the Early Olfactory System. Front Cell Neurosci 15: 684742.

McLaughlin CN, Brbić M, Xie Q, Li T, Horns F, Kolluru SS, Kebschull JM, Vacek D, Xie A, Li J, Jones RC, Leskovec J, et al. (2021) Single-cell transcriptomes of developing and adult olfactory receptor neurons in Drosophila. Elife 10: e63856.

Meijer JH, Michel S, vanderLeest HT, Rohling JHT (2010) Daily and seasonal adaptation of the circadian clock requires plasticity of the SCN neuronal network. European Journal of Neuroscience 32(12): 2143–2151.

Miazzi F, Hansson BS, Wicher D (2016) Odor-induced cAMP production in Drosophila melanogaster olfactory sensory neurons. Journal of Experimental Biology 219(12): 1798–1803.

Mombaerts P, Wang F, Dulac C, Chao SK, Nemes A, Mendelsohn M, Edmondson J, Axel R (1996) Visualizing an Olfactory Sensory Map. Cell 87(4): 675–686.

Nagel KI, Hong EJ, Wilson RI (2015) Synaptic and circuit mechanisms promoting broadband transmission of olfactory stimulus dynamics. Nat Neurosci 18: 56–65.

Nagel KI, Wilson RI (2011) Biophysical mechanisms underlying olfactory receptor neuron dynamics. Nat Neurosci 14(2): 208–216.

Nagel KI, Wilson RI (2016) Mechanisms Underlying Population Response Dynamics in Inhibitory Interneurons of the Drosophila Antennal Lobe. The Journal of Neuroscience 36(15): 4325–4338.

Nakamura T, Gold GH (1987) A cyclic nucleotide-gated conductance in olfactory receptor cilia. Nature 325: 442–444.

Oland LA, Biebelhausen JP, Tolbert LP (2008) Glial Investment of the Adult and Developing Antennal Lobe of Drosophila. J Comp Neurol 509(5): 526–550.

Olsen SR, Bhandawat V, Wilson RI (2010) Divisive Normalization in Olfactory Population Codes. Neuron 66(2): 287–299.

Olsen SR, Wilson RI (2008) Lateral presynaptic inhibition mediates gain control in an olfactory circuit. Nature 452: 956–960.

Pace U, Hanski E, Salomon Y, Lancet D (1985) Odorant-sensitive adenylate cyclase may mediate olfactory reception. Nature 316: 255–258.

Pettis JS, Winston ML, Slessor AKN (1995) Behavior of Queen and Worker Honey Bees (Hymenoptera: Apidae) in Response to Exogenous Queen Mandibular Gland Pheromone. Ann Entomol Soc Am 88(4): 580–588.

Reisert J, Matthews HR (1999) Adaptation of the odour-induced response in frog olfactory receptor cells. Journal of Physiology 519(3): 801–813.

Reisert J, Zhao H (2011) Response kinetics of olfactory receptor neurons and the implications in olfactory coding. Journal of General Physiology 138(3): 303–310.

Reuter D, Zierold K, Schröder WH, Frings S (1998) A Depolarizing Chloride Current Contributes to Chemoelectrical Transduction in Olfactory Sensory Neurons In Situ. The Journal of Neuroscience 18(17): 6623–6630.

Riffell JA, Abrell L, Hildebrand JG (2008) Physical Processes and Real-Time Chemical Measurement of the Insect Olfactory Environment. J Chem Ecol 34(7): 837–853.

Root CM, Masuyama K, Green DS, Enell LE, Nässel DR, Lee CH, Wang JW (2008) A Presynaptic Gain Control Mechanism Fine-Tunes Olfactory Behavior. Neuron 59(2): 311–321.

Sargsyan V, Getahun MN, Llanos SL, Olsson SB, Hansson BS, Wicher D (2011) Phosphorylation via PKC regulates the function of the Drosophila odorant co-receptor. Front Cell Neurosci 5: 5.

Sato K, Pellegrino M, Nakagawa T, Nakagawa T, Vosshall LB, Touhara K (2008) Insect olfactory receptors are heteromeric ligand-gated ion channels. Nature 452: 1002–1006.

Scheffer LK, Xu CS, Januszewski M, Lu Z, Takemura SY, Hayworth KJ, Huang GB, Shinomiya K, Maitin-Shepard J, Berg S, Clements J, Hubbard PM, et al. (2020) A connectome and analysis of the adult Drosophila central brain. Elife 9: e57443.

Schenk JE, Gaudry Q (2023) Nonspiking Interneurons in the Drosophila Antennal Lobe Exhibit Spatially Restricted Activity. eNeuro 10(1).

Schlegel P, Bates AS, Stürner T, Jagannathan SR, Drummond N, Hsu J, Capdevila LS, Javier A, Marin EC, Barth-Maron A, Tamimi IFM, Li F, et al. (2021) Information flow, cell types and stereotypy in a full olfactory connectome. Elife 10: e66018.

Schlief ML, Wilson RI (2007) Olfactory processing and behavior downstream from highly selective receptor neurons. Nat Neurosci 10(5): 623–630.

Semke E, Distel H, Hudson R (1995) Specific Enhancement of Olfactory Receptor Sensitivity Associated with Foetal Learning of Food Odors in the Rabbit. Naturwissenschaften 82(3): 148–149.

Sinnarajah S, Dessauer CW, Srikumar D, Chen J, Yuen J, Yilma S, Dennis JC, Morrison EE, Vodyanoy V, Kehrl JH (2001) RGS2 regulates signal transduction in olfactory neurons by attenuating activation of adenylyl cyclase III. Nature 409: 1051–1055.

Sklar PB, Anholt RRH, Snyder SH (1986) The Odorant-sensitive Adenylate Cyclase of Olfactory Receptor Cells. Differential Stimulation by Distinct Classes of Odorants. J Biol Chem 261(33): 15538–15543.

Song Y, Cygnar KD, Sagdullaev B, Valley M, Hirsh S, Stephan A, Reisert J, Zhao H (2008) Olfactory CNG Channel Desensitization by Ca^{2+}/CaM via the B1b Subunit Affects Response Termination but Not Sensitivity to Recurring Stimulation. Neuron 58(3): 374–386.

Sourjik V, Wingreen NS (2012) Responding to chemical gradients: bacterial chemotaxis. Curr Opin Cell Biol 24: 262–268.

Störtkuhl KF, Hovemann BT, Carlson JR (1999) Olfactory Adaptation Depends on the Trp Ca^{2+} Channel in Drosophila. The Journal of Neuroscience 19(12): 4839–4846.

Su CY, Menuz K, Carlson JR (2009) Olfactory Perception: Receptors, Cells, and Circuits. Cell 139: 45–59.

Turrigiano G (2012) Homeostatic Synaptic Plasticity: Local and Global Mechanisms for Stabilizing Neuronal Function. Cold Spring Harb Perspect Biol 4: a005736.

Vergoz V, Mcquillan HJ, Geddes LH, Pullar K, Nicholson BJ, Paulin MG, Mercer AR (2009) Peripheral modulation of worker bee responses to queen mandibular pheromone. PNAS 106(49): 20930–20935.

Vosshall LB, Stocker RF (2007) Molecular Architecture of Smell and Taste in Drosophila. Annu Rev Neurosci 30: 505–533.

Wahl S, Engelhardt M, Schaupp P, Lappe C, Ivanov I V. (2019) The inner clock—Blue light sets the human rhythm. J Biophotonics 12(12): e201900102.

Walter AM, Böhme MA, Sigrist SJ (2018) Vesicle release site organization at synaptic active zones. Neurosci Res 127: 3–13.

Wark B, Lundstrom BN, Fairhall A (2007) Sensory adaptation. Curr Opin Neurobiol 17(4): 423–429.

Weber AI, Krishnamurthy K, Fairhall AL (2019) Coding Principles in Adaptation. Annu Rev Vis Sci 5: 427–449.

Wicher D (2018) Tuning Insect Odorant Receptors. Front Cell Neurosci 12: 94.

Wicher D, Schäfer R, Bauernfeind R, Stensmyr MC, Heller R, Heinemann SH, Hansson BS (2008) Drosophila odorant receptors are both ligand-gated and cyclic-nucleotide-activated cation channels. Nature 452: 1007–1011.

Willmore BDB, King AJ (2023) Adaptation in auditory processing. Physiol Rev 103(2): 1025–1058.

Wilson RI, Laurent G (2005) Role of GABAergic Inhibition in Shaping Odor-Evoked Spatiotemporal Patterns in the Drosophila Antennal Lobe. The Journal of Neuroscience 25(40): 9069–9079.

Wilson RI, Mainen ZF (2006) Early Events in Olfactory Processing. Annu Rev Neurosci 29: 163–201.

Wu A, Yu B, Komiyama T (2020) Plasticity in olfactory bulb circuits. Curr Opin Neurobiol 64: 17–23.

Zald DH, Pardo J V. (1997) Emotion, olfaction, and the human amygdala: Amygdala activation during aversive olfactory stimulation. PNAS 94(8): 4119–4124.

Zufall F, Leinders-Zufall T (2000) The Cellular and Molecular Basis of Odor Adaptation. Chem Senses 25: 473–481.

Zufall F, Shepherd GM, Firestein S (1991) Inhibition of the olfactory cyclic nucleotide gated ion channel by intracellular calcium. Proc R Soc Lond B 246(1317): 225–230.

Züfle P, Batista LL, Brandão SC, D'Uva G, Daniel C, Martelli C (2025) Impact of developmental temperature on neural growth, connectivity, and function. Sci Adv 11: eadp9587.

7 Acknowledgements

8 Appendix

8.1 List of Abbreviations

ACh	acetylcholine
AL	antennal lobe
cAMP	cyclic adenosine monophosphate
CNG	cyclic-nucleotide gated
GABA	gamma-aminobutyric acid
GC	granule cell
IP3	inositol triphosphate
Ir	ionotropic receptor
JND	just noticeable difference
LN	local neuron
MC	mitral cell
Or	odorant receptor
Orco	odorant-receptor co-receptor
ORN	olfactory receptor neuron
PGC	periglomerular cell
PN	projection neuron
SCN	suprachiasmatic nucleus
TC	tufted cell

8.2 Declaration of Independence

Hiermit erkläre ich,

dass ich die vorliegende Arbeit selbstständig verfasst und keine anderen als die angegebenen Quellen und Hilfsmittel (dazu zählen auch KI-basierte Anwendungen oder Werkzeuge[1]) benutzt habe. Sämtliche wörtlichen oder sinngemäßen Übernahmen und Zitate sind kenntlich gemacht und nachgewiesen. Ich versichere, dass ich keine Hilfsmittel verwendet habe, deren Nutzung die Prüferin oder der Prüfer explizit ausgeschlossen hat. Im Anhang habe ich die verwendeten KI-Tools dokumentiert.

Mit Abgabe der vorliegenden Leistung übernehme ich die Verantwortung für das eingereichte Gesamtprodukt. Ich verantworte damit auch jegliche KI-generierten Inhalte, die ich in meine Arbeit übernommen habe. Die Richtigkeit übernommener (KI-generierter) Aussagen und Inhalte habe ich nach bestem Wissen und Gewissen geprüft.

Ich habe die Arbeit nicht zum Erwerb eines anderen Leistungsnachweises in gleicher oder ähnlicher Form eingereicht.

Mir ist bekannt, dass ein Verstoß gegen die genannten Punkte prüfungsrechtliche Konsequenzen hat und insbesondere dazu führen kann, dass die Studien- und Prüfungsleistung als mit „nicht bestanden“ bewertet wird. Die Einschreibung kann für bis zu zwei Jahre widerrufen werden, wenn Studierende zweimal oder häufiger bei Prüfungsleistungen täuschen (§ 69 Abs. 4 und S5 HochSchG).

_____

Ort, Datum und Unterschrift

AI-Tool	Purpose
DeepL Translate	Translation of abstract from English to German Translation into English of regulation documents in German
Google Translate	Translation into English of regulations/formularies in German
Consensus	Help with finding relevant papers
NotebookLM	Help with reading some papers
ChatGPT	Help with clarifying concepts and exploring scientific ideas Help improve minor parts of the text

Note: I carefully reviewed and validated all concepts and literature. This dissertation is the result of my writing, critical thinking and interpretations.

[1] Weiterführende Informationen zu KI-basierte Anwendungen oder Werkzeuge unter: https://digitale-lehre.uni-mainz.de/lehren-pruefen/ki-in-der-hochschulbildung/

8.3 Declaration of Honor

Hiermit versichere ich gemäß § 12, (2) der Promotionsordnung vom 01.04.2018:

Ich habe die heute als Dissertation vorgelegte Arbeit selbst angefertigt und ausschließlich die angegebenen Quellen und Hilfsmitte verwendet.

Ich habe oder hatte die jetzt als Dissertation vorgelegte Arbeit noch an keiner anderen deutschen oder ausländischen Hochschule oder vergleichbaren Einrichtung zur Erlangung eines akademischen Grades eingereicht.

Ich habe noch kein Promotions- PhD,- oder ein vergleichbares Graduierungsverfahren im Promotionsfach erfolglos beendet.

Ich habe noch kein Promotions- PhD,- oder ein vergleichbares Graduierungsverfahren im Promotionsfach erfolgreich beendet.

Für die Anfertigung der vorgelegten Arbeit wurde keine entgeltliche Hilfe Dritter, insbesondere eine Promotionsberatung oder –vermittlung in Anspruch genommen.

_____

Ort, Datum und Unterschrift

Curriculum Vitae